

May 2013

Rolling Contact Fatigue of Low Hardness Steel for Slewing Ring Application

Jason A. Knuth

University of Wisconsin-Milwaukee

Follow this and additional works at: <https://dc.uwm.edu/etd>



Part of the [Materials Science and Engineering Commons](#)

Recommended Citation

Knuth, Jason A., "Rolling Contact Fatigue of Low Hardness Steel for Slewing Ring Application" (2013). *Theses and Dissertations*. 123.
<https://dc.uwm.edu/etd/123>

This Thesis is brought to you for free and open access by UWM Digital Commons. It has been accepted for inclusion in Theses and Dissertations by an authorized administrator of UWM Digital Commons. For more information, please contact open-access@uwm.edu.

**ROLLING CONTACT FATIGUE OF LOW HARDNESS STEEL FOR
SLEWING RING APPLICATION**

by

Jason A. Knuth

A Thesis Submitted in
Partial Fulfillment of the
Requirements for Degree of

Master of Science

in Engineering

at

The University of Wisconsin-Milwaukee

May 2013

ABSTRACT

ROLLING CONTACT FATIGUE OF LOW HARDNESS STEEL FOR SLEWING RING APPLICATION

by

Jason A. Knuth

The University of Wisconsin-Milwaukee, 2013
Under the Supervision of Professor Anoop K. Dhingra

This thesis discusses the rolling contact fatigue of steel utilized in anti-friction bearings, also referred to as slewing bearings. These slewing bearings are utilized in cranes, excavators, wind turbines and other similar applications. Five materials composed of two different material types were tested. The two material types were high carbon steel and medium carbon alloy steel. The test specimens were processed from forged rolled rings. Two machines were evaluated a ZF-RCF and 3-Ball test machine. The evaluation was to determine which machine can best simulate the application in which the slewing bearing is utilized.

Initially, each specimen will be pretested to determine the appropriate testing direction from within the forged rolled rings. Pretesting is needed in order to establish consistent failure modes between samples. The primary goal of the test is to understand the life differences and failure modes between high carbon steel and medium carbon alloy steel. The high carbon steel ring was cut into two sections, one of which was stress relieved and the other was quenched and tempered. The medium carbon alloy steel was

cut into three sections, all of which were quenched and tempered to different hardness levels. The test program was dynamically adjusted based upon the previous sample's life and load. An S-N curve was then established from the 5 materials tested at two target loads. The samples were run until the first sign of a crack was detected by an eddy current.

At the completion of the rolling contact test, select sample's microstructure was evaluated for crack initiation location. The selected samples were divided into four groups which represent different maximum shear stress levels. These samples displayed indications of material deformation in which the high carbon steel experienced an increased amount of cold work when compared to medium carbon alloy steel. The life of the high carbon steel was nearly equivalent to the expected life of the medium carbon alloy. The work hardening of the high carbon steel increased the surface hardness that exceeded the medium carbon alloy steel surface hardness.

© Copyright by Jason A. Knuth, 2013
All Rights Reserved

TABLE OF CONTENTS

ABSTRACT.....	ii
TABLE OF CONTENTS.....	v
LIST OF FIGURES	viii
LIST OF TABLES	xii
ACKNOWLEDGEMENTS	xiii
Chapter 1	1
1.1 Background.....	1
1.2 Literature review.....	3
1.3 Research Objectives and Scope	6
1.4 Thesis Organization	7
Chapter 2.....	10
2.1 Introduction.....	10
2.2 Rolling Contact Fatigue	10
2.3 Slewing Ring Application Failures.....	12
2.4 Summary.....	14
Chapter 3.....	18
3.1 Introduction.....	18
3.2 Objective for Testing	18
3.3 ZF-RCF testing machine.....	19
3.4 Three-Ball Test Machine	20
3.5 Test apparatus Comparison.....	21
3.6 Testing Parameters.....	23

3.7 Summary	24
Chapter 4.....	30
4.1 Introduction.....	30
4.2 Material Samples	30
4.3 Determining RCF test Specimen Orientation	31
4.4 Equations used for testing.....	34
4.5 Pretesting for Specimen Orientation.....	36
4.6 Summary	38
Chapter 5.....	46
5.1 Introduction.....	46
5.2 Test Program Setup.....	46
5.3 High Carbon Steel.....	47
5.3.1 RCF-1-XX.....	47
5.3.2 RCF-2-XX.....	48
5.4 Medium Carbon Alloy Steel	50
5.4.1 RCF-3-XX.....	50
5.4.2 RCF-4-XX.....	52
5.4.3 RCF-5-XX.....	53
5.5 Metallurgical Analysis of the Samples	54
5.5.1 Stress Level 1 (73%).....	55
5.5.2 Stress Level 2 (90%).....	56
5.5.3 Stress Level 3 (100%).....	58
5.5.4 Stress Level 4 (110%).....	62
5.6 Discussion of Results.....	64
5.7 Summary	67
Chapter 6.....	88
6.1 Summary of research	88

6.2 Scope of Future work.....	91
References.....	93
Appendix A: Rolling Surface evaluation of RCF-1-XX.....	95
Appendix B: Rolling Surface evaluation of RCF-2-XX.....	105
Appendix C: Rolling Surface evaluation of RCF-3-XX.....	109
Appendix D: Rolling Surface evaluation of RCF-4-XX.....	113
Appendix E: Rolling Surface evaluation of RCF-5-XX.....	119
Appendix F: Weibull Curve.....	123

LIST OF FIGURES

Figure 1.1: Applications that utilize a slewing bearing	8
Figure 1.2: Multiple slewing bearing configurations.....	8
Figure 1.3 Slewing bearing degrees of freedom	9
Figure 1.4 Three row roller slewing ring configuration	9
Figure 2.1: Medium carbon alloy steel application failure	15
Figure 2.2: Medium carbon alloy steel application failure subsurface crack	15
Figure 2.3: Top view of medium carbon alloy steel failure.....	16
Figure 2.4: Material structure changes due to rolling contact forces (ref).....	16
Figure 2.5: High carbon steel application failure mode.....	17
Figure 3.1: Schematic of ZF-RCF testing machine	27
Figure 3.2: Photograph of ZF-RCF testing machine	27
Figure 3.3: Diagram of three-ball test or ball-rod test	28
Figure 3.4: Photograph of three-ball test or ball-rod test apparatus	28
Figure 3.5: Eddy current crack detection	29
Figure 4.1: Specimen testing direction	42
Figure 4.2: Specimen testing direction of machined bar	42
Figure 4.3: Direction of inclusions in test specimen.....	43
Figure 4.4: RCF-1-01-PRE Crack location.....	43
Figure 4.5: RCF-1-01-PRE microstructure of crack.....	44
Figure 4.6: RCF-5-03-PRE inclusion direction	44
Figure 4.7: RCF-5-03-PRE Crack and Microstructure	45
Figure 5.1: RCF-3-04, crack location. Unetched (201X)	73
Figure 5.2: RCF-3-04, Microstructure. 2% Nital (50X)	73
Figure 5.3: RCF-1-07, Crack location. Unetched (201X)	74
Figure 5.4: RCF-1-07, Microstructure. 2% Nital (50X)	74
Figure 5.5: RCF-1-07, Transgranular crack. 2% Nital (494X).....	75
Figure 5.6: RCF-1-07, Fine lamellar pearlite with small amounts of ferrite. (494X).....	75
Figure 5.7: RCF-4-12, Crack location. Unetched (201X)	76
Figure 5.8: RCF-4-12, Microstructure. 2% Nital (50X)	76
Figure 5.9: RCF-1-14, Crack location. Unetched (201X)	77

Figure 5.10: RCF-1-14, Microstructure. 2% Nital (50X)	77
Figure 5.11: RCF-2-01, Crack location. Unetched (201X)	78
Figure 5.12: RCF-2-01, Near surface microstructure. 2% Nital (494X)	78
Figure 5.13: RCF-2-05, Crack location. Unetched (201X)	79
Figure 5.14: RCF-5-02, Crack location. Unetched (201X)	79
Figure 5.15: RCF-5-02, Microstructure. 2% Nital (50X)	80
Figure 5.16: RCF-2-07, Crack location. Unetched (201X)	80
Figure 5.17: RCF-2-07, Microstructure. 2% Nital (50X)	81
Figure 5.18: RCF-5-09, Crack Location Unetched (201X)	81
Figure 5.19: RCF-5-09, Microstructure. 2% Nital (50X)	82
Figure 5.20: S-N Curve of 10% Failure with 95% Confidence	82
Figure 5.21: S-N Curve of 50% Failure with 95% Confidence	83
Figure 5.22: Subsurface hardness specific application material	83
Figure 5.23: Percent subsurface hardness increase specific application material	84
Figure 5.24: Range 1 shear stress level 73% micro hardness	84
Figure 5.25: Range 2 shear stress level 90% micro hardness	85
Figure 5.26: Range 3 shear stress level 100% micro hardness	85
Figure 5.27: Range 4 shear stress level 110% micro hardness	86
Figure 5.28: Comparison of application failure to testing failures	87
Figure A.1: RCF-1-06, 30.8% Increased Contact Width, crack 2.1mm	95
Figure A.2: RCF-1-06, Crack Tip	95
Figure A.3: RCF-1-07, 30% Increased Contact Width, crack 1.24mm	96
Figure A.4: RCF-1-07, Crack Tip	96
Figure A.5: RCF-1-08, 24.3% Increased Contact Width, crack 1.7mm	97
Figure A.6: RCF-1-08, Surface Condition	97
Figure A.7: RCF-1-09, 27.5% Increased Contact Width, crack 2.4mm	98
Figure A.8: RCF-1-09, Crack Tip	98
Figure A.9: RCF-1-10, 28.8% Increased Contact Width, crack 1.3mm	99
Figure A.10: RCF-1-10, Crack Tip	99
Figure A.11: RCF-1-11, 33.7% Increased Contact Width, crack 1.64mm	100
Figure A.12: RCF-1-11, Crack Tip	100
Figure A.13: RCF-1-12, 40.0% Increased Contact Width, crack 1.5mm	101
Figure A.14: RCF-1-12, Surface Condition	101
Figure A.15: RCF-1-13, 42.0% Increased Contact Width, crack 1.7mm	102
Figure A.16: RCF-1-13, Crack Tip at Edge of Rolling Surface	102
Figure A.17: RCF-1-14, 37.8% Increased Contact Width, crack 3mm	103
Figure A.18: RCF-1-14, Surface Condition	103
Figure A.19: RCF-1-15, 38.5% Increased Contact Width, crack 1.3mm	104

Figure A.20: RCF-1-15, Surface Condition.....	104
Figure B.1: RCF-2-01, 11.8% Increased Contact Width, crack 1.4mm	105
Figure B.2: RCF-2-02, 9.8% Increased Contact Width, crack 2.15mm	105
Figure B.3: RCF-2-03, 11.8% Increased Contact Width, crack 1.2mm	106
Figure B.4: RCF-2-04, 11.8% Increased Contact Width, crack unknown	106
Figure B.5: RCF-2-05, 11.8% Increased Contact Width, crack 1.4mm	107
Figure B.6: RCF-2-06, 17.6% Increased Contact Width, crack 1.1mm	107
Figure B.7: RCF-2-07, 17.6% Increased Contact Width, crack 1.5mm	107
Figure B.8: RCF-2-08, 13.7% Increased Contact Width, crack 1.5mm	108
Figure B.9: RCF-2-09, 17.6% Increased Contact Width, crack 1.0mm	108
Figure B.10: RCF-2-10, 17.6% Increased Contact Width, crack 1.3mm	108
Figure C.1: RCF-3-04, 9.4% Increased Contact Width, crack 1.9mm	109
Figure C.2: RCF-3-05, 7.8% Increased Contact Width, crack 2.2mm	109
Figure C.3: RCF-3-06, 7.3% Increased Contact Width, crack 1mm	110
Figure C.4: RCF-3-07, 9.2% Increased Contact Width, crack 0.62mm	110
Figure C.6: RCF-3-08, 4.9% Increased Contact Width, crack 1.5mm	111
Figure C.7: RCF-3-09, 9.8% Increased Contact Width, crack 1.5mm	111
Figure C.8: RCF-3-10, 9.8% Increased Contact Width, crack 1.5mm	111
Figure C.9: RCF-3-11, 7.8% Increased Contact Width, crack 1.7mm	112
Figure C.10: RCF-3-11, 9.8% Increased Contact Width, crack 1.35mm	112
Figure D.1: RCF-4-03, 11.2% Increased Contact Width, crack 1.5mm.....	113
Figure D.2: RCF-4-04, 11.6% Increased Contact Width, crack 0.7mm, Chunk Missing	113
Figure D.3: RCF-4-05, 8.4% Increased Contact Width, crack 1.5mm.....	113
Figure D.4: RCF-4-06, 12.2% Increased Contact Width, crack 0.9x1.2mm.....	114
Figure D.5: RCF-4-07, 14.7% Increased Contact Width, crack 2.1mm.....	114
Figure D.6: RCF-4-08, 7.8% Increased Contact Width, crack 1mm.....	115
Figure D.7: RCF-4-10, 8.8% Increased Contact Width, crack 1.1mm.....	115
Figure D.8: RCF-4-12, 19.6% Increased Contact Width, crack 1.5mm.....	115
Figure D.9: RCF-4-14, 14.9% Increased Contact Width, crack 1x0.6mm.....	116
Figure D.10: RCF-4-15, 7.6% Increased Contact Width, Missing Chunk 2.2x2.1mm..	116
Figure D.11: RCF-4-16, 7.8% Increased Contact Width.....	117
Figure D.12: RCF-4-18, 12.5% Increased Contact Width, crack 2.1mm.....	117
Figure D.13: RCF-4-19, 10.2% Increased Contact Width, crack 1.2mm.....	118
Figure D.14: RCF-4-21, 13.9% Increased Contact Width, crack 1.7mm.....	118

Figure E.1: RCF-5-01, 17.6% Increased Contact Width, crack 1.5mm	119
Figure E.2: RCF-5-02, 5.1% Increased Contact Width	119
Figure E.3: RCF-5-04, 4.9% Increased Contact Width, Crack 1.6mm	120
Figure E.4: RCF-5-05, 3.5% Increased Contact Width, Crack 1.2mm	120
Figure E.5: RCF-5-06, 3.9% Increased Contact Width, Crack 1.5mm	121
Figure E.6: RCF-5-08, 6.9% Increased Contact Width, Crack 1.5mm	121
Figure E.7: RCF-5-09, 4.7% Increased Contact Width, Crack 1.6mm	121
Figure E.8: RCF-5-10, 4.1% Increased Contact Width, Crack 1.5mm	121
Figure E.9: RCF-5-11, 4.1% Increased Contact Width	122
Figure E.10: RCF-5-11, 4.1% Increased Contact Width, Crack 1.5mm	122
Figure F.1: RCF-1-XX, Low Range, Weibull Plot.....	123
Figure F.2: RCF-1-XX, High Range, Weibull Plot	123
Figure F.3: RCF-2-XX, Low Range, Weibull Plot.....	124
Figure F.4: RCF-2-XX, High Range, Weibull Plot	124
Figure F.5: RCF-3-XX, Low Range, Weibull Plot.....	125
Figure F.6: RCF-3-XX, High Range, Weibull Plot	125
Figure F.7: RCF-4-XX, Low Range, Weibull Plot.....	126
Figure F.8: RCF-4-XX, High Range, Weibull Plot	126
Figure F.9: RCF-5-XX, Low Range, Weibull Plot.....	127
Figure F.10: RCF-5-XX, High Rang, Weibull Plot.....	127

LIST OF TABLES

Table 3.1: Test machine Comparison	26
Table 4.1: Tested Material	40
Table 4.2: Metallurgy & heat treatment process of material	40
Table 4.3: Mechanical Properties of the Material.....	41
Table 4.4: Results of Pre-test.....	41
Table 5.1: Results of RCF-1-XX test.....	48
Table 5.2: Results of RCF-2-XX test.....	49
Table 5.3: Results of RCF-3-XX test.....	51
Table 5.4: Results of RCF-4-XX test.....	52
Table 5.5: Results of RCF-5-XX test.....	54
Table 5.6: Reviewed metallurgical specimen ID and test results	70
Table 5.7: Micro hardness from the rolling surface of Range 1 (200 gm. Load)	70
Table 5.8: Micro hardness from the rolling surface of range 2 (200 gm. Load)	71
Table 5.9: Micro hardness from the rolling surface of range 3 (200 gm. Load)	71
Table 5.10: Micro hardness from the rolling surface of range 4 (200 gm. Load)	72
Table 5.11: Comparison of crack origin to hardness increase	72

ACKNOWLEDGEMENTS

I would like to thank my advisor Dr. Anoop Dhingra for his support throughout this project. I am especially grateful to Dr. Gottfried Hoffmann for his mentoring during the fatigue testing of the specimen utilizing the ZF-RCF rig. Additionally, I would like to thank Thomas Tefelske, P.E. Metallurgical Engineer, for his guidance in the preparation and evaluation of the of the test specimen. I would also like to extend my gratitude to Joy Global Inc. for the financial support and background information used for this research. Thank you as well to Michael Linstroth for your time spent reviewing my thesis. I also want to thank Prof. Perez and Prof. Lopez for serving on my committee and for the time spent reviewing my thesis.

Finally, I would like to thank my wife and family for their encouragement and patience while I have been pursuing my Master of Science in Engineering Degree.

Chapter 1

Introduction

1.1 Background

Cranes, excavators and wind turbines (Figure 1.1) utilize anti-friction bearings, also referred to as slewing bearings. A slewing bearing allows for rotation in opposite directions between two structures. In the above applications, a typical slewing bearing can range in size from three to twenty feet in diameter. Typical operating conditions for these applications include low rotational speeds (between 5-10 rpm) and oscillating loads. A slewing bearing assembly can consist of multiple configurations (Figure 1.2). The typical slewing bearing configuration consists of two raceways fixed to opposing structures with cylindrical or ball rolling elements in between. The slewing bearing allows for one open degree of freedom; restricting all translational and two rotational degrees of freedom (Figure 1.3).

The specific application that will utilize the results of this research has relatively large amounts of structural deflection and load profiles which are difficult to obtain due to various operational conditions. Slewing bearing loads can be described with three forces; axial, radial, and moment loads [Rotec]. Axial load is determined by the force applied in parallel to the slewing bearing's axis of rotation. This force arises from the opposing structures either pulling apart or pushing together the raceways. Radial load is the force acting perpendicular to the slewing bearing's axis of rotation. The magnitude of the force can vary depending on the installation and operational position of the bearing due to gravity shearing the raceways apart. The moment load is a force nonconcentric to

the slewing bearing's axis of rotation. The load is multiplied by the distance from the slewing bearing's axis of rotation. The application's axial force can exceed seven hundred and fifty short tons, have a radial load above five hundred short tons, and a moment load in excess of fifty million foot pounds. The three forces along with the large amount of structural deflection require a special size and type of slewing bearing.

The focus of this research is on the material selection of the raceway for a configuration similar to a three row roller (Figure 1.4). Slewing bearing raceways can utilize many different types of materials including: chrome steel, stainless steel, low or medium carbon alloy steel, ceramic, and plastic. The raceway material selection for a given application will significantly affect the performance and reliability of the slewing bearing. Some factors used in the selection of a raceway material are: application, hardness, fatigue resistance, anticipated lubrication cleanliness, and expected failure modes. Knowing the specific application's applied loads and forces determines the required material strength and ductility. The material hardness of the raceway is a key parameter for determining the bearing's capacity. Fatigue resistance under rolling contact conditions governs the allowed number of cycles for a given application. Contamination in the lubrication will cause the bearing to wear, increasing the internal geometric tolerances. The expected failure mode of a raceway influences the predictability and statistical variance of a failure occurring.

The design of the slewing ring used for this application has been in existence prior to this research. The standard slewing ring raceway material is high carbon steel, but the new specific application's raceway material used medium carbon alloy steel. Due to the structural deflections and manufacturing considerations the raceway and rolling element

material used for the specific design has a hardness of Rockwell C30-C42 in comparison to a standard slewing bearing hardness of Rockwell C55-C60. Fatigue resistance and failure mode are critical in this application due to the size and expense of repair and/or replacement of the slewing ring. This application is well lubricated with a low amount of contamination. Premature raceway failures have occurred on the slewing rings of the specific application in which utilize the medium carbon alloy steel. The medium carbon alloy steel was thought to have significantly better mechanical properties along with excellent harden-ability. It was believed that this would increase the overall raceway's hardness for a higher load capacity. However, when the medium carbon alloy steel was put into service the raceway lasted approximately half of the expected component life. The raceway would develop spalls and deep subsurface cracks. Prior to failure, the raceway rolling surface did not indicate a failure was about to occur. Due to a lack of any advance warning, the application's end user was unable to plan for the outage, which added frustration and expense.

This research qualifies which of the two raceway materials i.e. a high carbon or medium carbon alloy steel is better suited for the specific slewing ring application. The material will be subjected to rolling contact fatigue near the slewing ring's hardness level to determine which material has a more favorable failure mode and higher load capacity.

1.2 Literature review

The majority of rolling contact fatigue research focused on applications for the bearing and gearing industries. Depending upon the researcher's objectives and

hypothesis, several testing parameters were evaluated, such as elliptical or line contact. These types of contacts will affect the subsurface stress profile and the material's contact surface. The test specimen's mechanical and microstructural properties will influence crack propagation rate along with fatigue life of the specimen. These specimens can be subject to different environmental conditions. One example would be the rotational speed of the specimen which can modify the elastohydrodynamic lubricating conditions and oil temperatures. The magnitude of relative speed between the load rollers and the test specimen is defined as the sliding ratio. This ratio will produce a difference in the depth at which the maximum subsurface shear stress occurs.

Choi and Lee (2001) tested low carbon alloy steel under line contact conditions with a rotating speed of 8,000 rpm, applying a constant force to the test specimen ranging from 25-100 kgf. The test specimen had a microstructure of martensite with a mixture of bainite formed from the thermomechanical processing. The maximum shear stress zone was found in the area of increased hardness and was in agreement with the calculated depth of maximum shear stress according to distortion energy hypothesis and maximum shear stress hypothesis. The authors discuss the transformation and deformation behavior of the microstructure during rolling contact fatigue at the surface and in the maximum shear stress zones. The criteria used to determine the failure of each sample is unknown. The surfaces of each test specimen were examined for surface deformation using a Taylor Hobson surface roughness tester.

Hoffmann & Jandeska (2007) conducted a series of tests on powered metallurgy material for automotive gearing applications. Four different materials were tested with two distinctive heat treatment methods. Materials AISI 5120 & 8620 were carburized

and the remaining two materials were induction hardened using AISI 1060 & 4150 material. The materials were tested with line contact conditions at rotational speeds of 3,000 rpm. The load rollers on the test specimen applied pressures of 1250 Mpa to 4000 MPa. The research described methods for determining test ranges of material with unknown properties such as the endurance stress. The test apparatus's load was set to encourage crack initiation, at which time the apparatus's load was significantly reduced. The load was gradually increased every ten million cycles until crack growth resumed. The load level at which the crack resumed was considered to be the materials endurance stress. The test demonstrated how the method of processing and heat treating the material will affect the endurance strength along with the crack propagation rates.

Oila and Bull (2005) evaluated the metallurgical phase transformation during rolling and sliding contact. Their research focused on gear tooth contact; however this phenomenon is applicable for rolling contact in bearings as well. The test material used for their evaluation was carburized low carbon alloy steel with a martensitic structure with fifteen percent retained austenite. The authors observed three prominent features in the microstructure of the test specimens. Alternating stresses during rolling contact caused plastic deformation which changed the dislocation density resulting in increased hardness of the material. During this time they felt the temperature was high enough to activate the diffusion of carbon. Then, within the boundaries of plastic deformation, recrystallization occurred. This new structure was deemed a dark etching region near the contact surface which had initiated at prior austenite grain boundaries. Below these features lay white etching bands, where carbon from the bands migrated in their vicinity

causing the space between bands to have elevated hardness. This study has shown the effect on martensitic structure during rolling contact fatigue.

Research on rolling contact fatigue is dependent upon multiple parameters. These parameters have to be adjusted depending on the objective of the research. The above research has demonstrated key parameters, of which is having a consistent failure criterion for determining when the first initiated crack or pit occurred. Also, the test specimen's material processing and microstructure will affect the endurance strength of the specimen. To quantify differences between specific materials used in a given application, an independent test is required due to the inconsistency of the parameters between studies.

1.3 Research Objectives and Scope

This research deals with:

1. Determining the appropriate testing apparatus and parameters to simulate the application's working conditions.
2. Developing test procedure in order to review different heat treatment processes of the high carbon and medium carbon alloy steels.
3. Executing the developed test procedure to determine which material has a more favorable failure mode and higher load capacity.
4. Evaluating the test specimens for similarity to the application's preexisting material and failures.

1.4 Thesis Organization

This Thesis is divided into six chapters. Chapter 1 presented an overview of the research problem including literature review, research objectives, and the scope of this thesis, as well as the organization.

Chapter 2 covers the different types of failure modes along with the failure modes associated with the application's preexisting material.

Chapter 3 covers the selection process used to determine the testing apparatus and parameters.

Chapter 4 covers the pretesting evaluation of the material used to select the appropriate testing procedure.

Chapter 5 covers the execution of the test procedure and preliminary result.

Finally, chapter 6 summarizes the main finding of this thesis and outlines the scope for future work.



Figure 1.1: Applications that utilize a slewing bearing

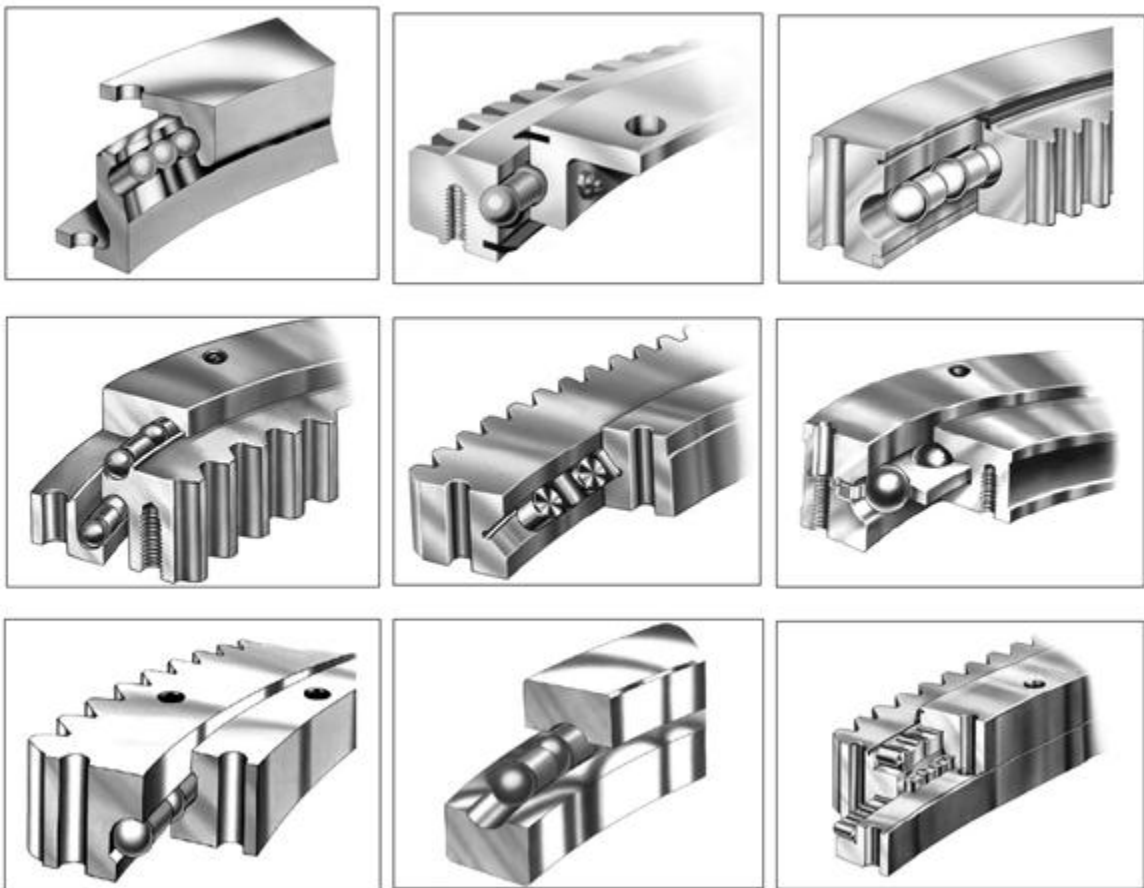


Figure 1.2: Multiple slewing bearing configurations

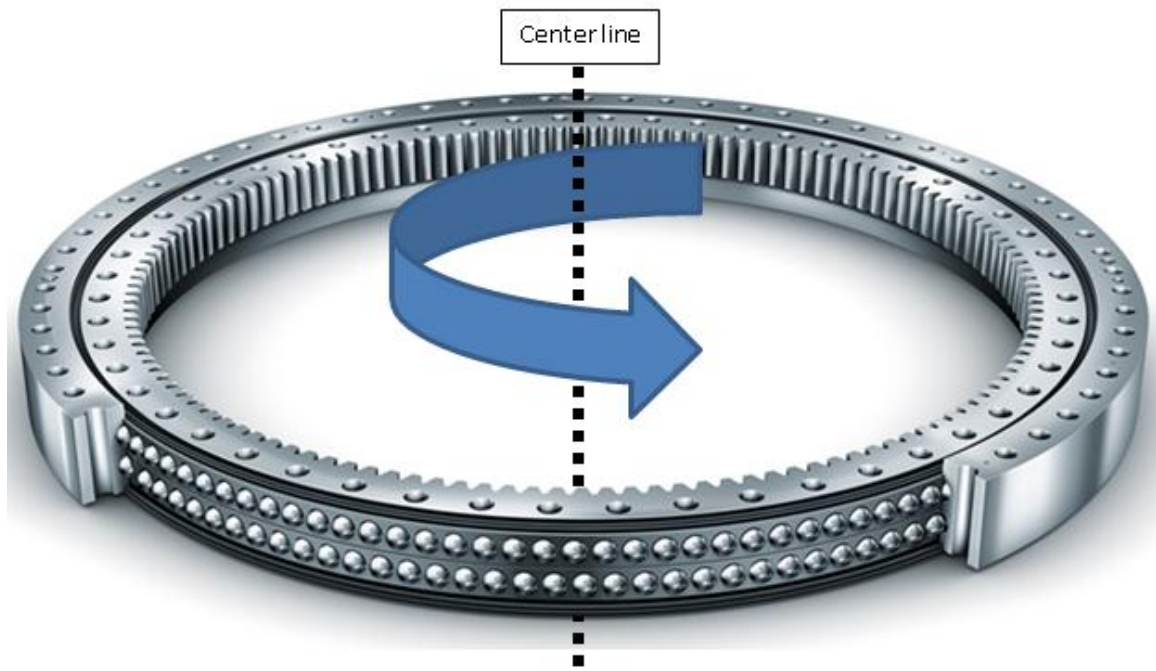


Figure 1.3 Slewing bearing degrees of freedom

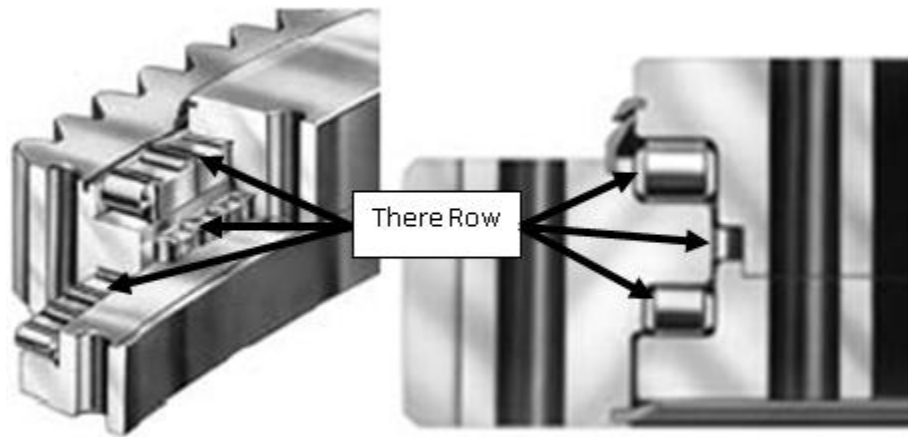


Figure 1.4 Three row roller slewing ring configuration

Chapter 2

Rolling Contact Fatigue Failures

2.1 Introduction

This chapter briefly reviews how cracks are formed from rolling contact fatigue. These cracks can be caused from the inherent imperfections in the material's microstructure. Furthermore, the microstructure can transform causing imperfections which are capable of generating cracks. These cracks will propagate under cyclic loading until they reach the rolling surface at which time final failure has occurred. This discussion is followed by background information of the specific slewing ring application's material, design changes, and life expectancy.

2.2 Rolling Contact Fatigue

RCF (Rolling Contact Fatigue) has been deemed to occur at a stress concentration that can initiate and propagate fatigue cracks under cyclic loading. Stress concentrations result from inclusions, chemical bands, carbides or anything else that caused the material to have uniform mechanical properties. The bearing industry produces materials that are considered "Clean" and homogeneous, which reduces the number of stress concentrations, but does not eliminate the concentration in the material.

Prior to a crack occurring due to RCF, a stress concentration is present either at the surface or subsurface. This stress concentration could have been preexisting during the materials processing, or may have been caused by microstructural changes due to the cyclic loading of rolling/sliding contact. [Oila and Bull (2005)] The local residual stress

around the stress concentration can cause the tensile stress to become greater than the materials ultimate strength thus creating the crack initiation site. The crack will propagate due to the cyclic loading. Research has demonstrated that the cracks will tend to propagate near a 30 degree angle relative to the rolling/sliding direction between boundaries of low hardness microstructure. [Nelias & Dumont 1999] When the crack comes to the surface, spalling or pitting will occur shortly after. This will cause debris to be released into the system. This debris will cause a post failure or secondary cracking due to the misalignment and excessive Hertzian contact stress.

The severity or depth of spalling/pitting depends on the location of the shear plane. If the shear plane is close to the surface, light pitting will occur and the crack will propagate to the surface. With increased loading beyond the material's dynamic capacity, the plane will be driven deeper within the material. Field reports for the slewing ring application considered in this thesis have demonstrated that cracks initiated at the deep shear plane will tend to travel inward (away from the rolling contact surface) and then turn parallel to the surface. The crack will propagate until the cyclic load causes bending stresses near the crack tip driving the crack to the surface. (Figures 2.1-2.3)

The process of determining the crack location is essentially one of seeking the weakest point in the material where the local strength is a minimum. Rolling contact fatigue plots have large amounts of scatter that follow a Weibull distribution closely. This scatter is due to the variation of the material strength on a micro level. These variations tend to occur around inclusions. In fact Figure 2.4 shows a common phenomenon that occurs from high rolling loads. This has been called the "butterfly" effect, which has been seen stemming from nonmetallic inclusions. This effect is

common in martensitic steels that have been quenched and tempered. High loading conditions causes the formation of untempered martensite to form around stress risers usually in front of the cracks. This increases the propagation rate, due to the brittle nature of the untempered martensite. When the material is subjected to high loads the grain structure absorbs the energy rather than deforming. This energy will cause the martensite to transform into untempered martensite. When this transformation occurs, the untempered martensite is a larger structure and requires more space, which causes local tensile residual stresses around the brittle untempered martensite [Sadeghi 2009].

2.3 Slewing Ring Application Failures

The specific slewing ring application has been in existence for several decades and has only utilized two raceways materials. The initial application utilized a version of high carbon steel, and only recently switched to a medium carbon alloy steel. The switch in materials was due to the increased axial, radial and moment loading on the application's slewing ring. Medium carbon alloy steel has better mechanical properties and hardenability than high carbon steel. Due to the diameter of the raceway and the risk of quench cracking the high carbon steel, the hardness ranged from 30-35 HRC. The medium carbon alloy steel allowed for the raceway material to be hardened to the machining restrictions of 37-42 HRC. With the increased hardness, the medium carbon alloy steel has higher tensile strength along with increased charpy values demonstrate the material's toughness to impacts. The switch to medium carbon alloy steel was initially made due to increased loading of the specific application.

The expected life of the application's slewing ring is five to seven years. After two years of the application utilizing the medium carbon alloy steel, there were reports of catastrophic failures of the raceway. These failures resulted in relatively large chunks of material breaking off and seizing up the application's rotation. This failure was deemed catastrophic due to the lack of notice prior to raceway failure, causing the application to become inoperable. Several raceways were returned for analysis. Figures 2.1-2.3 show examples of the medium carbon alloy steel failure. The rate of failures while using the new material was becoming more prevalent than the rate of failures utilizing the high carbon steel on the smaller applications. Additionally the failures utilizing high carbon steel were not deemed catastrophic, due to the predictability of raceway wear. Applications that utilized the high carbon steel did not experience large chunks of material breaking off and seizing up the applications rotation. The failure of the high carbon steel was found to be surface pitting causing excess surface wear (Figure 2.5). This type of failure was more acceptable to the application's user, allowing them adequate time to plan for the application's outage.

Further investigation is necessary in determining the material's demonstrated differences in failure modes. Determining these differences will show whether the difference was from the chemistry of the material or how the manufacturing processing i.e. heat treatment, affects the failure. Otherwise, the application's utilization or loading could have affected the failure.

2.4 Summary

In this chapter, subsurface cracks generated by rolling contact fatigue were briefly described along with the slewing ring's application failures. These cracks are associated with stress concentrations that will cause residual tensile stress. The stress concentrations in the material can be reduced by producing a "clean" or more homogenous material. The material's microstructure can cause additional stress concentrations under significant loading. The slewing ring design for the specific application has been in existence for decades. This slewing ring has only utilized two materials in that time. High carbon steel was initially used and this was recently switched to medium carbon alloy steel for the perceived increase in mechanical properties. This change has resulted in a significant reduction in the expected life of the slewing ring. In order to determine the cause of the failures, additional testing was required to compare the differences in the materials.

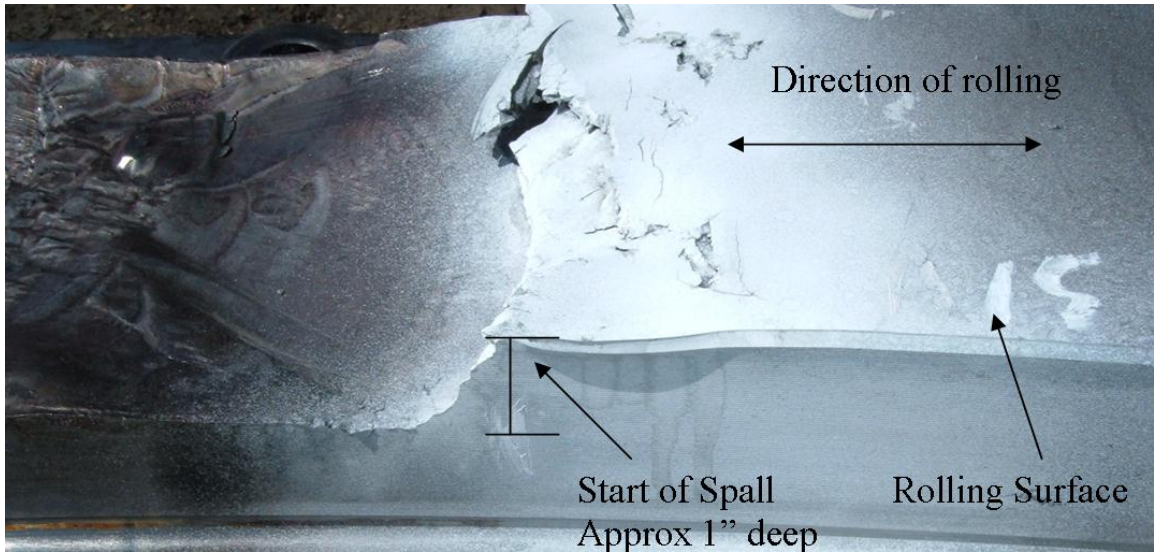


Figure 2.1: Medium carbon alloy steel application failure

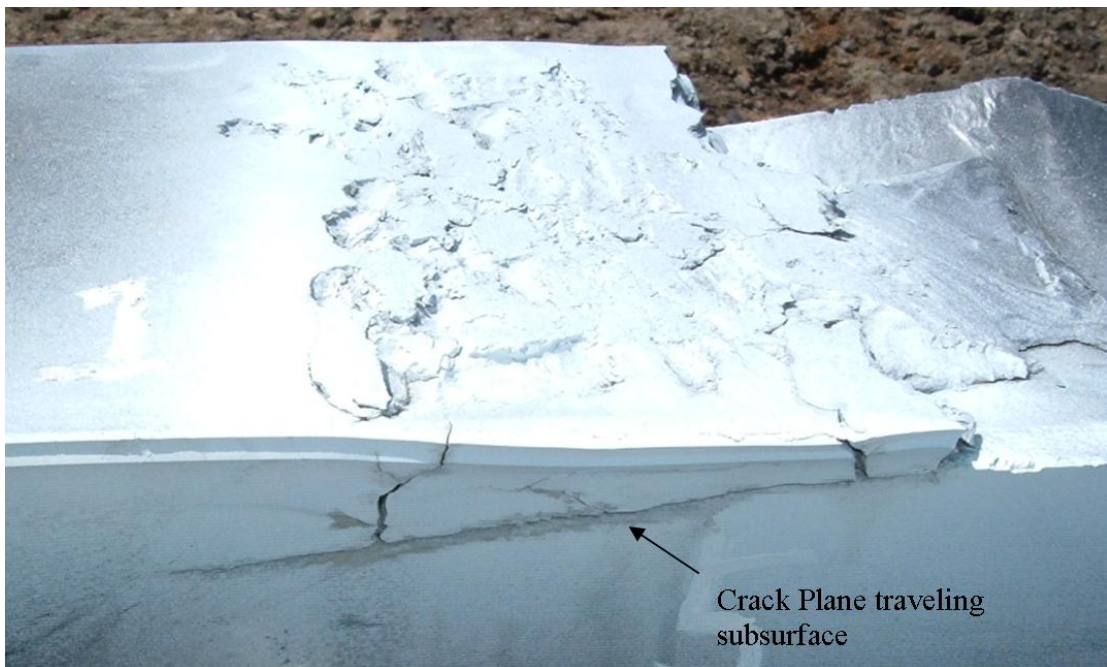


Figure 2.2: Medium carbon alloy steel application failure subsurface crack



Figure 2.3: Top view of medium carbon alloy steel failure

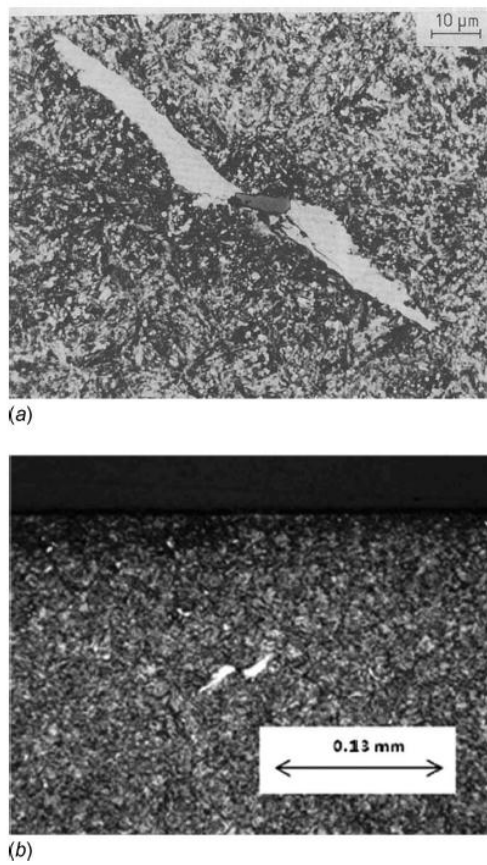


Fig. 7 Formation of butterflies around nonmetallic inclusion under rolling contact: (a) bearing steel AISI-52100 [78], and (b) bearing steel M50 074A [79]

Figure 2.4: Material structure changes due to rolling contact forces (ref)



Figure 2.5: High carbon steel application failure mode

Chapter 3

Testing Apparatus Selection

3.1 Introduction

This chapter discusses the selection process of the rolling contact fatigue testing apparatus. The testing objective will be discussed along with a review of two testing apparatuses, ZF-RCF and 3-Ball test machine. Both test machines have been utilized for determining rolling contact fatigue of standard bearing materials. After the individual discussion of the machines, a comparison will be made to select the appropriate machine for the specific slewing ring application. This is followed by the testing parameters and summary of the decision.

3.2 Objective for Testing

The primary goal for testing is to understand the life differences and failure modes between high carbon steel and medium carbon alloy steel. The medium carbon alloy steel has better harden-ability properties, along with superior toughness. The Charpy V-Notch impact energy at -40°F is fifteen to seventeen foot pounds, in comparison to the high carbon steel's two to three foot pounds. Low Charpy impact energy is an indicator of the material's brittleness, which does not guard against impact loading and uneven load distribution. Testing should determine the differences in failure modes between the two materials that have been used in the specific slewing ring application.

Secondly, the test apparatuses should determine the difference in rolling contact life with respect to the material's hardness. Increased material hardness will increase the chances of the first crack initiating, additionally. The specific application's slewing ring hardness cannot be at the ideal hardness for optimal life of bearings (near Rockwell C58) due to manufacturing limitations.

3.3 ZF-RCF testing machine

The machine shown in Figure 3.1 and Figure 3.2 tests the material specimen under line contact conditions; the test specimen in have a cylindrical or crowned test surface. There are three load rollers that are loaded hydraulically. Each load roller will represent one load cycle. This machine is set at 3000 RPM which is equivalent to 9,000 load cycles per minute or 540,000 load cycles an hour. This machine tests under the condition of full EHL (Elastic Hydrodynamic Lubrication) which means the oil film is thick enough to prevent and avoid metal-to-metal contact. This reduces the amount of friction to prevent wear of the mating surfaces. This particular test fixture has the capabilities to measure the coefficient of friction between the test sample and the load rollers. This machine as well can control the amount of sliding that takes place between the load rollers and the test specimen. The test fixture had been used only for 22% sliding, to simulate gear sliding contact. A benefit to this machine is the capability to detect the first instance of a crack. The machine uses Eddy current; this system records the response signal of current within the material (Figure 3.5). Surface and subsurface initiated cracks distort the current signal. Then a data system records the variance and magnitude of the signal. This will allow the first detection of a crack to be seen, along

with the rate of growth. There is no direct correlation between the magnitude of the current source and the size of the crack; but as the magnitude of the current increases the crack is increasing at the same theoretical rate.

The tests that have been performed in the past for this machine were in the 300 ksi Hertz contact stress range. The samples have been in the hardness range of around 60 HRC. These samples have lasted in the test fixture for 10-30 million load cycle equivalent to 0.8 to 2.3 days.

3.4 Three-Ball Test Machine

The fixture shown in Figure 3.3 and Figure 3.4 is considered to be the three-ball test or ball-rod test. This test fixture was originally designed to test ball bearings. The test material is made into a rod that is located in the center and three balls will contact the outside of the rod. The contact patch on this type of test has an elliptical area. This type of test will concentrate all the stress into a very small area. This allows the test fixture to operate under low loads but still be able to reach peak stresses. Each ball represents one load; the machine runs at 3600-RPM equivalent to 10,800 load cycles per minute or 648,000 load cycles per hour. The test is lubricated but the amount of lubrication between the balls and rod is unknown and may not have a full EHL test condition. This can lead to unwanted friction; friction can cause the depth of max stress to come to the surface, which can change the results along with changing the mode of failure. In the three ball test, it is difficult to eliminate the effects of friction and sliding due to the balls having three rotational degrees of freedom.

In previous testing, the three-ball machine has typically run material of high hardness. When this type of test is performed, the dynamic capacity of the material is exceeded in order to speed up the testing. The dynamic capacity of the material is the theoretical maximum load that the material can withstand in the time frame of one million load cycles. Running at these high stress loads will allow faster test times that could reduce the overall cost of testing. Eight tests can be performed on each rod decreasing the sample's machining cost. The three-ball machine runs tests between 500-700 ksi compressive stress, around 60 HRC. At this stress level, the testing times will be between ten and thirty million load cycles. Each machine has the capability to run four specimens at once.

A major difference between the slewing ring application and the three-ball test machine is the type of contact. The test fixture has an elliptical contact which cannot compare to the application's line contact. Correlations have been developed between elliptical and line contact testing. These correlations came from years of testing with a line contact machines. This correlation was based from tests run with standard bearing hardness material. Testing lower hardness material may have a different correlation.

3.5 Test apparatus Comparison

Table 3.1 shows the brief comparative summary of the test machines. The ZF-RCF machine utilizes rollers which have line contact similar to the specific slewing ring whereas the three-ball machine has the elliptical contact area. The three-ball machine has the advantage in load cycles per hour; keeping the overall testing time relatively short.

An important factor in comparing the slewing ring application to the test apparatuses specimen is having an equivalent stress range. The ZF-RCF machine can produce similar stresses while the three-ball machine would have to operate at lower stress levels due to the elliptical contact.

The specific slewing ring application has negligible amount of relative sliding between the roller and raceway. The ZF-RCF machines configuration can be changed to accommodate no relative sliding. The three-ball machine cannot control the amount of relative sliding.

The raceway material used in the specific slewing ring application has a reduced hardness, in comparison to the standard test specimens used in the test apparatuses. This will cause an unknown testing parameter of how the material will behave. Test specimen material with lower hardness could show some ductile properties during testing. These properties could be advantageous in the slewing ring to redistribute the load evenly or harmful due to the material plastically deforming. During testing, material deformation will change the stress levels, potentially causing the test to be invalid. The three-ball machine exerts a significant amount of stress on a small area, which could cause the material to deform in a matter dissimilar to the specific slewing ring application.

The stress level at which testing will be performed must be similar to the specific slewing ring application. The three-ball machine traditionally runs tests at high stress levels that exceeded the dynamic capacity of the material to reduce testing time. The estimated dynamic capacity for the specific slewing ring application is 558 ksi using the three-ball machine. The dynamic capacity using the ZF-RCF machine is 288 ksi. The

difference in dynamic capacity is primarily due to the rolling geometry elliptical and line contact. The ZF-RCF machine has line contact providing less of a chance for the material to deform, because the area in contact is greater than the three-ball machine.

The ability to determine crack growth is an additional feature that will show the time between crack initiation and final failure. This allows for the understanding of the failure modes between the two different materials. This could determine the root cause for the catastrophically failures of the medium carbon alloy steel of the specific slewing ring application. The ZF-RCF machine is able to map crack growth, where the three-ball machine is not.

The recommendation is to proceed with the ZF-RCF machine for testing. No test will give a 100% perfect correlation to the specific slewing ring application, but the ZF-RCF machine will give a good correlation difference between the two materials providing that the materials do not have significant material deformation in the test fixture. In order to determine the significance of material deformation four to five test samples will be pre tested. The ZF-RCF machine will have the capabilities to show how cracks are formed and how cracks travel through the material. The two types of materials have different microstructures: high carbon steel has a fine/course pearlitic structure whereas the medium carbon alloy steel has a fine grain tempered martensite.

3.6 Testing Parameters

The following testing conditions and failure criteria will be followed utilizing the ZF-RCF testing machine:

1. Speed was 3,000 rpm which was equivalent to 540,000 cycles an hour
2. Different load levels. The Load was controlled by hydraulic pressure which is applied to the three load rollers. Each load roller will affect one RCF cycle on the sample.
3. Constant loading conditions via hydraulic pressure control
4. Sliding = 0% (no relative speed between the load rollers and the test specimen)
5. Lubricant: Dexron III, automatic gear box oil
6. Operating temperature: $80C \pm 2C$
7. Failure criterion: the occurrence of first crack as detected by the eddy current sensor installed on the apparatus.
8. Eddy current setting: Excitation frequency = 1000kHz, evaluation mode = vector, sensitivity = 25dB, the threshold for shutting down the apparatus was set to 0.15 to 0.2V above the background noise.
9. 50 million load cycles will be considered a “run out” or no failure

3.7 Summary

In this chapter, the test objectives were briefly described followed by a description and comparison of the two test machines, a ZF-RCF and 3-Ball test machine. Due to the elliptical contact the 3-ball test machine will not be utilized. This type of contact is dissimilar to the specific slewing ring’s line contact. The specific slewing ring test specimen’s lower than standard hardness could be invalidated as a result of the excessive plastic deformation and different failure mode. The ZF-RCF machine has the capabilities to achieve most, if not all testing objectives. Prior to testing being

performed, the only unknown of the ZF-RCF machine is the initial load parameters due to the material's lower hardness. In order to determine the initial load setting and significance of material deformation, four to five test samples will be pre tested.

Table 3.1: Test machine Comparison

Test machine Comparison						
	Contact area	Load cycle per hour	Hardnes Rockwell C	Friction	Test per sample	Crack Growth Detection
Application	Line	1,200	30 to 39	NO		
ZF-RCF	Line	540,000	60	NO	1	YES
3-Ball	Elliptical	650,000	60	YES	8	NO

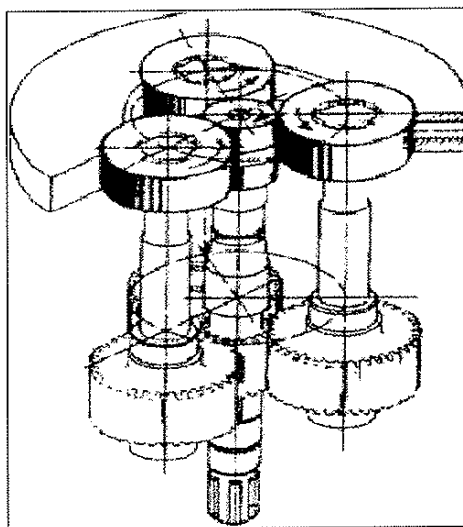


Figure 3.1: Schematic of ZF-RCF testing machine

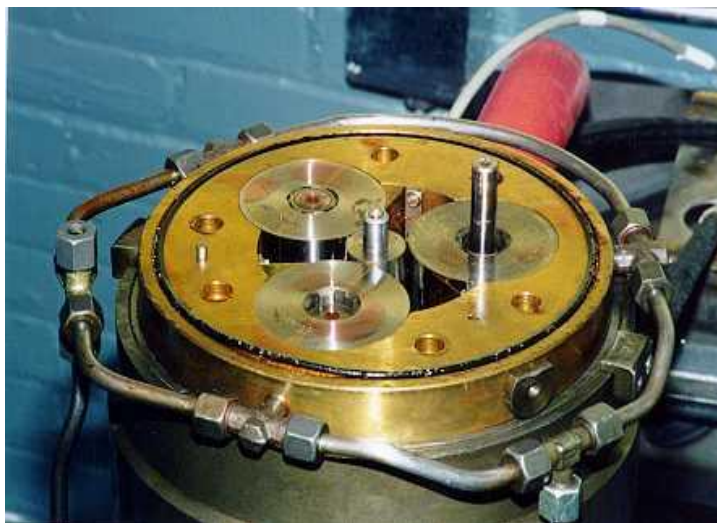


Figure 3.2: Photograph of ZF-RCF testing machine

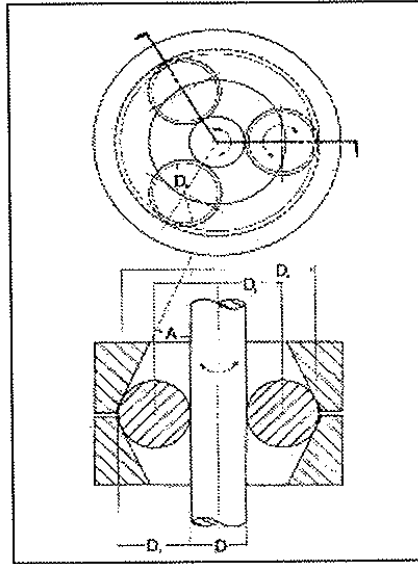


Figure 3.3: Diagram of three-ball test or ball-rod test

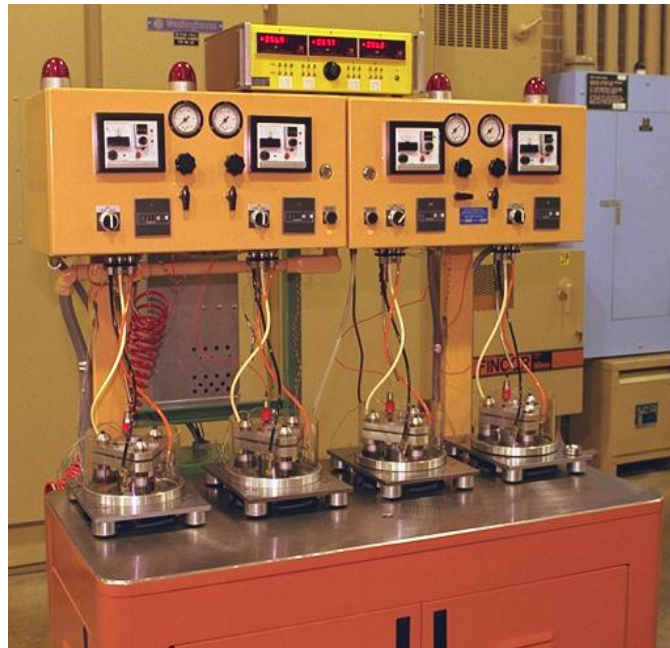


Figure 3.4: Photograph of three-ball test or ball-rod test apparatus

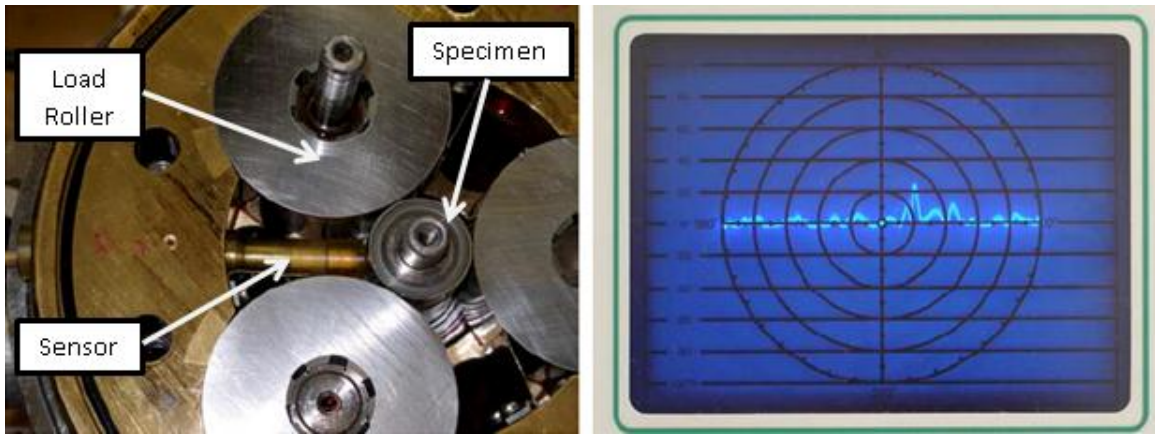


Figure 3.5: Eddy current crack detection

Chapter 4

Material and RCF Pre-Testing

4.1 Introduction

This chapter reviews the processing of the material specimens along with considerations for the machine sample orientation within the slewing ring raceway. Two orientations will be discussed, circumferential and radial. Of the two orientations, one will be chosen for pretesting to determine the correct sample direction. The pretesting will be followed by a summary of the result, detailing the sample orientation for final testing.

4.2 Material Samples

This research will test five materials composed of two different material types. The two material types are high carbon steel and medium carbon alloy steel. The test specimen was processed from forged rolled rings of a smaller diameter than that of the specific slewing ring's raceway diameter. The forged rings were processed with similar manufacturing techniques and forging ratios. The rings were cut into sections prior to heat treatment. The high carbon steel ring was cut into two sections, one section was stress relieved and the other was quenched and tempered. The medium carbon alloy steel was cut into three sections, all of which were quenched, but tempered to a different hardness. Table 4.1 shows the specific hardness for each sample. Table 4.2 shows the metallurgy of the samples and the heat treatment process. Table 4.3 shows the mechanical properties of both materials. The properties were taken from both sections of

the high carbon steel and one section of the medium carbon alloy steel. Figure 4.1 shows the orientation and direction of the specimen within the forged ring. The medium carbon alloy steel has significantly better tensile and yield properties in all directions compared to the high carbon steel. In addition the medium carbon alloy steel shows superior toughness properties in all testing directions.

4.3 Determining RCF test Specimen Orientation

Determining the test specimen orientation is a critical step in the testing process, however the step is rarely, if ever, discussed in current literature. The two specimen directions that will be reviewed are circumferential direction (A) and radial direction (B). Figure 4.2 shows orientations that were taken from the rolled rings. The specimens were taken from test bars machined near the top and bottom surfaces of the rolled ring. The two directions seemed to correlate to the specific slewing ring raceway failures. The following factors were reviewed prior to determining the final test samples orientation.

- Grain direction
- Inclusion direction
- Forging direction
- Applications rolling direction

Figure 4.3 shows the inclusion orientation in the two directions A and B. Due to the manufacturing of the forged ring, the grain structure and inclusion directions are elongated following the circumferential direction of the ring. Reviewing a transverse section of direction B shows the grain structure and inclusions are oriented transversely

across the specimen. During testing of the specimen in direction B the load rollers will travel around on the circumference simulating the raceway. The grain structure and inclusions will not remain in the same relative orientation to the load during the rotation of the specimen. The different orientations of the samples can be classified into quadrants. Failures in different quadrants could cause failure modes which differ in comparison to the specific slewing ring.

Direction A's transverse section shows the grain structure and inclusions are flowing perpendicular to the transverse section. During testing of the specimen in direction A, the load rollers will also travel around the circumference simulating the raceway. The grain structure and inclusions will remain in the same relative orientation to the load during the rotation of the specimen. Direction A's raceway is perpendicular to the specific slewing ring's raceway which could result in differing modes of failure. Below is a list of the pros and cons of the two specimen orientations. Figure 4.3 radial (B) orientation shows two modes with are zones or quadrants in which the microstructure and inclusion directions are different from each other.

Direction B (Radial)

Negative

- Two separate failure modes could occur.
- Mode 2 microstructural orientation does not represent the application's rolling surface
- There is an inconsistency of the rolling surface's microstructure around the circumference of the test sample

- Statistically the data could vary more in the radial direction because of the two separate failure modes
- If there was a difference in the material strength from mode 1 to mode 2, as the material transitions between the modes the strength of the material will change
- The specimen have to fail in the same orientation, otherwise the data will not be reliable without running a large number of test specimen.

Positive

- Mode 1 microstructural orientation represents the application's rolling direction accurately

Direction A (Circumferential)

Negative

- The orientation of the inclusions are not consistent with the application's inclusion orientation
- The inclusions are turned 90 degrees lateral

Positive

- Rolling surface microstructure is uniform 360 degrees around the test sample
- This direction would have more consistent results, which can decrease the statistical variation of the test.
- The microstructure variations can be eliminated as a testing variable

In order to eliminate concerns of the testing direction, a pretest was performed. During the pretest the material was subjected to step loading to determine the starting test pressures and parameters. The initial pretest utilized a specimen in direction B, to verify if the samples will fail in a constant quadrant.

4.4 Equations used for testing

The ZF-RCF testing apparatus has three load rollers 120 degrees apart around the circumference of the test specimen. The load rollers are hydrostatically controlled to apply a known load onto the test specimen. The load roller pressure will be referred to as a "load setting" in mega Pascal not to be confused with the applied load on the specified test specimen in Newtons. To convert the load setting to the applied load on the test specimen Eq. (4.1) was used. After each test was performed, an evaluation of the rolling surface was performed and a measurement was made of the increased rolling contact width, and a corrected load setting was determined. The increase of the width did not change the applied load on the specimen; rather the applied load remained constant throughout the test.

$$\mathbf{Applied_Load} = (\mathbf{LR}) \left[\frac{\mathbf{L}^2}{\left(\frac{1}{2\pi(1-\nu_1\nu_2)} \right) \left(\frac{2E_1E_2}{E_1+E_2} \right) \left(\frac{2060}{w} \right) \left(\frac{R_1+R_2}{R_1R_2} \right)} \right] \quad (4.1)$$

where,

LR=Load roller effective area, mm²

L=Load Setting, Mpa

W=Contact width, mm

E_1 =Modulus of Elasticity of the Load roller, Mpa

E_2 = Modulus of Elasticity of the Test Specimen, Mpa

R_1 =Radius of the Load roller, mm

R_2 = Radius of the Test Specimen, mm

ν_1 =Poisson's ratio of the Load roller

ν_2 =Poisson's ratio of the Test Specimen

The maximum shear stress of the test specimen is determined from the Hertz theory of elastic contact of cylindrical bodies. The cylindrical body axes lie parallel with each other and come in contact with a force per unit length of contact, allowing the problem to become two-dimensional. Furthermore, the depth at which the maximum shear stress occurs is derived from the same theory. The depth at which maximum shear occurs tends to create the initiation site of subsurface cracks during rolling contact fatigue. The applied load on the test specimen from the apparatus was used in Eq. (4.2) and Eq. (4.3). Maximum shear stress was calculated in pounds per square inch and the depth at maximum shear stress was calculated in the units of inch.

$$\tau_{\max} = 0.3p \quad (4.1)$$

$$\tau_{\max_{\text{Depth}}} = 0.78a \quad (4.2)$$

$$p = \frac{c_0 \times a}{h} \quad (4.3)$$

$$a = \sqrt{\frac{2 \times \frac{\text{Applied load}}{w} \times h}{\pi}} \quad (4.4)$$

$$\mathbf{h} = \left(\frac{1}{\left(\frac{1}{2R_1} + \frac{1}{2R_2} \right)} \right) \left(\frac{1-\nu_1^2}{E_1} + \frac{1-\nu_2^2}{E_2} \right) \quad (4.5)$$

where,

Applied_load=Contact width, lbf

W=Contact width, in

C_o =Coefficient from a chart dependent on the amount of friction 1=no friction

E_1 =Modulus of Elasticity of the Load roller, psi

E_2 = Modulus of Elasticity of the Test Specimen, psi

R_1 =Radius of the Load roller, in

R_2 = Radius of the Test Specimen, in

ν_1 =Poisson's ratio of the Load roller

ν_2 =Poisson's ratio of the Test Specimen

4.5 Pretesting for Specimen Orientation

The results from this pretest will help in determining the final test plan. Not all five materials will be tested in the pretest, only the two materials that represent the highest and lowest material hardness. This will allow the testing range to be determined. Three samples of each material will be tested. The two materials selected for testing are the high carbon steel which has been stress relieved, and quenched and tempered medium carbon alloy steel at 411 HB. The specimens were machined in the radial direction to determine if the failures would occur in consistent quadrants. If the specimens fail in a

similar quadrant, the final test will utilize a specimen machined from the radial direction. If any of the specimens fails in an inconsistent quadrant or manner, the final test will utilize a specimen machined from the circumferential direction.

If the sample runs for at least seven to ten million load cycles, the load roller pressure will be increased in steps until the first sign of failure occurs which will be determined by the eddy current setting. Table 4.4 shows the pretest results for all six samples. Notice that at the high hardness level the medium carbon alloy steel was able to endure a high stress prior to failure. This is in line with what is expected.

The high carbon steel sample was started at a load roller pressure of 900 Mpa. The sample was stepped up in pressure twice until failing after 6.8 million cycles at a load setting of 1300 Mpa. The number of cycles was lower than the preferred value of seven to ten million cycles. The next two specimens were tested at a load setting of 1200 Mpa with 33 and 4.5 million cycles until the first crack. These samples showed significant inconsistency in number of cycles but each had similar failure modes.

The medium carbon alloy steel sample was initially tested at a load setting of 1100 Mpa. The load was quickly incremented five times until reaching a final value of 2000 Mpa and failing at 8.4 million cycles. The next two test specimens had an initial load setting of 1900 and 1700 Mpa respectively and failed at 1.04 and 2.1 million cycles. These specimens did not achieve a failure at the desired amount of cycles. Both the high carbon steel and medium carbon alloy steel exhibited inconsistent cycles to failure, creating a large variance between load settings. Some speculation as to the difference is that the stepping of the load setting caused the crack tips to blunt, increasing the crack growth rates. This theory was never confirmed.

One sample of each material was sectioned and mounted in order to view the crack location and metallurgical changes if any. Notice that the inclusion directions can be seen in the unetched samples. The crack initiation location of high carbon steel specimen RCF-1-01-PRE is shown in Figure 4.4, and Figure 4.5. From this sample, some key points to notice are:

- Crack initiated subsurface
- Crack propagated near 30 degrees from the surface inward
- Crack did not follow the grain boundaries

The crack initiation location of medium carbon alloy steel specimen RCF-5-03-PRE is shown in Figure 4.6 and Figure 4.7. From this sample some key points to notice are:

- The alloy steel is “cleaner” with less inclusions than the carbon steel.
- Crack surfaces were removed during testing the initiation site is not conclusive.
- Fine martensite at the crack tip, unsure if the crack is following the grain boundaries
- The surface did not show signs of cold work

4.6 Summary

The pretested specimen of high carbon steel failed in consistent quadrants. The medium carbon alloy steel specimen did not fail in similar quadrants. In fact the specimen tended to fail in between quadrants. Due to the variance in failure mode and cycles to failure, the final test specimen will be machined from the circumferential

direction. This direction cannot be correlated with the specific slewing bearing rolling direction. The rolling direction of the test specimen is perpendicular to the specific slewing ring's rolling direction. However, the circumferential direction will have a constant rolling surface which should allow for a tighter statistical range of data compared to the radial direction. This will make the testing more reliable between materials.

The surfaces of the pre-test samples were closely reviewed for signs of deformation. The plastic deformation that was found was initially unexpected but not surprising. The test apparatus typically tests material with significantly higher hardness which is less prone to cold working. The deformation occurred after the first 50,000 cycles. After the initial plastic deformation, the material's contact surface remained constant. The sample's plastic deformation leads to a change in the test width which would reduce the contact pressure if the test apparatus's three hydraulic load rollers are not adjusted. Due to the fact that the deformation occurred in the first 50,000 cycles, the tests were completed with constant load settings. After the tests were completed, the contact widths of all samples were measured and a corrected load setting was determined. For a given test pressure and material, the amount of contact width deformation was nearly the same.

Table 4.1: Tested Material

Material Tested			
Hardness Rockwell C	High Carbon Steel Stress Relieved	High Carbon Steel Quenched & Tempered	Medium Carbon Alloy Steel Quenched & Tempered
30	RCF-1-XX		
32		RCF-2-XX	
33			RCF-3-XX
39			RCF-4-XX
44			RCF-5-XX

Table 4.2: Metallurgy & heat treatment process of material

Test Sample Metallurgy	
High Carbon Steel Stress Relief	
Sample ID	RCF-1-XX
Grain Structure	Coarse Pearlite
Grain Direction	Follows Forging Direction
Inclusion Direction	Follows Forging Direction
Parallel with rolling surface	Inclusion/Grains
High Carbon Steel Quenched and Tempered	
Sample ID	RCF-2-XX
Grain Structure	Fine Pearlite
Grain Direction	Homogenous
Inclusion Direction	Follows Forging Direction
Parallel with rolling surface	Inclusion
Medium Carbon Alloy Steel Quenched and Tempered	
Sample ID	RCF-3-XX, RCF-4-XX, RCF-5-XX
Grain Structure	Fine Martensite
Grain Direction	Homogenous
Inclusion Direction	Follows Forging Direction
Parallel with rolling surface	Inclusion

Table 4.3: Mechanical Properties of the Material

Test Sample Mechanical Properties								
Sample Orientation	Circumferential			Radial		Longitudinal		
Sample ID	RCF-1-XX	RCF-2-XX	RCF-4-XX	RCF-1-XX	RCF-2-XX	RCF-1-XX	RCF-2-XX	RCF-4-XX
Tensile Strength (psi) %	54%	73%	91%	57%	84%	53%	69%	82%
Yield Strength (psi) %	52%	41%	83%	50%	61%	51%	38%	72%
Yield/tensile Ratio	0.96	0.57	0.91	0.87	0.72	0.96	0.56	0.88
Elongation %	15	15	15	2	10	2	6	14.7
Reduction in Area %	39	23	50.2	12	10	2	5	48.8
Charpy V-Notch -40 F %	13%	17%	193%	13%	13%	13%	10%	133%

Table 4.4: Results of Pre-test

Pre-Testing of Material			
	ID #	Load Setting (Mpa)	# Cycles Million
High Carbon Steel	RCF-1-01-PRE	900	7.5
		1100	12
		1300	6.84
	RCF-1-02-PRE	1200	4.5
	RCF-1-03-PRE	1200	33.5
		1400	12
1600		2.25	
Medium Carbon Alloy Steel	RCF-5-01-PRE	1100	12.18
		1300	13.6
		1500	12.45
		1700	14.25
		1900	11.1
		2000	8.4
	RCF-5-02-PRE	1900	1.04
	RCF-5-03-PRE	1700	2.1

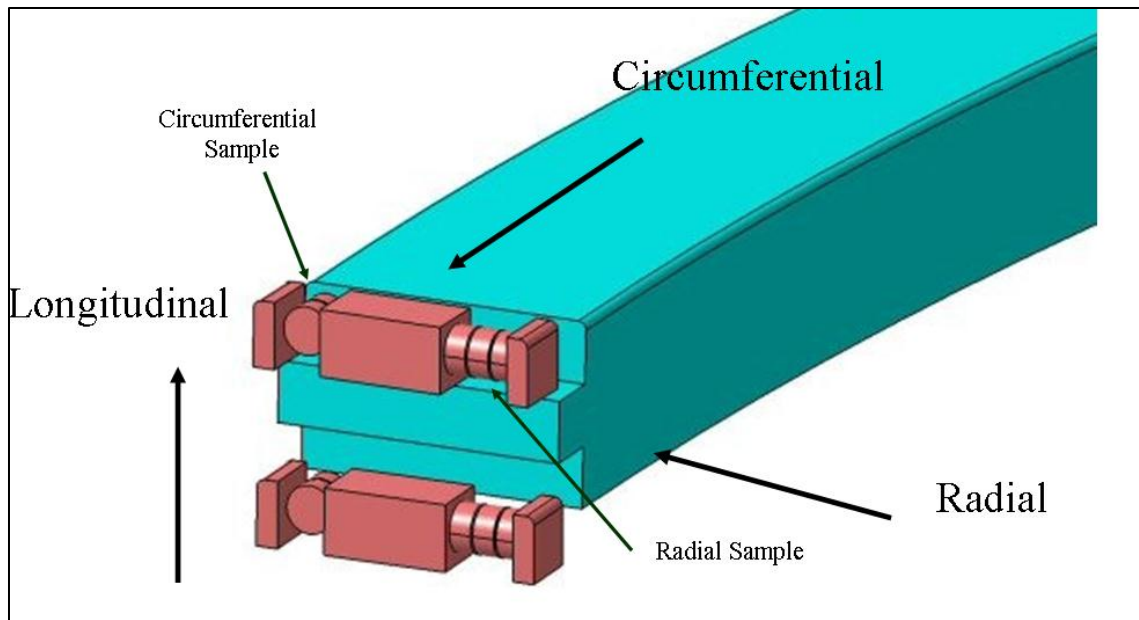


Figure 4.1: Specimen testing direction

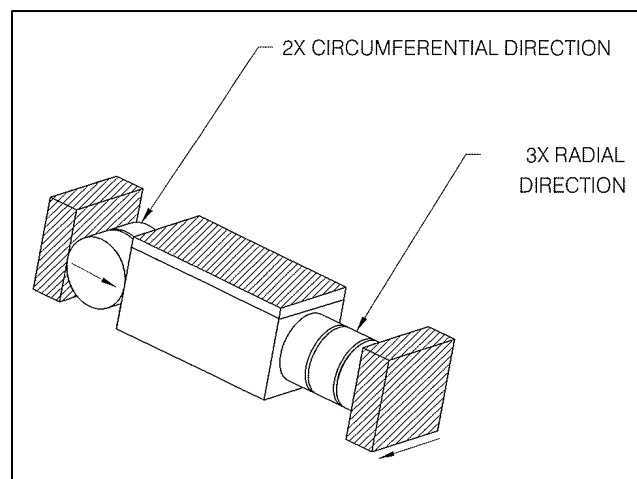


Figure 4.2: Specimen testing direction of machined bar

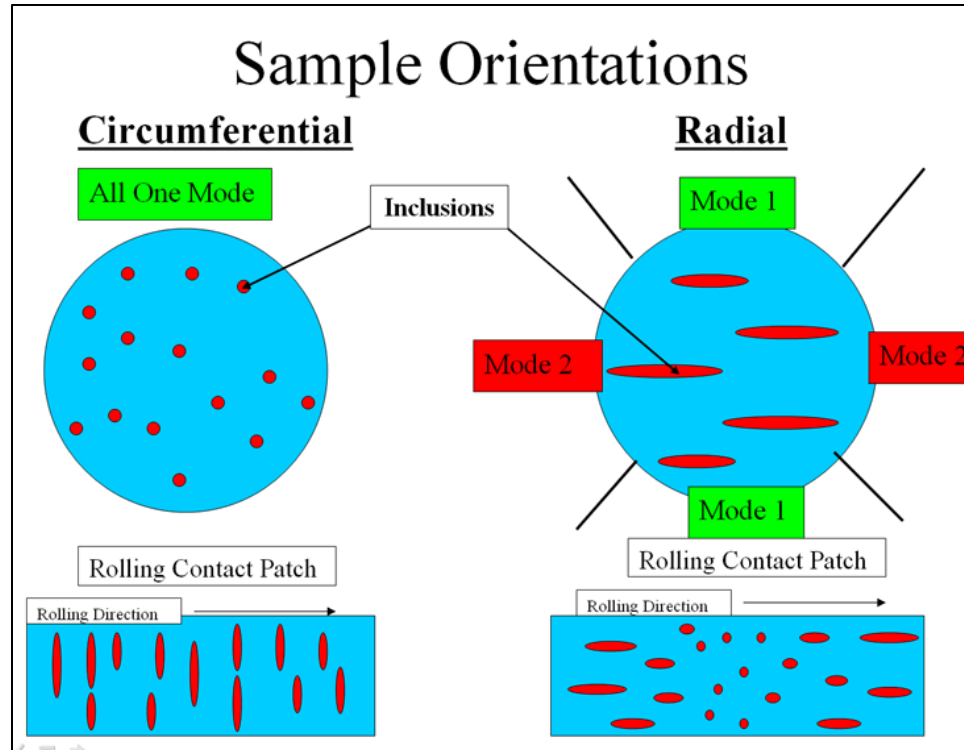


Figure 4.3: Direction of inclusions in test specimen

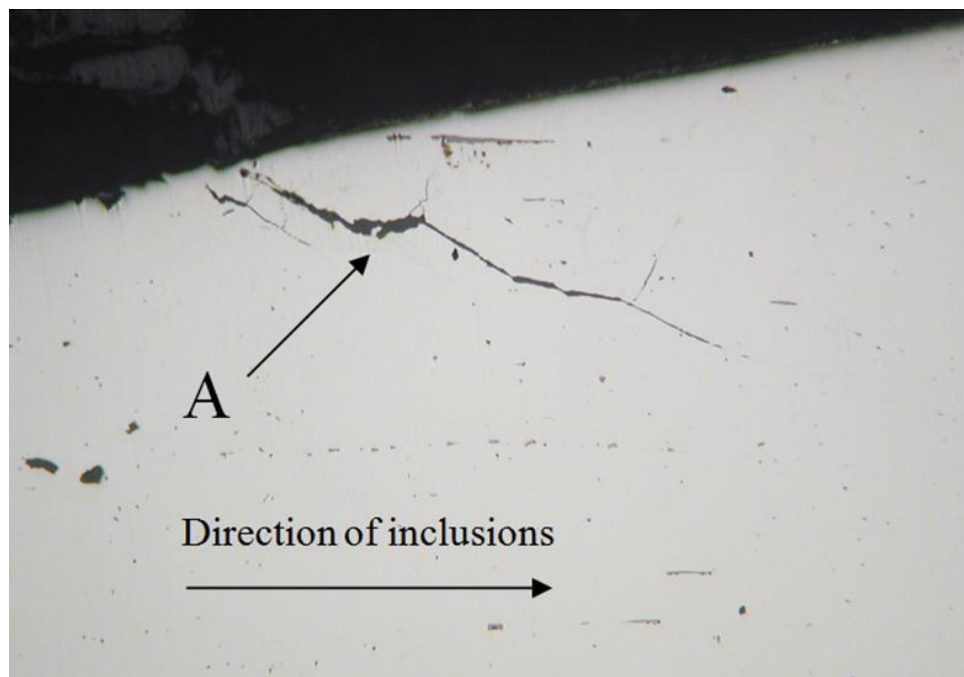


Figure 4.4: RCF-1-01-PRE Crack location



Figure 4.5: RCF-1-01-PRE microstructure of crack

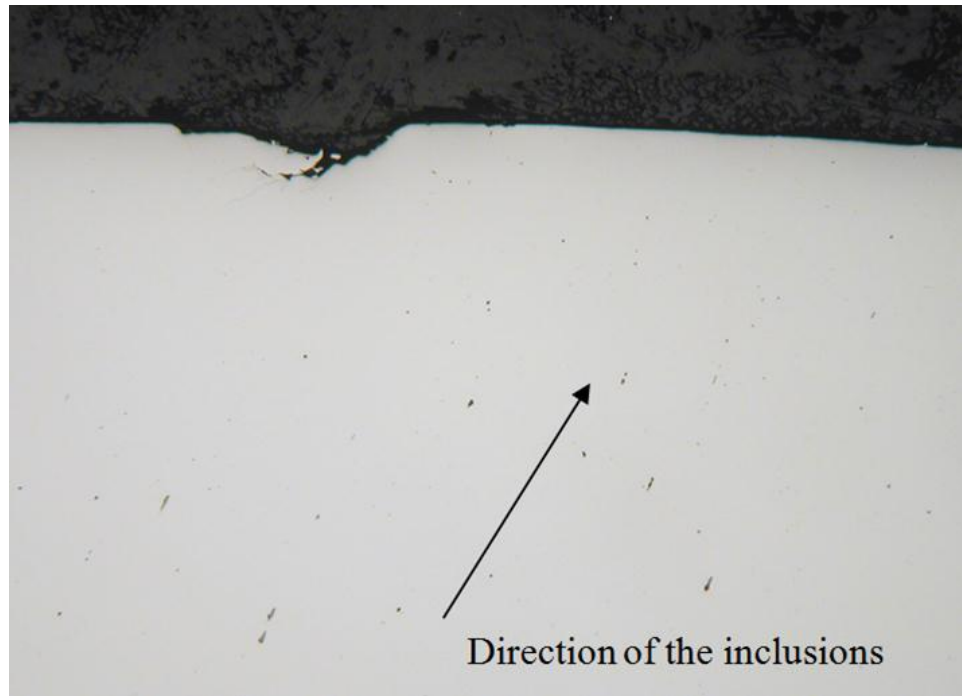


Figure 4.6: RCF-5-03-PRE inclusion direction



Figure 4.7: RCF-5-03-PRE Crack and Microstructure

Chapter 5

Rolling Contact Fatigue Testing

5.1 Introduction

This chapter discusses the final testing of five materials composed of two different material types. The two material types are high carbon steel and medium carbon alloy steel. Rolling contact fatigue testing will utilize the ZF-RCF testing apparatus. After the completion of each test, the specimen's rolling contact surface will be evaluated. From the evaluation and test results multiple samples will be metallurgically assessed. Subsequently, the samples test results will be compared in an S-N curve to determine which material is better suited for the specific slewing ring application.

5.2 Test Program Setup

The final RCF test program was dynamically adjusted based upon the previous sample's life and load. The statistical scatter in the data helped to determine the number of samples need at each load level. Due to the funding of the project, certain samples were allowed a higher amount of scatter. In order to develop an accurate S-N curve with the minimum number of samples, two target loads will be applied. The first target load will have a desired number of cycles prior to failure of between three and eight million load cycles. The next target load will be at a lower setting in order to fail specimens at between five and ten million load cycles. This criterion determines the load applied to the specimens during testing. The samples were run until the first sign of a crack was

detected by an eddy current. At the end of each test a measurement of the raceway's contact width was completed. The effective load was determined from the increase in contact width. A ratio of the maximum subsurface shear stress change from the start and end of the test was compared to the percent change of the effective load setting vs. the initial load setting.

5.3 High Carbon Steel

5.3.1 RCF-1-XX

The first sample to be tested was the stress relieved high carbon steel at the pressure setting determined from the pre-test. The first specimen RCF-1-01 was tested at the targeted lower level pressure of 1400 Mpa, and failed at 1.97 million load cycles. The results of RCF-1-01 were unexpected. For the following test specimen, RCF-1-02 pressure was reduced to 1200 Mpa at which the sample "ran out" which means the test exceeded fifty million cycles and was considered an infinite life. With the following samples RCF-1-03, RCF-1-04, and RCF-1-05 testing pressures were increased by 100 Mpa and all of these samples exceed fifty million cycles. The first sample to fail was specimen RCF-1-06 was at a pressure setting of 1800 Mpa after 5.1 million cycles. The initial specimen RCF-1-01 that had an early failure was considered an outlier and the data was voided.

Four additional samples were tested at the lower pressure setting of 1800 Mpa. Test Specimen RCF-1-07, RCF-1-08, RCF-1-09 and RCF-1-10 had an average life of 5.4 million load cycles. After reviewing the sample's life at the low pressure level, the high

pressure level was only able to be increased by 200 Mpa. Five additional specimens were tested at a higher pressure setting of 2000 Mpa RCF-1-11, RCF-1-12, RCF-1-13, RCF-1-14 and RCF-1-15 with an average life of 3.5 million cycles. Table 5.1 shows the results from the high carbon steel stress relieved RCF-1-XX specimen. During testing the specimens effective rolling contact width increased. The lower pressure setting of 1800 Mpa caused the sample's width to increase an average of 28% effectively changing the pressure setting to 1590 Mpa. The width of specimen that was subjected to 2000 Mpa increased an average of 39% effectively changing the pressure to 1700 Mpa. **Error! Reference source not found.** shows the rolling surface evaluation and measured width percent increase.

Table 5.1: Results of RCF-1-XX test

High Carbon Steel RCF-1-XX							
	ID #	Load Setting (Mpa)	Effective Load (Mpa)	# Cycles Million	Width % Increase	Shear Stress	
						%	(mm)
Run Out or Quick Failure	RCF-1-01	1400	1347	1.97	8.0%	78.9%	0.197
	RCF-1-02	1200	1138	50.00	11.2%	66.6%	0.166
	RCF-1-03	1300	1240	50.00	10.0%	72.6%	0.181
	RCF-1-04	1400	1306	50.00	15.0%	76.5%	0.191
	RCF-1-05	1600	1468	50.00	18.8%	86.0%	0.215
Low Load Range	RCF-1-06	1800	1574	5.11	30.8%	92.2%	0.230
	RCF-1-07	1800	1579	8.52	30.0%	92.5%	0.231
	RCF-1-08	1800	1615	4.85	24.3%	94.6%	0.236
	RCF-1-09	1800	1594	5.10	27.5%	93.4%	0.233
	RCF-1-10	1800	1586	3.6	28.8%	92.9%	0.232
High Load range	RCF-1-11	2000	1730	2.73	33.7%	101.3%	0.253
	RCF-1-12	2000	1690	5.10	40.0%	99.0%	0.247
	RCF-1-13	2000	1678	0.74	42.0%	98.3%	0.245
	RCF-1-14	2000	1704	5.10	37.8%	99.8%	0.249
	RCF-1-15	2000	1699	3.90	38.5%	99.5%	0.248

5.3.2 RCF-2-XX

RCF-2-XX is high carbon steel that has been quenched and tempered to 301 HB.

In order to review and compare the materials with a limited number of samples the RCF-

2-XX will be tested with similar pressure settings to RCF-1-XX. Five samples were tested at each test set pressure of 1800 Mpa and 2000 Mpa. The samples at the low pressure level averaged 3.4 million cycles at an effective pressure of 1800 Mpa. The samples at the high pressure level averaged 2.7 million cycles at an effective pressure of 2000 Mpa.

The lower pressure setting of 1800Mpa resulted in the samples width increasing an average of 11% effectively changing the pressure setting to 1706 Mpa. The specimens that were subjected to 2000 Mpa saw their width increase an average of 17% effectively changing the pressure to 1850 Mpa. The RCF-2-XX material had a shorter life than RCF-1-XX material at the given set pressures. In comparison, the RCF-2-XX had a higher effective pressure which caused the samples to fail sooner. This observation would indicate that quenching and tempering the material will reduce the amount of plastic deformation on the rolling surface which will increase the load carrying capacity. The RCF-2-XX had an average of 20% less plastic deformation when compared to RCF-1-XX. 0 shows the rolling surface evaluation and measured width percent increase.

Table 5.2: Results of RCF-2-XX test

High Carbon Steel RCF-2-XX							
	ID #	Load Setting (Mpa)	Effective Load (Mpa)	# Cycles Million	Width % Increase	Shear Stress	
						%	(mm)
Low Load Range	RCF-2-01	1800	1703	4.26	11.8%	99.7%	0.249
	RCF-2-02	1800	1718	2.37	9.8%	100.6%	0.251
	RCF-2-03	1800	1703	1.83	11.8%	99.7%	0.249
	RCF-2-04	1800	1703	6.96	11.8%	99.7%	0.249
	RCF-2-05	1800	1703	3.45	11.8%	99.7%	0.249
High Load range	RCF-2-06	2000	1844	0.92	17.6%	108.0%	0.269
	RCF-2-07	2000	1844	6.18	17.6%	108.0%	0.269
	RCF-2-08	2000	1875	4.08	13.7%	109.8%	0.274
	RCF-2-09	2000	1844	1.22	17.6%	108.0%	0.269
	RCF-2-10	2000	1844	1.29	17.6%	108.0%	0.269

5.4 Medium Carbon Alloy Steel

The next three materials tested were of the medium carbon alloy steel at different hardness. The objective of using three different hardness levels is to understand how the increased hardness affects the material's life. In the case of the specific slewing ring application, the original material used a high carbon steel which successfully met cycle requirements and exhibited predictable failures once the calculated life was passed. As the specific application's stresses increased, the slewing ring's material changed to medium carbon alloy steel. With the change in steel and the increased hardness of the material, the assumed life should be similar to or better than the high carbon steel. However the life requirement of the medium carbon alloy steel in the specific application was not achieved. In fact the life was unpredictable and the failures that occurred were unexpected. The test of these three materials will be compared to the high carbon steel in order to understand why the high carbon steel in the application seemed to be better than the medium carbon alloy steel.

5.4.1 RCF-3-XX

RCF-3-XX is medium carbon alloy steel that has been quenched and tempered to 311BHN. The test life objectives remained the same at the high and low pressures levels for the desired number of cycles. Specimen RCF-3-01 and RCF-3-02 were tested at 2000 Mpa and failed quickly, at fewer than 1 million cycles. RCF-3-03 was tested at 1800 Mpa and failed at just over 1 million cycles. The load setting was reduced for the following specimen's to a value comparable to the pretest values of 1300 Mpa. The next five test specimens averaged 9.36 million cycles at an effective pressure of 1253 Mpa.

The samples at the high pressure level averaged 4.65 million cycles at an effective pressure of 1483 Mpa. The average percent increase of the contact width was 8.4% compared to the 17-39% increase seen in the high carbon steel specimen. Comparatively this medium carbon alloy steel material is the most similar to or the “closest” to the hardness of the carbon steels, with less load capacity. If the pressure was set similar to pressures of which the high carbon steel were subjected to (1800 – 2000 Mpa) the sample would fail immediately. 0 shows the rolling surface evaluation and measured width percent increase.

Table 5.3: Results of RCF-3-XX test

Medium Carbon Alloy Steel RCF-3-XX							
	ID #	Load Setting (Mpa)	Effective Load (Mpa)	# Cycles Million	Width % Increase	Shear Stress	
						%	(mm)
Pre Test	RCF-3-01	2000	1981	0.74	2.0%	116.0%	0.289
	RCF-3-02	2000	1953	0.83	4.9%	114.4%	0.285
	RCF-3-03	1800	1733	1.27	7.8%	101.5%	0.253
Low Load Range	RCF-3-04	1300	1243	11.3	9.4%	72.8%	0.182
	RCF-3-05	1300	1252	9	7.8%	73.3%	0.183
	RCF-3-06	1300	1255	8.4	7.3%	73.5%	0.183
	RCF-3-07	1300	1244	8.8	9.2%	72.9%	0.182
	RCF-3-08	1300	1269	9.3	4.9%	74.3%	0.185
High Load range	RCF-3-09	1550	1479	5.13	9.8%	86.6%	0.216
	RCF-3-10	1550	1479	4.15	9.8%	86.6%	0.216
	RCF-3-11	1550	1493	4.8	7.8%	87.4%	0.218
	RCF-3-12	1550	1479	4.53	9.8%	86.6%	0.216

5.4.2 RCF-4-XX

RCF-4-XX is a medium carbon alloy steel that has been quenched and tempered to 363BHN. Testing of this material started at RCF-3-XX's high load setting of 1550 Mpa. Due to the large variation in cycle results, ten specimens were run. The tests resulted in an average of 7.5 million cycles at an effective load of 1452 Mpa, which is a reduction of 4.8% in load. The average number of cycles to failure was within the low load range criteria. Eleven samples were tested at the high load range averaging 4.9 million cycles at an effective pressure of 1593 Mpa. 0 shows the rolling surface evaluation and measured width percent increase.

Table 5.4: Results of RCF-4-XX test

Medium Carbon Alloy Steel RCF-4-XX							
	ID #	Load Setting (Mpa)	Effective Load (Mpa)	# Cycles Million	Width % Increase	Shear Stress	
						%	(mm)
Low Load Range	RCF-4-01	1550	1457	12.8	13.1%	85.3%	0.213
	RCF-4-02	1550	1493	4.96	7.8%	87.4%	0.218
	RCF-4-03	1550	1470	3.33	11.2%	86.1%	0.215
	RCF-4-04	1550	1467	11.3	11.6%	85.9%	0.214
	RCF-4-05	1550	1489	7.32	8.4%	87.2%	0.217
	RCF-4-06	1550	1464	9.9	12.2%	85.7%	0.214
	RCF-4-07	1550	1447	7.71	14.7%	84.8%	0.211
	RCF-4-08	1550	1493	4.35	7.8%	87.4%	0.218
	RCF-4-09	1550	1493	11.4	7.8%	87.4%	0.218
	RCF-4-10	1550	1486	2.8	8.8%	87.0%	0.217
High Load range	RCF-4-11	1700	1518	3.1	25.5%	88.9%	0.222
	RCF-4-12	1700	1554	7.56	19.6%	91.0%	0.227
	RCF-4-13	1700	1608	6.1	11.8%	94.2%	0.235
	RCF-4-14	1700	1586	2.75	14.9%	92.9%	0.232
	RCF-4-15	1700	1639	0.456	7.6%	96.0%	0.239
	RCF-4-16	1700	1637	1.86	7.8%	95.9%	0.239
	RCF-4-17	1700	1546	4.32	21.0%	90.5%	0.226
	RCF-4-18	1700	1602	8.58	12.5%	93.9%	0.234
	RCF-4-19	1700	1619	2.91	10.2%	94.8%	0.237
	RCF-4-20	1700	1621	9.1	10.0%	94.9%	0.237
	RCF-4-21	1700	1593	7.92	13.9%	93.3%	0.233

5.4.3 RCF-5-XX

RCF-5-XX is medium carbon alloy steel that has been quenched and tempered to 411BHN. Testing for this material began at RCF-4-XX's high load setting of 1700Mpa. Seven specimens were run with an average life of 20.8 million cycles. Three of the seven specimens had a significantly higher life; RCF-5-03 and RCF-5-07 exceeded 50 million while RCF-5-01 achieved 28.2 million cycles. The 1700 Mpa load setting was considered the lowest load to result in a failure for this specific material. This point can also be referred to as the knee on the S-N curve. These three specimens were excluded from the data in order to establish the knee point on the S-N curve. The remaining four specimens averaged 4.4 million cycles at an effective load of 1664 Mpa. The high pressure level was at 1900 Mpa with an effective pressure of 1859 Mpa. Five samples were tested at this level with an average life of 2.7 million cycles. It was determined that this material was behaving in an unpredictable manor by reviewing the scatter at both pressure levels. Table 5.5 shows the test results for the alloy steel at 411 HB. 0 shows the rolling surface evaluation and measured width percent increase.

Table 5.5: Results of RCF-5-XX test

Medium Carbon Alloy Steel RCF-5-XX							
	ID #	Load Setting (Mpa)	Effective Load (Mpa)	# Cycles Million	Width % Increase	Shear Stress	
						%	(mm)
Low Load Range	RCF-5-01	1700	1567	28.2	17.6%	91.8%	0.229
	RCF-5-02	1700	1658	2.03	5.1%	97.1%	0.242
	RCF-5-03	1700	1690	50	1.2%	99.0%	0.247
	RCF-5-04	1700	1660	5.7	4.9%	97.2%	0.242
	RCF-5-05	1700	1671	5.8	3.5%	97.9%	0.244
	RCF-5-06	1700	1668	4.25	3.9%	97.7%	0.244
	RCF-5-07	1700	1660	50	4.9%	97.2%	0.242
High Load range	RCF-5-08	1900	1838	0.924	6.9%	107.6%	0.269
	RCF-5-09	1900	1857	6.18	4.7%	108.7%	0.271
	RCF-5-10	1900	1862	4.08	4.1%	109.1%	0.272
	RCF-5-11	1900	1862	1.22	4.1%	109.1%	0.272
	RCF-5-12	1900	1874	1.29	2.7%	109.8%	0.274

5.5 Metallurgical Analysis of the Samples

The microstructure, crack initiation location, and the review of increased near surface hardness due cold working were evaluated on nine test specimens. The identification number and summary of the test results of the evaluated samples can be found in Table 5.6. All of the samples were visually examined and transverse metallographic sections were prepared through the estimated crack origin locations. Knoop micro hardness traverses were made from the roller contact surfaces of selected samples adjacent to the cracks. The nine selected specimen represent four different maximum shear stress levels. The shear stress values have been converted to a percentage of the theoretical operational maximum shear stress of the specific application's slewing ring raceway. The four targeted levels are 73%, 90%, 100% and 110% respectively. All of the samples exhibited a single, generally longitudinally cracked area in the roller contact surfaces. These cracks exhibit some parallel smaller

secondary cracks. The cracks are located adjacent to one edge of the roller contact areas, which exhibit burnished textures. Some plastic deformation was present along the edges of the roller contact areas which are indicative of some plastic deformation of the surface during testing. This is consistent with the measured results showing an increase in the roller contact surface widths after testing. Some of the cracks had joined, resulting in the formation of a pit on the contact surface. These pits exhibit steep sides relative to the roller contact surfaces and are consistent with subsurface initiated pitting contact fatigue.

5.5.1 Stress Level 1 (73%)

RCF-3-04 was the only sample evaluated at this stress level. The primary objective of evaluation at this load level was to determine if abnormality existed in this sample. This was the lowest stress level which caused a consistent failure. This stress level was used in testing the medium carbon alloy steel samples at a hardness of 311BHN. The high carbon steel samples were able to withstand a higher stress range even with lower sample hardness of 301 HB. The evaluated sample exhibited multiple branching subsurface cracks at the location of the visually evident surface crack which is consistent with subsurface initiated pitting contact fatigue as shown in Figure 5.1. The crack branches indicate that the origin is located approximately 0.127mm below the roller contact surface. No other cracks are present around the remainder of the circumference in the plane of this metallographic section. The microstructure of this sample consists of uniform fine grained tempered martensite as shown in Figure 5.2. No microstructural changes are evident adjacent to the roller contact surface that could be indicative of any significant plastic deformation from the cyclic compressive (hertz) stresses generated by

the mating roller contact during testing. Slight chemical segregation is evident which is typical of this type of medium carbon alloy steel forging.

The maximum near surface hardness of RCF-3-04 is equivalent to approximately 41 Rockwell C at a depth of 0.152mm, as shown in Table 5.7. The location of the maximum near surface hardness is consistent with the location of the subsurface crack origin. The average core hardness (at depths of 0.75mm to 1.50mm) is equivalent to approximately 37 Rockwell C. This indicates that the applied cyclic compressive (hertz) stress during testing resulted in cold-working the near surface material which increased the hardness approximately 4 Rockwell C points. This hardness increase extends to a depth of approximately 0.305mm.

5.5.2 Stress Level 2 (90%)

Samples RCF-1-07 and RCF-4-12 were evaluated in the second stress range. RCF-1-07 is high carbon steel that has been stress relieved to 285 HB core hardness. RCF-4-12 is medium carbon alloy steel that has been quenched and tempered to 363 HB core hardness. The evaluation and comparison of the two different materials at the same stress may indicate differences in the failures modes that were observed on the specific application.

Sample RCF-1-07 exhibits multiple branching subsurface cracks at the location of the visually evident surface crack. These are typical of subsurface initiated pitting contact fatigue as shown in Figure 5.3. The crack branches indicate that the origin is located approximately 0.0685mm below the roller contact surface. No other cracks are

present around the remainder of the circumference in the plane of this metallographic section. A 0.558mm deep layer exhibiting a slightly different microstructure extends from the roller contact surface as shown in Figure 5.4. The near surface microstructure consists of fine lamellar pearlite as shown in Figure 5.5. The branching subsurface cracks are transgranular. The core microstructure also consists of fine lamellar pearlite with very small amounts of ferrite as shown in Figure 5.6.

Sample RCF-4-12 exhibits multiple branching subsurface cracks at the location of the visually evident surface crack that are typical of subsurface initiated pitting contact fatigue as shown in Figure 5.7. The crack branches indicate that the origin is located approximately 0.187mm below the roller contact surface. No other cracks are present around the remainder of the circumference in the plane of this metallographic section. The microstructure of this sample consists of uniform fine grained tempered martensite that is similar to sample RCF-3-04 as shown in Figure 5.8. No microstructural changes are evident adjacent to the roller contact surface that could be indicative of any significant plastic deformation from the cyclic compressive (hertz) stresses generated by the mating roller contact during testing. Slight chemical segregation is also evident in this sample.

The maximum near surface hardness of RCF-1-07 is equivalent to approximately 48 Rockwell C at a depth of 0.101mm, as shown in Table 5.8. The location of the maximum near surface hardness is slightly shallower than the location of the subsurface crack origin. The average core hardness is equivalent to approximately 33 Rockwell C. This indicates that the applied cyclic compressive (hertz) stress during testing resulted in cold-working the near surface material leading to an increased hardness of approximately

15 Rockwell C points. This hardness increase extends to a depth of approximately 0.508mm.

The maximum near surface hardness of sample RCF-4-12 is equivalent to approximately 43 Rockwell C at a depth of 0.101mm, as shown in Table 5.8. The location of the maximum near surface hardness is slightly deeper than the location of the subsurface crack origin. The average core hardness is equivalent to approximately 40 Rockwell C. This indicates that the applied cyclic compressive (hertz) stress during testing resulted in cold-working the near surface material that increased the hardness approximately 3 Rockwell C points. This hardness increase extends to a depth of approximately 0.152mm.

5.5.3 Stress Level 3 (100%)

Stress level three targets the samples that were run near the theoretical maximum shear stress level of the specific application's slewing ring. Four samples were evaluated in total. Three of the samples were high carbon steel and the remaining sample was medium carbon alloy steel. Only one of the three medium carbon alloy steel groups was subjected to stress level 3.

RCF-1-14 exhibits multiple branching subsurface cracks at the location of the visually evident surface crack which is typical of subsurface initiated pitting contact fatigue as shown in Figure 5.9. The crack branches indicate that the origin is located approximately 0.213mm below the roller contact surface. No other cracks are present around the remainder of the circumference in the plane of this metallographic section. A

0.558mm deep layer exhibiting a slightly different microstructure extends from the roller contact surface as shown in Figure 5.10. The near surface microstructure and core microstructures are similar to sample RCF-1-07.

Sample RCF-2-01 exhibits multiple branching subsurface cracks at the location of the visually evident surface crack which is typical of subsurface initiated pitting contact fatigue as shown in Figure 5.11. The crack branches indicate that the origin is located approximately 0.155mm below the roller contact surface. No other cracks are present around the remainder of the circumference in the plane of this metallographic section. The near surface microstructure consists of fine lamellar pearlite as shown in Figure 5.12. The branching subsurface cracks are transgranular. The core microstructure also consists of fine lamellar pearlite with very small amounts of ferrite as shown in Figure 5.6. The near surface and core microstructures are very similar to the stress relieved high carbon steel sample RCF-1-07. This indicates that the oil quench and the relatively low hardenability of this material were not sufficient to quench the test sample location to martensite during the quench and temper heat treatment.

Sample RCF-2-05 exhibits multiple branching subsurface cracks at the location of the visually evident surface crack which is typical of subsurface initiated pitting contact fatigue as shown in Figure 5.13. The crack branches indicate that the origin is located approximately 0.142mm below the roller contact surface. The near surface and core microstructures show similarity to the stress relieved high carbon steel sample RCF-1-07 and quenched and tempered high carbon steel sample RCF-2-01.

Sample RCF-5-02 exhibits multiple branching subsurface cracks at the location of the visually evident surface crack which is typical of subsurface initiated pitting contact fatigue as shown in Figure 5.14. The crack branches indicate that the origin is located approximately 0.203mm below the roller contact surface. No other cracks are present around the remainder of the circumference in the plane of this metallographic section. The microstructure of this sample consists of uniform fine grained tempered martensite that is similar to samples RCF-3-04 and RCF-4-12. A 0.406mm deep layer exhibiting a slightly different microstructure extends from the roller contact surface as shown in Figure 5.15. This is indicative of some plastic deformation from the cyclic compressive (hertz) stresses applied by the mating rollers during testing. Slight chemical segregation is also evident.

The maximum near surface hardness of sample RCF-1-14 is equivalent to approximately 50 Rockwell C at a depth of 0.152mm, as shown in Table 5.9. The location of the maximum near surface hardness is slightly shallower than the location of the subsurface crack origin. The average core hardness is equivalent to approximately 37 Rockwell C. This indicates that the applied cyclic compressive (hertz) stress during testing resulted in cold-working the near surface material which increased the hardness approximately 13 Rockwell C points. This hardness increase extends to a depth of approximately 0.508mm.

Sample RCF-2-01 has a maximum near surface hardness equivalent to approximately 45 Rockwell C at a depth of 0.102mm, as shown in Table 5.9. The location of the maximum near surface hardness is slightly shallower than the location of the subsurface crack origin. The average core hardness is equivalent to approximately 37

Rockwell C. This indicates that the applied cyclic compressive (hertz) stress during testing resulted in cold-working the near surface material which increased the hardness approximately 8 Rockwell C points. This hardness increase extends to a depth of approximately 0.304mm.

The RCF-2-05 sample's maximum near surface hardness is equivalent to approximately 47 Rockwell C at a depth of 0.152mm, as shown in Table 5.9. The location of the maximum near surface hardness is slightly deeper than the location of the subsurface crack origin. The average core hardness is equivalent to approximately 38 Rockwell C. This indicates that the applied cyclic compressive (hertz) stress during testing resulted in cold-working the near surface material that increased the hardness approximately 9 Rockwell C points. This hardness increase extends to a depth of approximately 0.355mm.

The maximum near surface hardness of sample RCF-5-02 is equivalent to approximately 51 Rockwell C at a depth of 0.203mm, as shown in Table 5.9. The location of the maximum near surface hardness is similar to the location of the subsurface crack origin. The average core hardness is equivalent to approximately 45 Rockwell C. This indicates that the applied cyclic compressive (hertz) stress during testing resulted in cold-working the near surface material that increased the hardness approximately 6 Rockwell C points. This hardness increase extends to a depth of approximately 0.406mm.

5.5.4 Stress Level 4 (110%)

Stress level four targets the samples that were run over the theoretical maximum shear stress level of the specific application's slewing ring. Two samples were evaluated at this level. One high carbon steel sample and one medium carbon alloy steel. There were a limited number of material groups that were able to achieve 10% over the stress level.

Sample RCF-2-07 exhibits multiple branching subsurface cracks at the location of the visually evident surface crack which is typical of subsurface initiated pitting contact fatigue as shown in Figure 5.16. The crack branches indicate that the origin is located approximately 0.142mm below the roller contact surface. No other cracks are present around the remainder of the circumference in the plane of this metallographic section. A 0.508mm deep layer exhibiting a slightly different microstructure extends from the roller contact surface as shown in Figure 5.17. This is indicative of some plastic deformation from the cyclic compressive (hertz) stresses applied by the mating rollers during testing. The near surface and core microstructures are very similar to the previous high carbon steel samples RCF-1-07, RCF-2-01, and RCF-2-05.

Sample RCF-5-09 exhibits multiple branching subsurface cracks at the location of the visually evident surface crack which is typical of subsurface initiated pitting contact fatigue as shown in Figure 5.18. The crack branches indicate that the origin is located approximately 0.157mm below the roller contact surface. No other cracks are present around the remainder of the circumference in the plane of this metallographic section. A 0.025mm deep layer exhibiting a slightly different microstructure extends from the roller contact surface as shown in Figure 5.19 which is indicative of some plastic deformation

from the cyclic compressive (hertz) stresses applied by the mating rollers during testing. The microstructure of this sample consists of uniform fine grained tempered martensite that is similar to samples RCF-3-04, RCF-4-12, and RCF-5-02. Slight chemical segregation is also evident.

The maximum near surface hardness of sample RCF-2-07 is equivalent to approximately 51 Rockwell C at a depth of 0.10mm to 0.15mm, as shown in Table 5.10. The location of the maximum near surface hardness is similar to the location of the subsurface crack origin. The average core hardness is equivalent to approximately 39 Rockwell C. This indicates that the applied cyclic compressive (hertz) stress during testing resulted in cold-working the near surface material which increased the hardness approximately 12 Rockwell C points. This hardness increase extends to a depth of approximately 0.457mm.

The maximum near surface hardness of sample RCF-5-09 is equivalent to approximately 48 Rockwell C at a depth of 0.152mm, as shown in Table 5.10. The location of the maximum near surface hardness is similar to the location of the subsurface crack origin. The average core hardness is equivalent to approximately 45 Rockwell C. This indicates that the applied cyclic compressive (hertz) stress during testing resulted in cold-working the near surface material which increased the hardness approximately 3 Rockwell C points. This hardness increase extends to a depth of approximately 0.203mm.

5.6 Discussion of Results

Traditional bearing calculations and methodology reduces the expected life of the bearing with decreasing levels of hardness, regardless of the material type. Under this notion, the high carbon steel has the lowest hardness. This would predict the life would be worse than the medium carbon alloy steel. The results of the cycles to failure were evaluated utilizing a Weibull distribution seen in 0. The predicted number of cycles that cause 10% and 50% of failures at a 95% confidence were plotted. All five material types at a high and low load setting were plotted on a log normal plot. Figure 5.20 shows the 10% failure S-N plot and Figure 5.21 shows the 50% failure S-N plot. The results of the S-N plot show that the traditional bearing calculation and methodology of calculating life base on hardness hold true only for similar material types. The result demonstrates that material type affects the life results of materials with a hardness less than the traditional minimum bearing hardness of 50 Rockwell C. The stress relieved high carbon at a core hardness of 30 Rockwell C has a slightly lower expected life than the quenched and tempered high carbon steel at 32 Rockwell C. The stress relieved high carbon steel has a higher expected life when compared to two of the medium carbon alloy steels at a hardness level of 33 Rockwell C and 39 Rockwell C. If judgment was made on only the S-N plots, the high carbon quenched and tempered steel at 33 Rockwell C would be equivalent to the medium carbon alloy steel at 44 Rockwell C. However, this trend was not similar to the specific application's raceway life. A majority of the medium carbon alloy steel raceways would meet the equivalent life of the high carbon steel, although a handful of raceways catastrophically failed prematurely. These failures gave little to no

warning of the impending failure, which illustrates the importance of understanding how and where the cracks initiate.

The evaluated samples contain single areas of generally longitudinal cracking which is consistent with subsurface initiated pitting contact fatigue. These crack initiated depths are consistent with the depths of the increased maximum hardness that resulted from cold working of the roller contact surfaces during testing as summarized in Table 5.11. Except for sample RCF-1-07, these crack origin depths are in the range of 0.127mm to 0.213mm and are relatively independent of the applied cyclic compressive (hertz) stress range. The crack origins are generally slightly deeper in the quenched and tempered medium carbon alloy steel samples when compared to the stress relieved and quenched and tempered high carbon steel samples. This trend is consistent with the results seen in the specific application's service history with the two materials. In addition, the stress relieved or quenched and tempered high carbon steel exhibits substantially greater amounts of cold working due to the compressive loading of the roller contact surfaces to the medium carbon alloy steel as indicated by the greater near surface hardness increases.

Figure 5.22 records the near surface hardness of failed slewing ring raceways from the specific application utilizing the two different materials. The high carbon steel reaches the same or higher level of hardness as the medium carbon alloy steel near the depth of theoretical maximum shear stress. This level of hardness increase is significant when compared to the base hardness of the material. Figure 5.23 demonstrates the percent hardness of increase over the base hardness for those failed applications. High carbon steel reaches about 55% increase of hardness. If there is a relationship between

the percent increase of hardness of the material and amount of compressive residual; the high carbon steel will have a higher resistance to crack initiation along with a decrease in crack growth rate. The test specimen subsurface micro hardness followed the same trend seen in all four stress ranges seen in the following figures: Figure 5.24, Figure 5.25, Figure 5.26, and Figure 5.27. The high carbon steel showed a significant amount of cold working in comparison to the medium carbon alloy steel confirming the increased hardness results from this test. In addition, Figure 5.28 shows a comparison of the failed surfaces of the two materials during this test to the failed surfaces of the actual slewing ring raceway of the specific application.

The results of this test indicate a few factors are the probable cause of the variations in the service performances of the medium carbon alloy steel slewing ring raceways and the stress relieved or quenched and tempered high carbon steel slewing ring raceways. First the increased cold working of the high carbon steel contact surfaces increases the near surface residual compressive stresses. These compressive stresses offset some of the applied subsurface tensile stresses during testing or in service. The increased cold working of the high carbon steel also permits the roller contact surface to better conform to the roller configuration. This is especially true for the specific application's slewing ring which is several feet in diameter. Substantial plastic deformation of the roller contact surfaces was proven in the evaluation of failed high carbon steel slewing ring raceways. The decreased amount of cold working of the medium carbon alloy steel may result in localized variations in the contact stresses due to slight dimensional differences when applied on such a large scale.

Secondly, the heat treatment of the medium carbon alloy steel test samples utilized a water quench. The greater quench severity associated with a water quench in comparison to oil or polymer quench increases the section sizes that can be completely transformed to martensite. However, this will increase the amount of internal residual quenching stresses. Some of these residual tensile quenching stresses are relieved during tempering. The residual internal tensile stresses are additive to the tensile stresses associated with surface contact stresses. This would decrease the time required for cracks to initiate and propagate. These residual tensile stresses could also affect the location of crack initiation as well as the crack propagation direction. This could account for the deep spalling of the medium carbon alloy steel raceways in service and the average subsurface crack depth during testing being deeper than the high carbon steel's crack depth.

5.7 Summary

Rolling contact fatigue testing utilizing a ZF-RCF testing apparatus occurred with five material groups composed of two different material types. The two material types are high carbon steel and medium carbon alloy steel. Each of the five material groups was subjected to two load levels for a targeted number of cycles, one to fail specimens between five and ten million load cycles and the other to fail the specimens between three and eight million. A total of seventy test specimens were tested until the first sign of a crack was detected by an eddy current. At the end of each test an evaluation of the rolling surface was completed along a measurement of the raceway's contact surfaces width. The effective load setting was determined from the increase in contact width. The

maximum shear stress percentage was calculated after each test. This is the percentage of theoretical maximum shear stress level of the specific application's slewing ring raceway.

The results of the cycles to failure were evaluated utilizing a Weibull distribution. The predicted number of cycles that cause 10% and 50% of failures at a 95% confidence were plotted on a log normal plot. This plot is also used as an S-N plot to compare the expected life of the five material groups. Both 10% and 50% failure rates depicted the high carbon quench and tempered steel at 33 Rockwell C as having near equivalent expected life as the medium carbon alloy steel at 44 Rockwell C.

Nine of the seventy samples were metallographically evaluated for the microstructure, crack initiation location, and reviewed for increased near surface hardness due cold working. Knoop microhardness traverses were made from the roller contact surfaces of selected samples adjacent to the cracks. The selected specimens represent four different maximum shear stress levels; 73%, 90%, 100% and 110% of the theoretical maximum shear stress of the specific application's slewing ring raceway. The results of this test indicated a few factors that are the probable cause of the variations in the service performances of the medium carbon alloy steel slewing ring raceways and the stress relieved or quenched and tempered high carbon steel slewing ring raceways. First, the increased cold working of the high carbon steel when compared to the medium carbon alloy steel increased the near surface residual compressive stresses. These compressive stresses offset some of the applied subsurface tensile stresses during testing or in service. Furthermore, the severity of the heat treatment quench process could lead to residual tensile stresses which are additive to the tensile stresses associated with surface contact stresses.

Overall the high carbon steel at 33 Rockwell C has nearly equivalent expected life of the medium carbon alloy steel at 44 Rockwell C. Along with the work hardening of the high carbon steel, increases of the surface hardness to a level above the medium carbon alloy steel with the possible addition of compressive residual stresses at the surface decrease the crack growth rate. The amount of compressive residual stress at the surface was not evaluated, but only assumed from the amount of plastic deformation seen at the surface.

Table 5.6: Reviewed metallurgical specimen ID and test results

Stress Range	Specimen ID #	Maximum Shear Stress %	Cycles to failures (million)
1 (73%)	RCF-3-04	72.8%	11.3
2 (90%)	RCF-1-07	92.5%	8.52
	RCF-4-12	91.0%	7.56
3 (100%)	RCF-1-14	99.8%	5.10
	RCF-2-01	99.7%	4.26
	RCF-2-05	99.7%	3.45
	RCF-5-02	97.1%	2.03
4 (110%)	RCF-2-07	108.0%	6.18
	RCF-5-09	108.7%	6.18

Table 5.7: Micro hardness from the rolling surface of Range 1 (200 gm. Load)

Range 1 - 73% Shear Stress		
Depth, mm	RCF-3-04	
	Knoop	Aproximate Equivalent Rockwell C
0.050	375	37.5
0.100	408	40.5
0.150	417	41.3
0.200	408	40.5
0.250	394	39.3
0.300	373	37.3
0.350	366	36.6
0.400	361	36.1
0.450	358	35.8
0.500	366	36.6
0.625	363	36.3
0.750	351	35.0
0.875	375	37.5
1.000	381	38.1
1.125	378	37.8
1.250	356	35.5
1.375	349	34.8
1.500	381	38.1

Table 5.8: Micro hardness from the rolling surface of range 2 (200 gm. Load)

Range 2 - 90% Shear Stress				
Depth, mm	RCF-4-12		RCF-1-07	
	Knoop	Aproximate Equivalent Rockwell C	Knoop	Aproximate Equivalent Rockwell C
0.050	399	39.8	479	45.9
0.100	438	43.0	510	48.0
0.150	432	42.5	476	45.7
0.200	420	41.6	498	47.2
0.250	411	40.8	479	45.9
0.300	402	40.0	445	43.5
0.350	423	41.8	441	43.2
0.400	423	41.8	411	40.8
0.450	411	40.8	388	38.8
0.500	414	41.1	363	36.3
0.625	411	40.8	349	34.8
0.750	411	40.8	349	34.8
0.875	399	39.8	347	34.5
1.000	383	38.3	325	31.9
1.125	386	38.6	347	34.5
1.250	405	40.3	317	30.8
1.375	386	38.6	327	32.1
1.500	408	40.5	349	34.8

Table 5.9: Micro hardness from the rolling surface of range 3 (200 gm. Load)

Range 3 -100% Shear Stress								
Depth, mm	RCF-1-14		RCF-2-01		RCF-2-05		RCF-5-02	
	Knoop	Aproximate Equivalent Rockwell C						
0.050	476	45.7	426	42.0	432	42.5	426	42.0
0.100	490	46.7	461	44.7	487	46.5	461	44.7
0.150	539	49.8	432	42.5	498	47.2	432	42.5
0.200	515	48.3	408	40.5	476	45.7	408	40.5
0.250	506	47.7	405	40.3	441	43.2	405	40.3
0.300	479	45.9	399	39.8	420	41.6	399	39.8
0.350	435	42.8	388	38.8	399	39.8	388	38.8
0.400	429	42.3	383	38.3	375	37.5	383	38.3
0.450	429	42.3	397	39.6	402	40.0	397	39.6
0.500	391	39.0	414	41.1	378	37.8	414	41.1
0.625	386	38.6	370	37.0	408	40.5	370	37.0
0.750	366	36.6	378	37.8	391	39.0	378	37.8
0.875	397	39.6	370	37.0	381	38.1	370	37.0
1.000	354	35.3	402	40.0	397	39.6	402	40.0
1.125	370	37.0	366	36.6	386	38.6	366	36.6
1.250	368	36.8	388	38.8	373	37.3	388	38.8
1.375	363	36.3	349	34.8	386	38.6	349	34.8
1.500	345	34.3	361	36.1	378	37.8	361	36.1

Table 5.10: Micro hardness from the rolling surface of range 4 (200 gm. Load)

Range 4 - 110% Shear Stress				
Depth, mm	RCF-2-07		RCF-5-09	
	Knoop	Aproximate Equivalent Rockwell C	Knoop	Aproximate Equivalent Rockwell C
0.050	445	43.5	458	44.5
0.100	557	50.9	494	47.0
0.150	557	50.9	506	47.7
0.200	522	48.7	490	46.7
0.250	510	48.0	465	45.0
0.300	468	45.2	438	43.0
0.350	448	43.7	461	44.7
0.400	414	41.1	483	46.2
0.450	405	40.3	483	46.2
0.500	394	39.3	502	47.5
0.625	373	37.3	487	46.5
0.750	378	37.8	472	45.5
0.875	388	38.8	468	45.2
1.000	402	40.0	461	44.7
1.125	397	39.6	479	45.9
1.250	368	36.8	479	45.9
1.375	438	43.0	465	45.0
1.500	397	39.6	476	45.7

Table 5.11: Comparison of crack origin to hardness increase

Stress Range	Specimen ID #	Material	Crack origin depth (mm)	Cacluated Depth of Max shear stress (mm)	Near Surface Hardness Increase Rockwell C
1 (73%)	RCF-3-04	Alloy	0.127	0.182	4
2 (90%)	RCF-1-07	Carbon	0.069	0.231	15
	RCF-4-12	Alloy	0.188	0.227	3
3 (100%)	RCF-1-14	Carbon	0.213	0.249	13
	RCF-2-01	Carbon	0.155	0.249	8
	RCF-2-05	Carbon	0.142	0.249	9
	RCF-5-02	Alloy	0.203	0.242	6
4 (110%)	RCF-2-07	Carbon	0.142	0.269	12
	RCF-5-09	Alloy	0.157	0.271	3



Figure 5.1: RCF-3-04, crack location. Unetched (201X)



Figure 5.2: RCF-3-04, Microstructure. 2% Nital (50X)



Figure 5.3: RCF-1-07, Crack location. Unetched (201X)



Figure 5.4: RCF-1-07, Microstructure. 2% Nital (50X)



Figure 5.5: RCF-1-07, Transgranular crack. 2% Nital (494X)



Figure 5.6: RCF-1-07, Fine lamellar pearlite with small amounts of ferrite. (494X)



Figure 5.7: RCF-4-12, Crack location. Unetched (201X)



Figure 5.8: RCF-4-12, Microstructure. 2% Nital (50X)

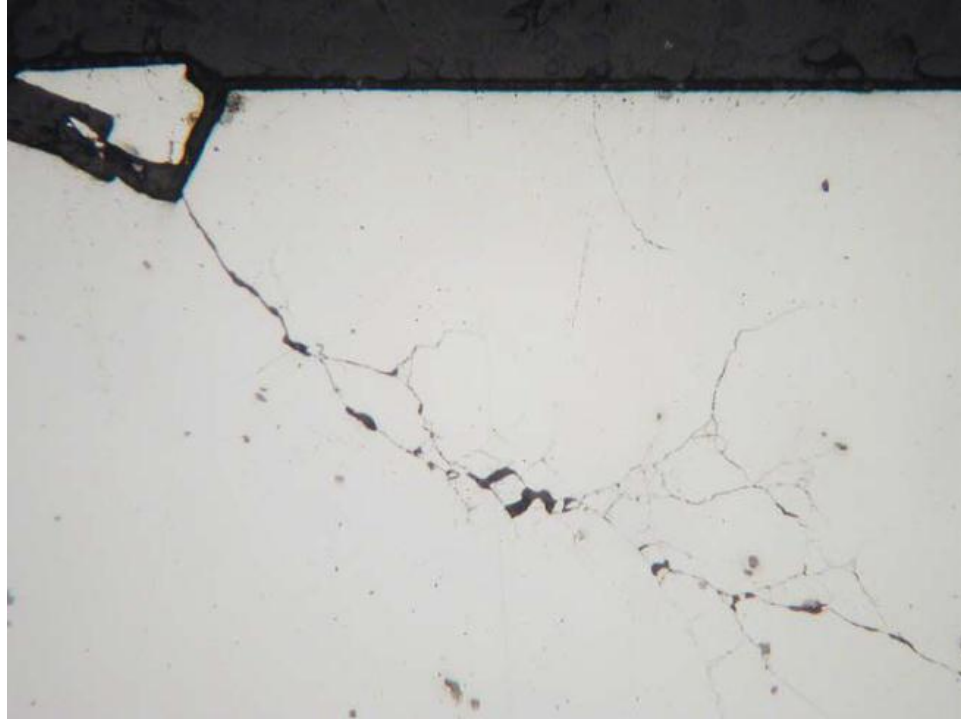


Figure 5.9: RCF-1-14, Crack location. Unetched (201X)



Figure 5.10: RCF-1-14, Microstructure. 2% Nital (50X)



Figure 5.11: RCF-2-01, Crack location. Unetched (201X)



Figure 5.12: RCF-2-01, Near surface microstructure. 2% Nital (494X)

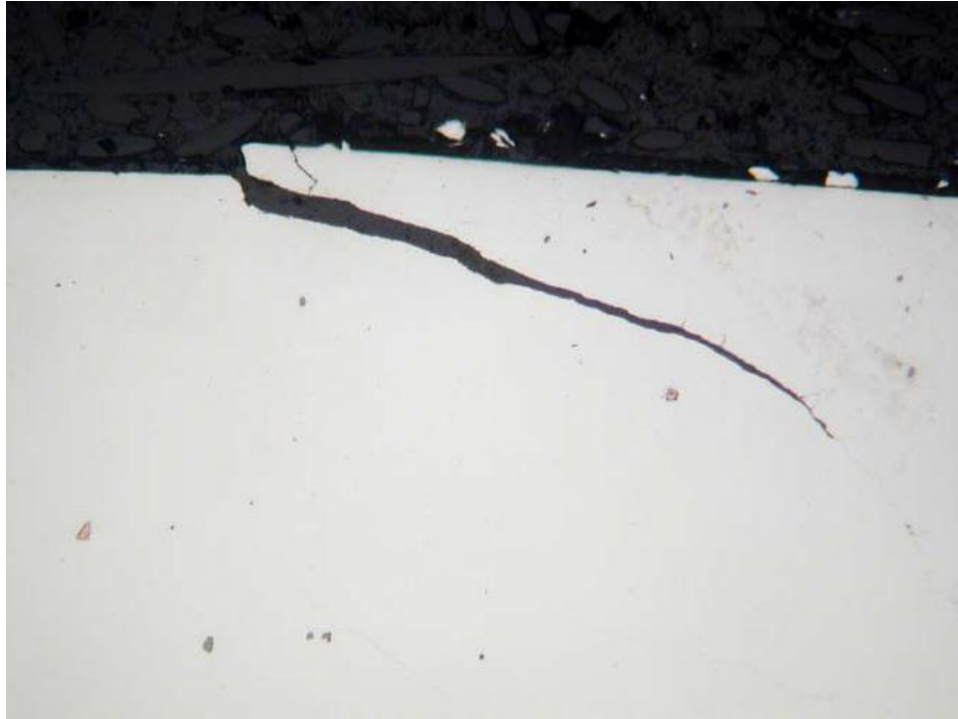


Figure 5.13: RCF-2-05, Crack location. Unetched (201X)



Figure 5.14: RCF-5-02, Crack location. Unetched (201X)



Figure 5.15: RCF-5-02, Microstructure. 2% Nital (50X)



Figure 5.16: RCF-2-07, Crack location. Unetched (201X)



Figure 5.17: RCF-2-07, Microstructure. 2% Nital (50X)



Figure 5.18: RCF-5-09, Crack Location Unetched (201X)



Figure 5.19: RCF-5-09, Microstructure. 2% Nital (50X)

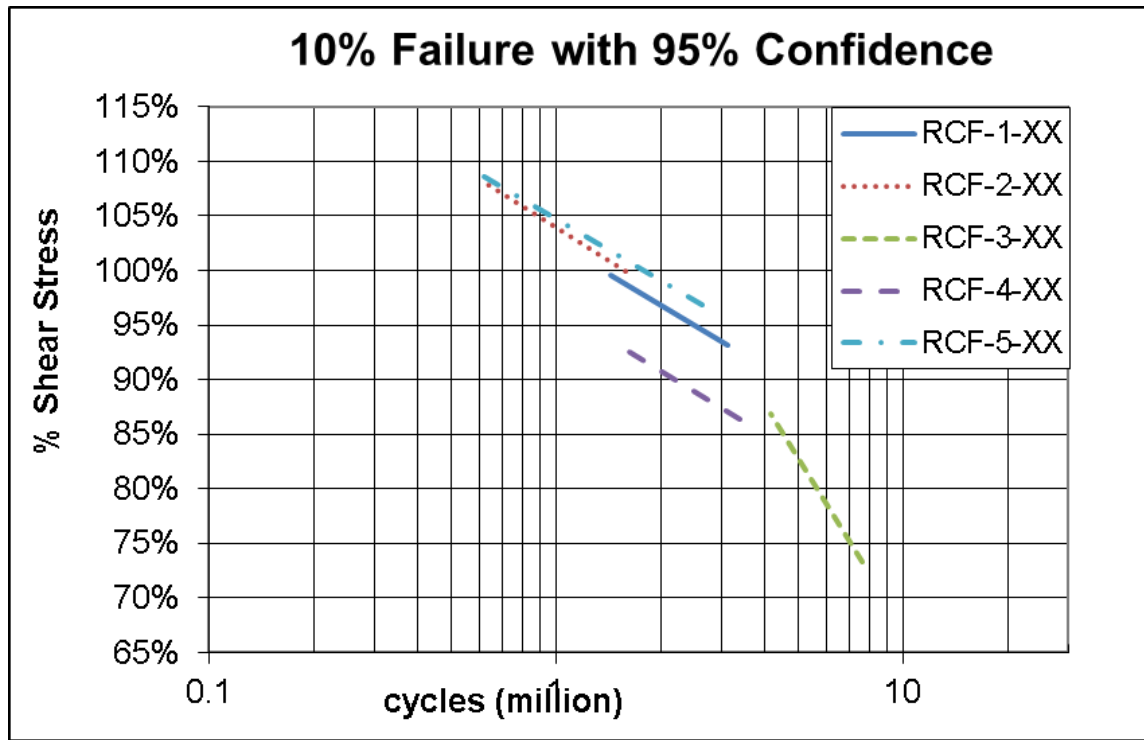


Figure 5.20: S-N Curve of 10% Failure with 95% Confidence

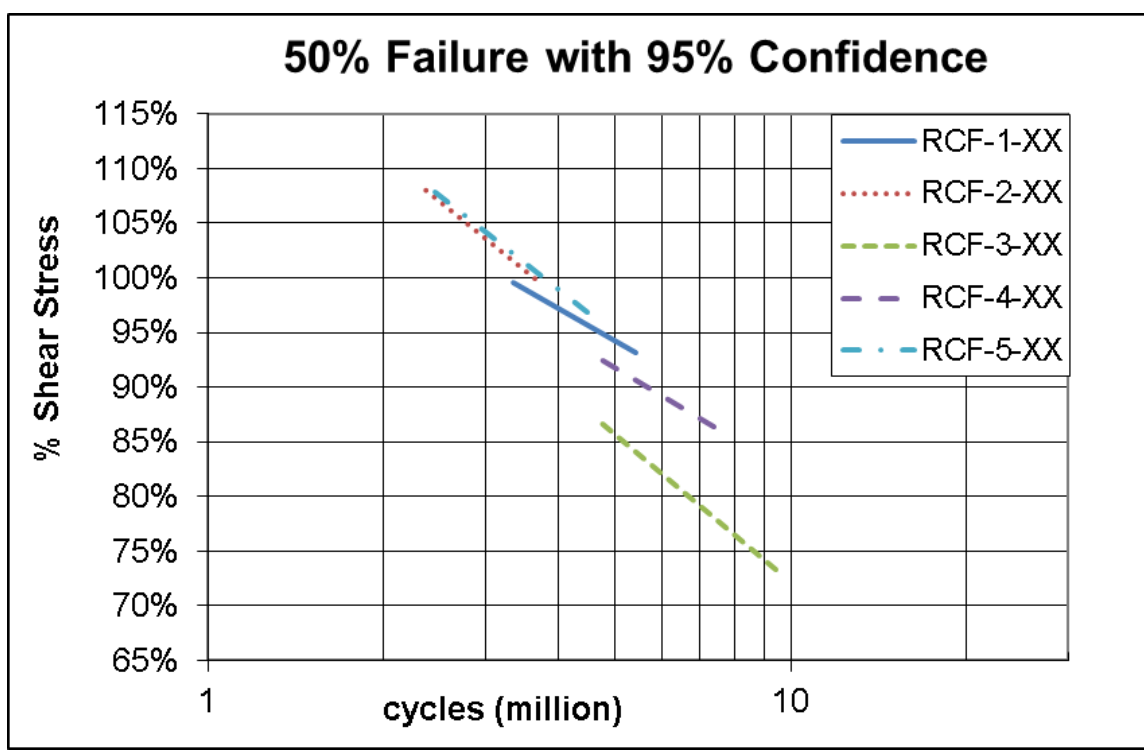


Figure 5.21: S-N Curve of 50% Failure with 95% Confidence

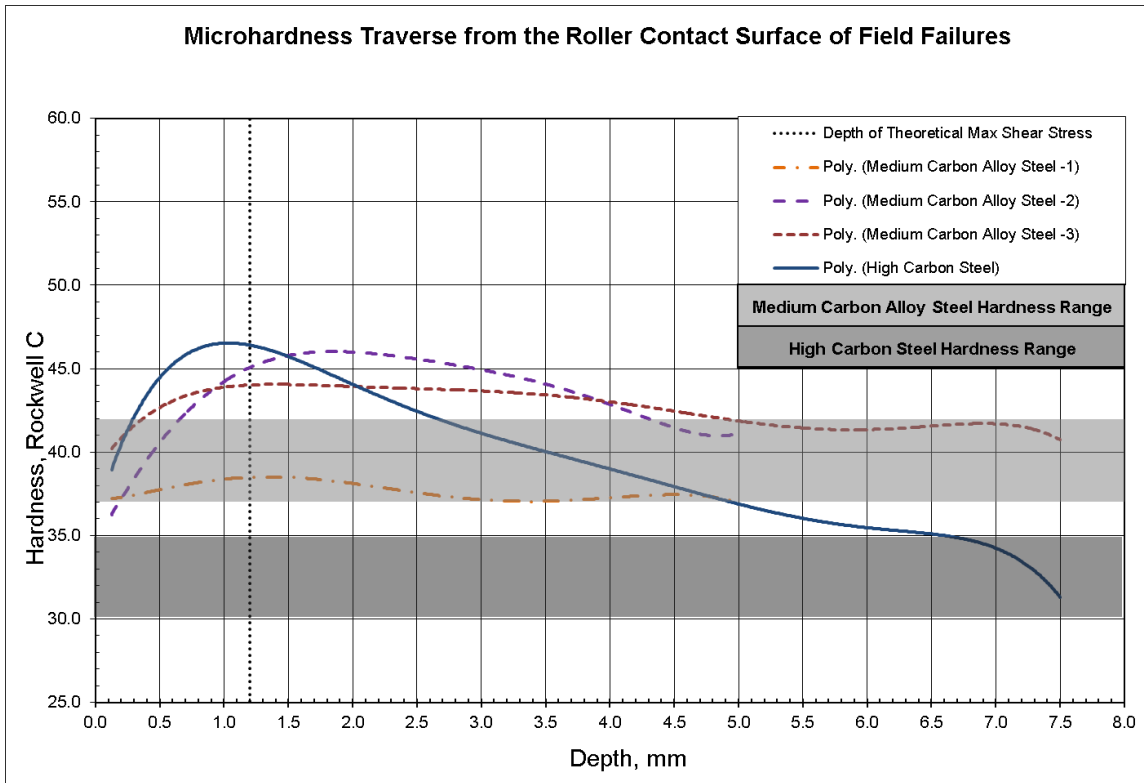


Figure 5.22: Subsurface hardness specific application material

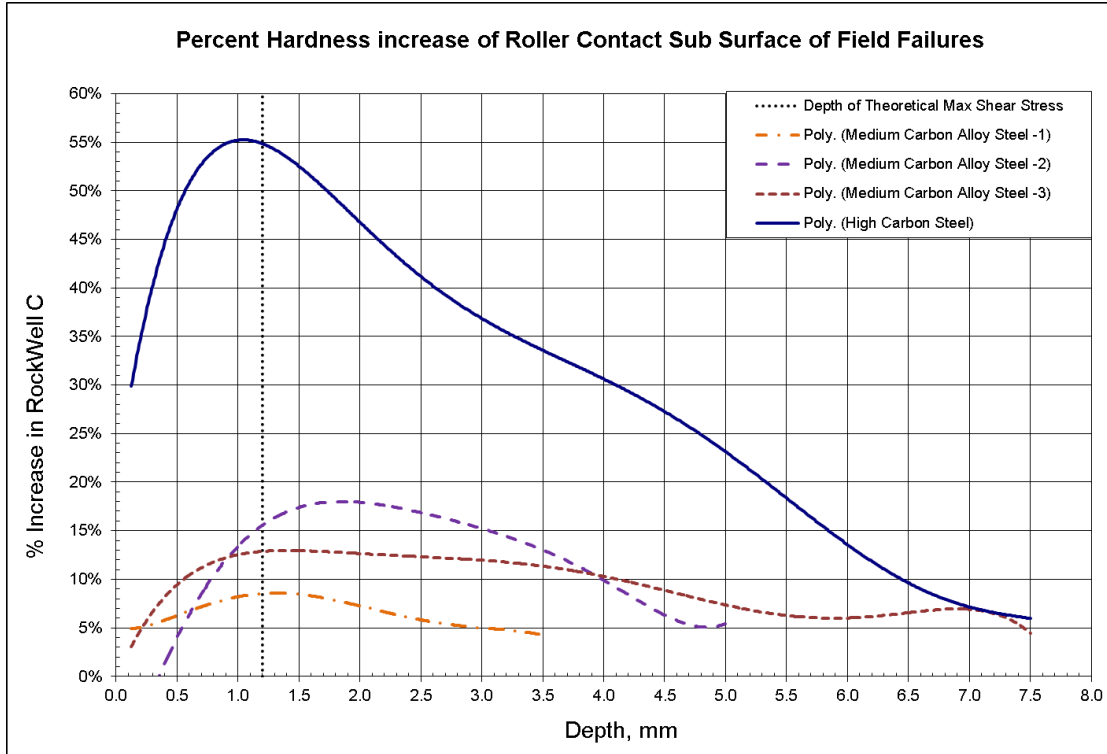


Figure 5.23: Percent subsurface hardness increase specific application material

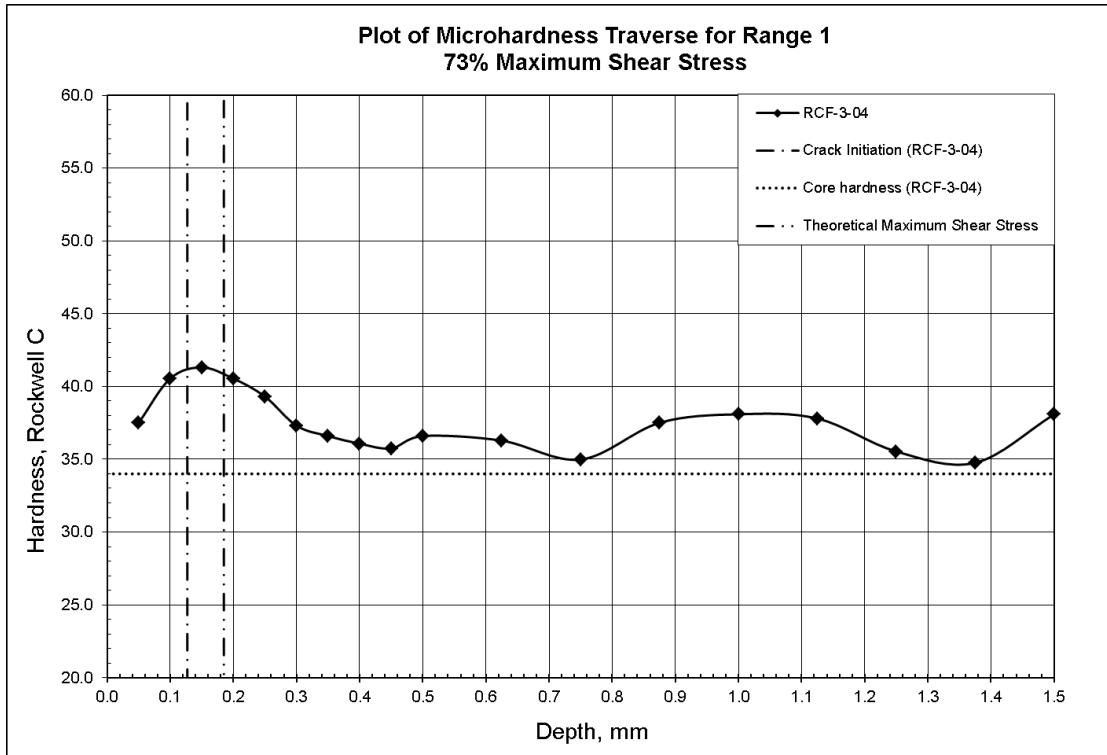


Figure 5.24: Range 1 shear stress level 73% micro hardness

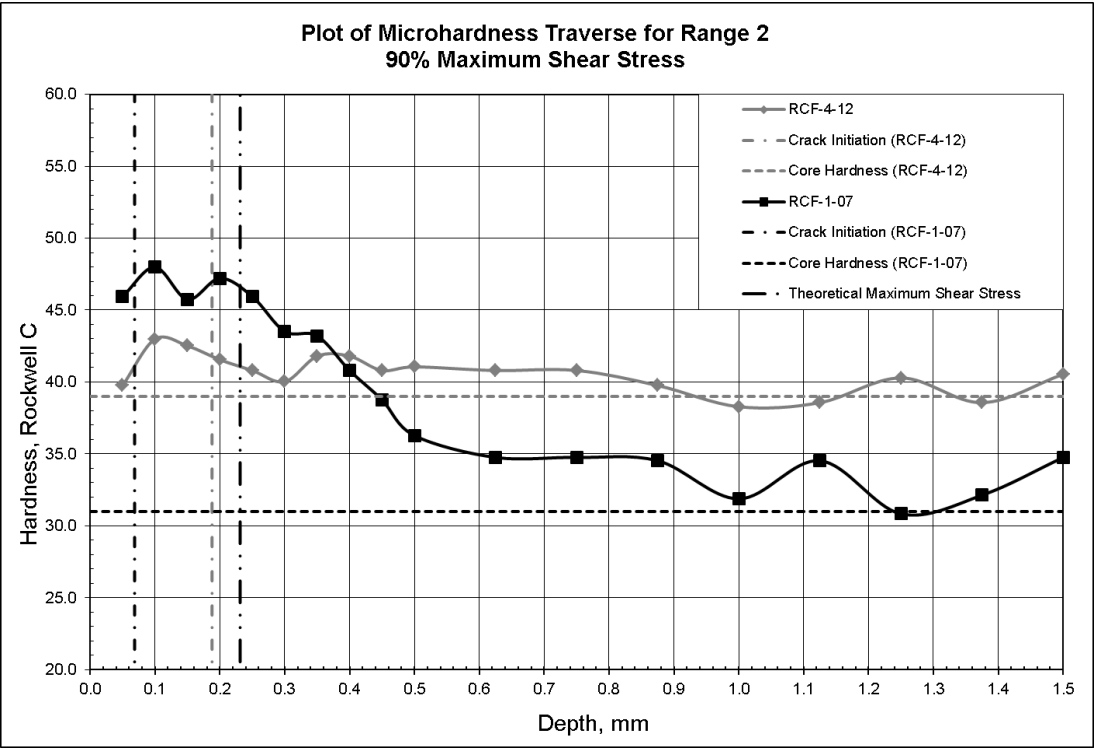


Figure 5.25: Range 2 shear stress level 90% micro hardness

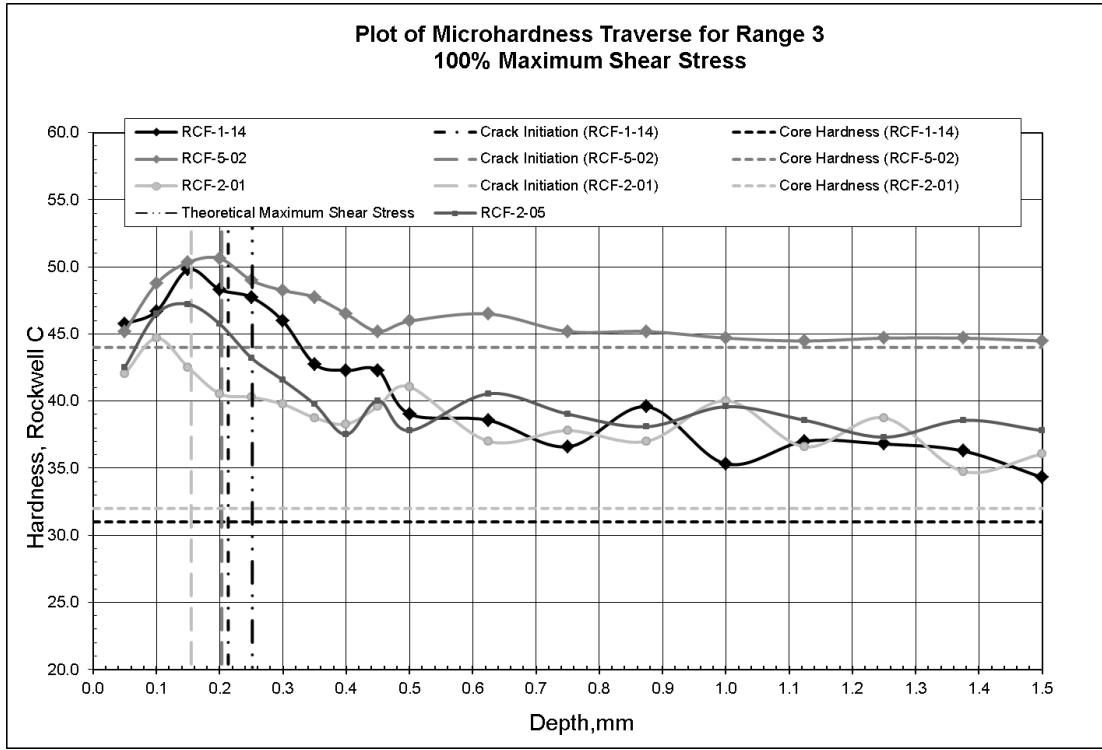


Figure 5.26: Range 3 shear stress level 100% micro hardness

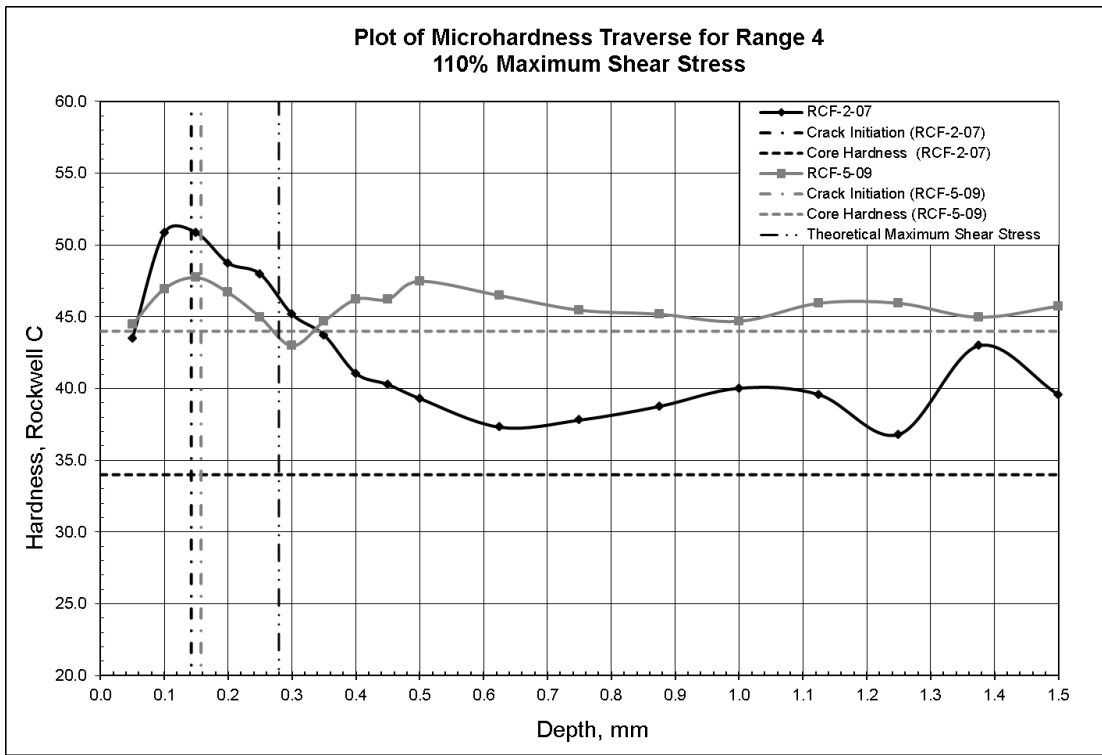


Figure 5.27: Range 4 shear stress level 110% micro hardness

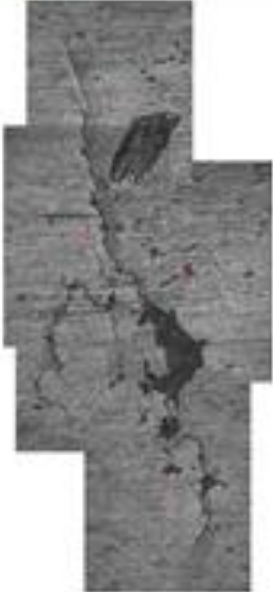
	High Carbon Steel	Medium Carbon Alloy Steel
Specific Application Failures		
Testing Failure		

Figure 5.28: Comparison of application failure to testing failures

Chapter 6

Conclusions

6.1 Summary of research

In this research, rolling contact fatigue testing of reduced hardness steels was performed using a ZF-RCF testing apparatus. These steels are utilized in anti-friction bearings, also referred to as slewing rings for cranes, excavators, and wind turbines. The reduced hardness of the steel is relatively low compared to slewing rings used in similar applications. Two previously used materials for a specific application were tested to facilitate the decision of future use as raceway material.

The specific application has relatively large amounts of structural deflection and load profiles which are difficult to obtain due to various operational conditions. The past slewing ring raceway material had been a high carbon steel, but was recently switched to medium carbon alloy steel. Due to structural deflections and manufacturing considerations, the raceway and rolling element material used for the specific design has a reduced hardness of 30 Rockwell C to 40 Rockwell C compared to a standard slewing ring hardness of 55 Rockwell C and greater. Fatigue resistance and failure mode are critical in this application due to the size and expense of repair and/or replacement of the slewing ring. The need for this research was due to the premature failures of the medium carbon alloy steel. The utilization of this material caused unpredictable failures which the application's end user was unable to plan for.

In order to simulate the specific application, care was to taken in the selection of the testing apparatus. Two testing apparatuses where reviewed, ZF-RCF and 3-Ball test

machine. The 3-ball test machine was not utilized due to the elliptical contact between the rod and balls, which is dissimilar to the specific application's slewing ring line contact. The application's slewing ring material is of lower hardness which can cause excessive plastic deformation the ZF-RCF testing apparatus was chosen due to the ability to stop and measure the rolling contact surface and adjust the applied load. The ZF-RCF machine was able to achieve all testing objectives.

Five material groups were tested. These groups were composed of the two material types, high carbon steel and medium carbon alloy steel. The material was processed from forged rolled rings of a smaller diameter than the specific application's slewing ring raceway diameter. The forged rings were processed with similar manufacturing techniques and forging ratios. The rings were cut into sections prior to heat treatment. The high carbon steel ring was cut into two sections. One section was stress relieved to a hardness of 30 Rockwell C and the other was quenched and tempered to a hardness of 32 Rockwell C. The medium carbon alloy steel was cut into three sections, all of which were quenched, but tempered to a different hardness. The samples were hardened to 33, 39, and 44 Rockwell C respectively.

The test specimen used in this research was processed from the ring sections described above. Consideration of the test specimen's orientation was also taken. Two possible directions were reviewed, the circumferential and the radial direction. The two directions seemed to correlate to the specific slewing ring raceway failures. Multiple factors were considered prior to the determination of the final test specimen orientation. The key factors were grain and inclusion orientation. The radial direction was initially pretested due to its orientation being comparable to the rolling direction of the specific

slewing ring. This specimen orientation introduced variance in the failure mode and cycles to failure. The final testing direction was determined to be the circumferential direction. This direction is not correlated with the specific slewing bearing rolling direction. The rolling direction of the test specimen was perpendicular to the specific slewing ring's rolling direction. Nevertheless, the circumferential direction had a constant rolling surface which reduced the testing variance seen in the radial direction.

Final testing of the five material groups was subjected to two load levels for a targeted specific number of cycles to failure. A total of seventy test specimens were tested until the first sign of a crack was detected by an eddy current. At the end of each test an evaluation of the rolling surface was completed along with a measurement of the raceway's contact surfaces width. The maximum shear stress percentage was calculated after each test. This percentage was based on the theoretical maximum shear stress level of the specific application's slewing ring raceway.

The results of the cycles to failure were evaluated utilizing a Weibull distribution. The predicted number of cycles was plotted on a log normal plot. This plot was used as an S-N plot to compare the expected life of the five material groups. Both ten and fifty percent failure rates depicted the high carbon quench and tempered steel at 33 Rockwell C with near equivalent expected life as the medium carbon alloy steel at 44 Rockwell C.

Nine of the seventy samples were metallurgically evaluated for the microstructure, crack initiation location, and the review of increased near surface hardness due to cold working. The selected specimens were evaluated in four maximum

shear stress levels; 73%, 90%, 100% and 110%. The evaluation indicated the probable cause of the variations in the service performances of the medium carbon alloy steel and the stress relieved or quenched and tempered high carbon steel slewing ring raceways.

Increased cold working resulted in increased near surface residual compressive stresses when comparing high carbon steel to medium carbon alloy steel. These compressive stresses offset some of the applied subsurface tensile stresses during testing or in service. Furthermore the severity of the heat treatment quench process could lead to residual tensile stresses which are additive to the tensile stresses associated with surface contact stresses.

Overall the high carbon steel at 33 Rockwell C had nearly the equivalent expected life as the medium carbon alloy steel at 44 Rockwell C. The work hardening of the high carbon steel increased the surface hardness to a level above the medium carbon alloy steel. The work hardening possibly added compressive residual stresses to the surface decreasing the crack growth rate.

6.2 Scope of Future work

- Evaluate the compressive residual stress on the rolling surface with respect to the amount of plastic deformation.
- Assess the crack growth rate between the reduced hardness steel of a pearlitic and martensitic microstructure.
- Consider incrementally increasing the applied force onto the specimen, to understand if a break in period would be beneficial.

- Simulate oscillating applied loads that can be correlated to the specific application's duty cycle.
- Test a variation to the manufacturing process of the medium carbon steel to further relieve residual stresses due to the severity associated with the water quenching process.

References

- 1 Lohmann,G. and Schreiber, H., Zur bestimmung des lebensdauerexponenten von Walzlagern (Werkstatt and Betrieb 92 (1959), 4, 188-192).
- 2 Lunderg, G. and Palmgren, A., Dynamic capacity of roller bearings (acta Polytech. (1952) 96 Mechanical Engineering series 2-stockholm, Nr. 4)
- 3 Lunderg, G. and Palmgren, A., Dynamic capacity of roller bearings (acta Polytech. (1947) 7; Mechanical Engineering series 1-stockholm, Nr. 3; Kugellager-Z. (1947) ¾).
- 4 Farshid Sadeghi “A Review of Rolling Contact Fatigue” Journal of tribology J. Tribol. -- October 2009 -- Volume 131, Issue 4, 041403 (15 pages)
- 5 Harris, T.A., “Rolling Bearing Analysis,” John Wiley & Sons, 1965
- 6 Rotec Industries: <http://www.rotec-usa.com/>
- 7 Hoffmann, G. and Jandeska, W. 2007. Effects on rolling contact fatigue performance. Gear Technology January/February 2007
- 8 Oila, A. and Bull, S. 2005. Phase transformations associated with micropitting in rolling/sliding contacts. Journal of Materials Science 40: 4767-4774.
- 9 Choi, B. and Lee, C. 2001 Characteristics of rolling contact fatigue of steels produced by thermomechanical processing. Journal of Materials Science 36: 5237-5243
- 10 Popescu, G. 2006 An engineering model for three-dimensional elastic-plastic rolling contact analyses. Tribology Transactions, 49: 387-399
- 11 Nelias, D. and Dumont, M. 1999 Role of Inclusions, Surface roughness and operating conditions on rolling contact fatigue. ASME 121 April 1999: 240-251
- 12 Sadeghi, F. 2009 A review of Rolling Contact Fatigue. Journal of tribology, ASME 131 October 2009: 041403-1 – 041403-15
- 13 McCool, J. and Valori, R. 2009 Evaluating the validity of rolling contact fatigue test results. Tribology Transactions, 52:2, 223-230

- 14 Kim, T., Cho, Y. and Lee, H. 2003 The fatigue crack initiation life prediction based on several high-cycle fatigue criteria under spherical rolling contact. *Tribology Transactions*, 46:1, 76-82
- 15 Eden, H., Garnham, J. and Davis, C. 2005 Influential microstructural changes on rolling contact fatigue crack initiation in pearlitic rail steels. *Materials Science and Technology*, 21:6, 623-629
- 16 Bormetti, E., Donzella G. and Mazzu, A. 2002 Surface and subsurface cracks in rolling contact fatigue of hardened components. *Tribology Transactions*, 45:3, 274-283
- 17 Shimizu, S. 2002 Fatigue limit concept and life prediction model for rolling contact machine elements. *Tribology Transactions*, 45:1, 39-46
- 18 Kotzalas M. 2001 A theoretical study of residual stress effects on fatigue life prediction. *Tribology Transactions*, 44:4, 609-614
- 19 Iswanto, P., Nishida, S., Hattori, N. and Usui, I. 2006 Influence of residual stress and mean stress on fatigue strength improvement of austenitic stainless steel. *Strength, Fracture and Complexity*, IOS Press, 4: 117-127
- 20 Johnson, K. 1985. *Contact mechanics*. 9th printing 2003. New York: Cambridge University Press.

Appendix A: Rolling Surface evaluation of RCF-1-XX



Figure 0.1: RCF-1-06, 30.8% Increased Contact Width, crack 2.1mm

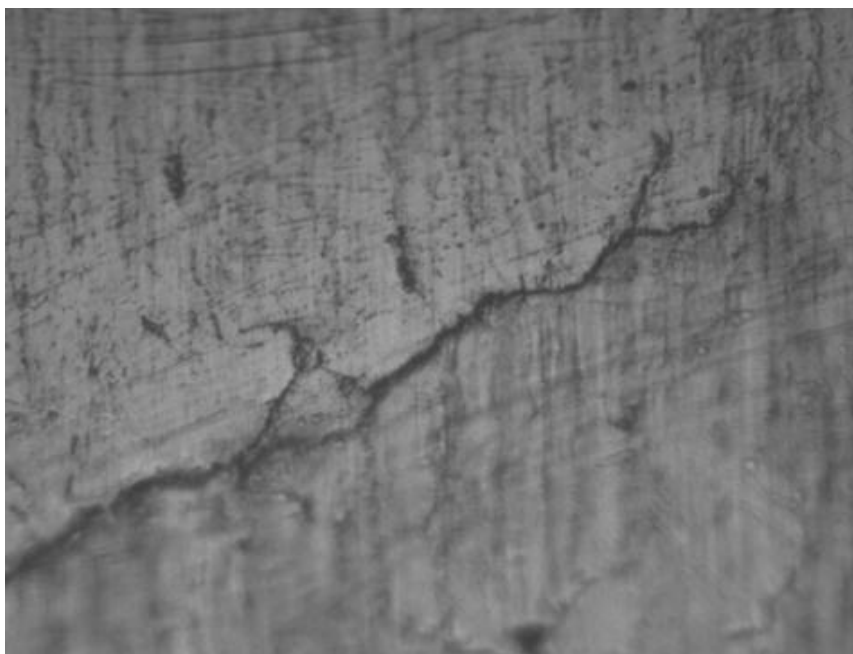


Figure 0.2: RCF-1-06, Crack Tip

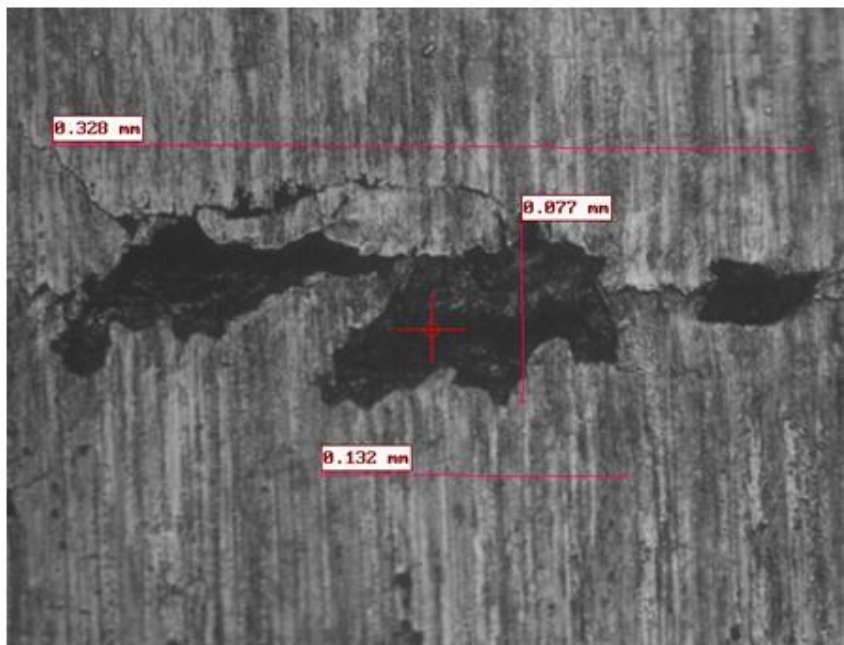


Figure 0.3: RCF-1-07, 30% Increased Contact Width, crack 1.24mm

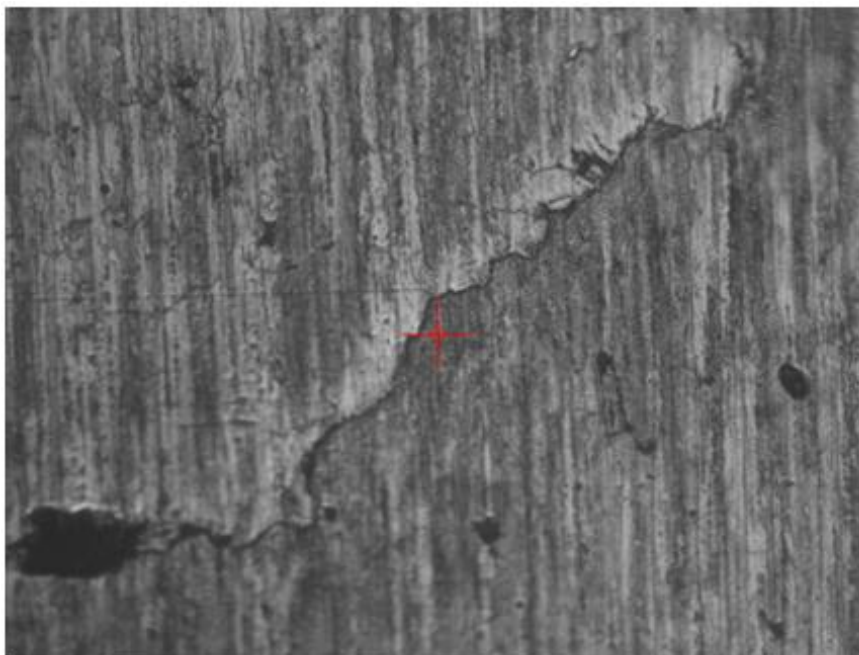


Figure 0.4: RCF-1-07, Crack Tip

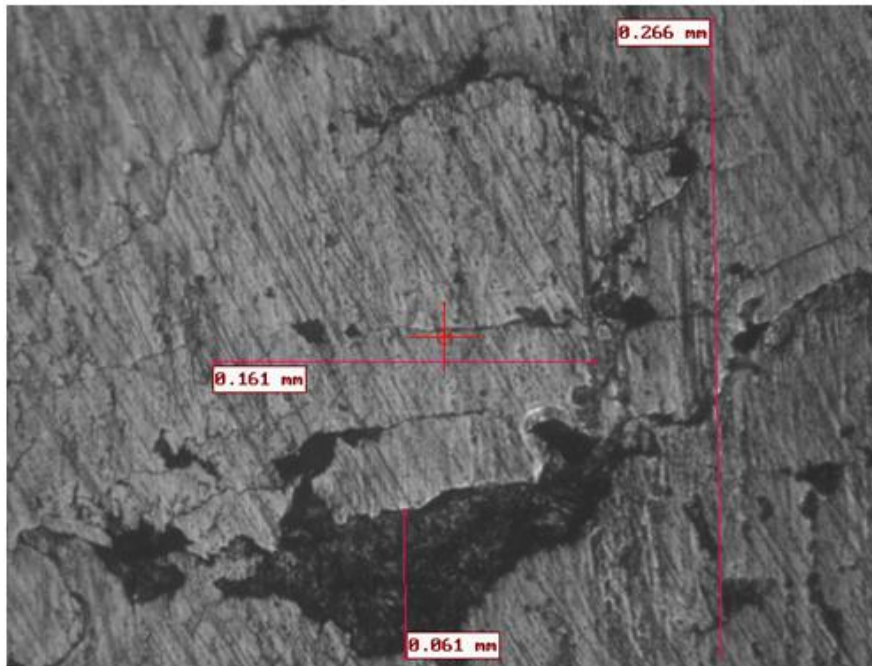


Figure 0.5: RCF-1-08, 24.3% Increased Contact Width, crack 1.7mm

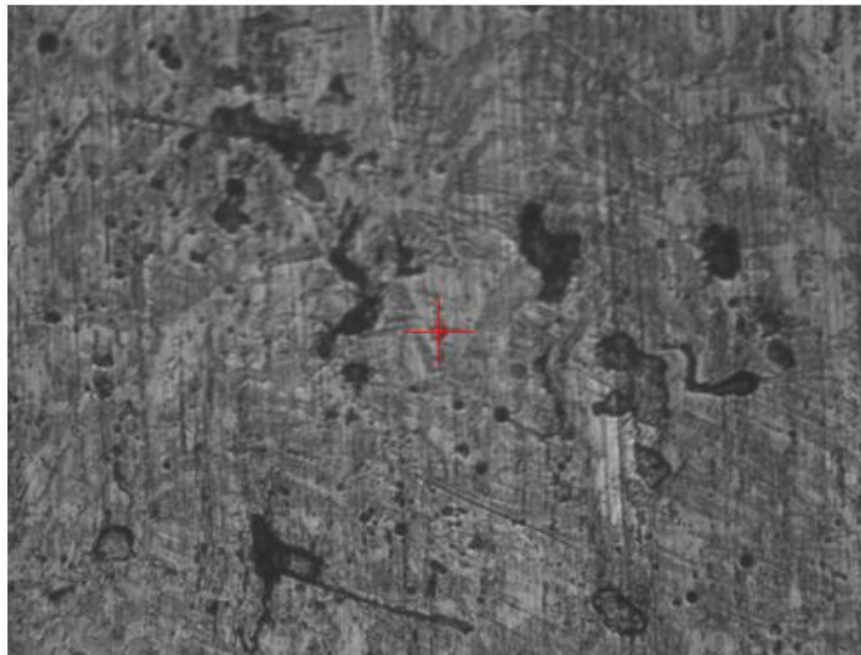


Figure 0.6: RCF-1-08, Surface Condition

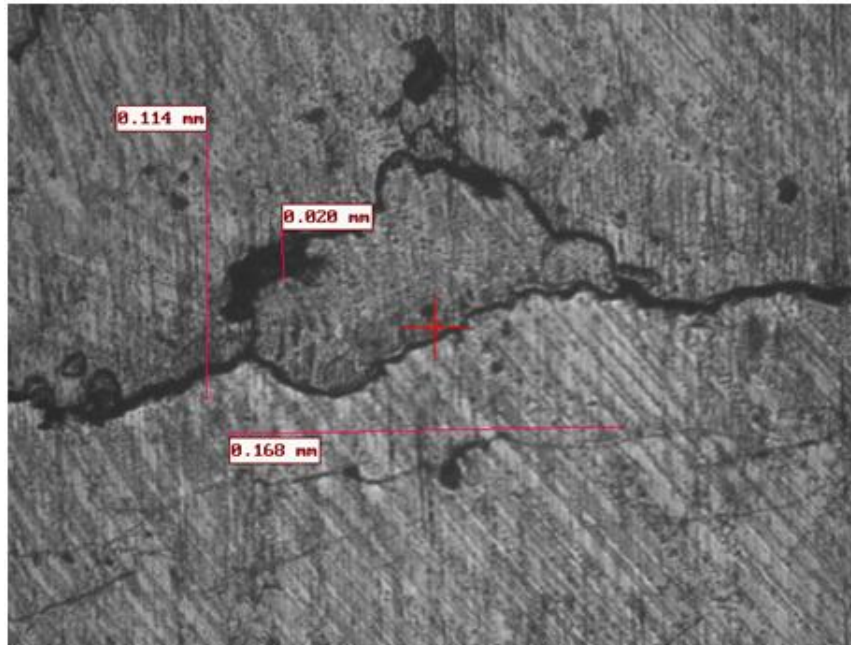


Figure 0.7: RCF-1-09, 27.5% Increased Contact Width, crack 2.4mm

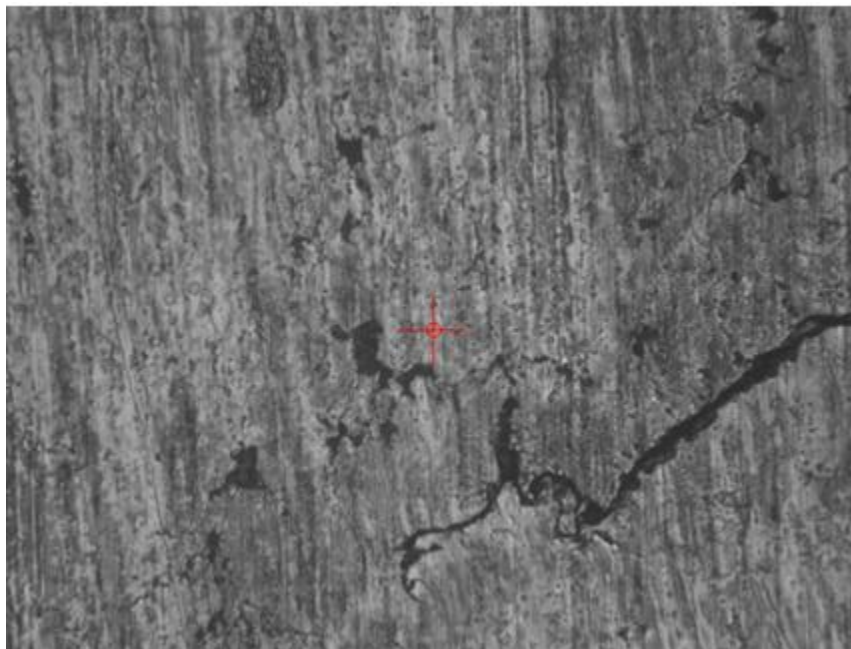


Figure 0.8: RCF-1-09, Crack Tip

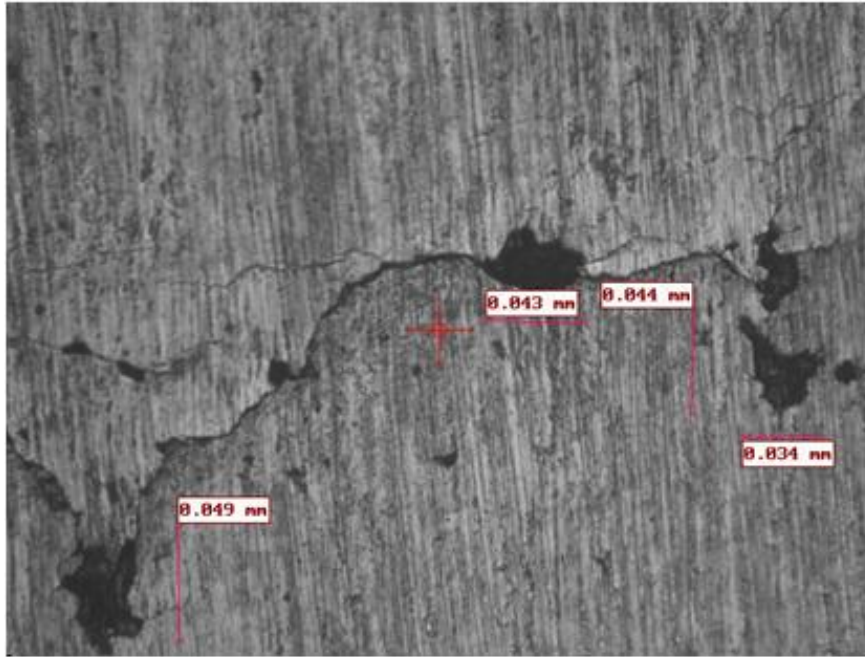


Figure 0.9: RCF-1-10, 28.8% Increased Contact Width, crack 1.3mm

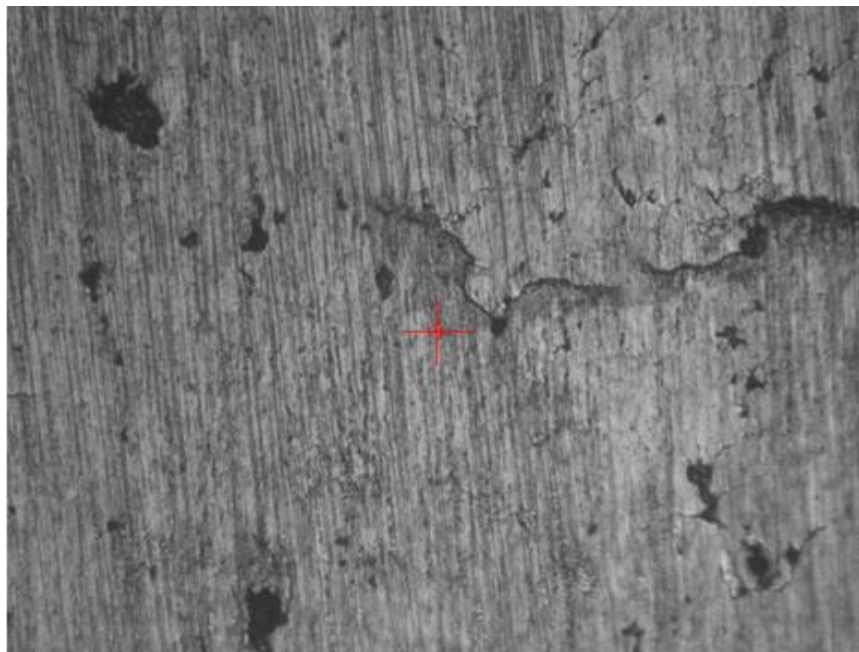


Figure 0.10: RCF-1-10, Crack Tip

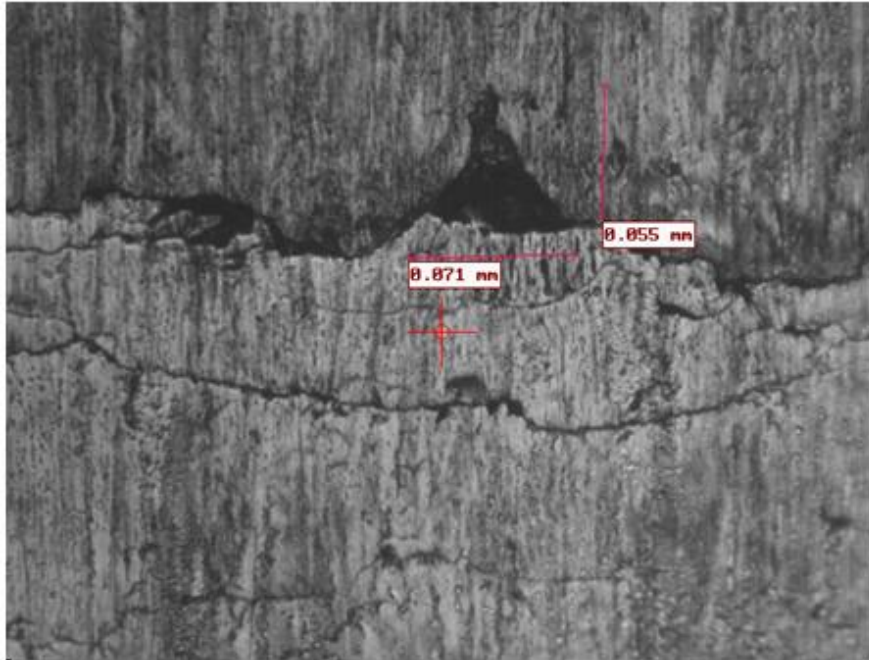


Figure 0.11: RCF-1-11, 33.7% Increased Contact Width, crack 1.64mm



Figure 0.12: RCF-1-11, Crack Tip

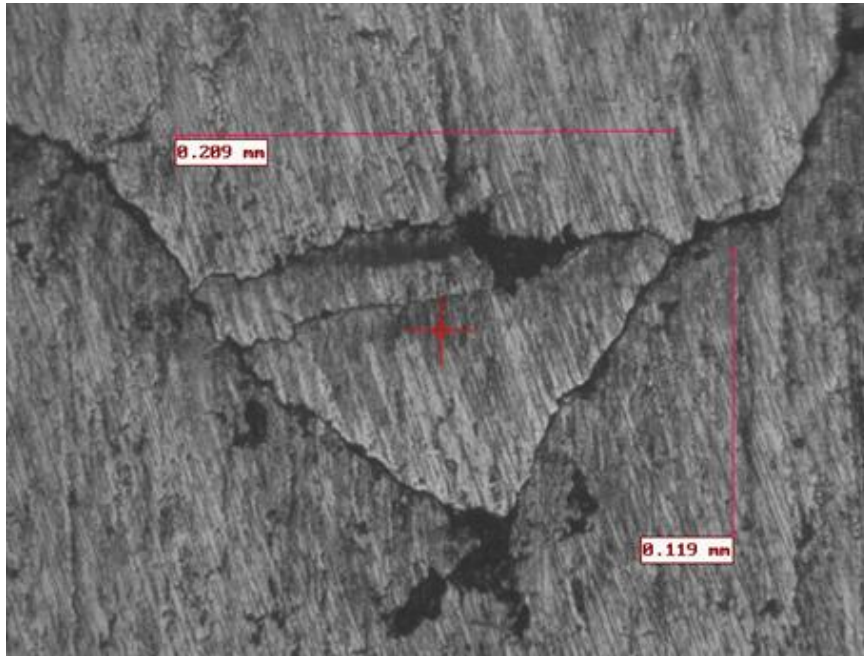


Figure 0.13: RCF-1-12, 40.0% Increased Contact Width, crack 1.5mm

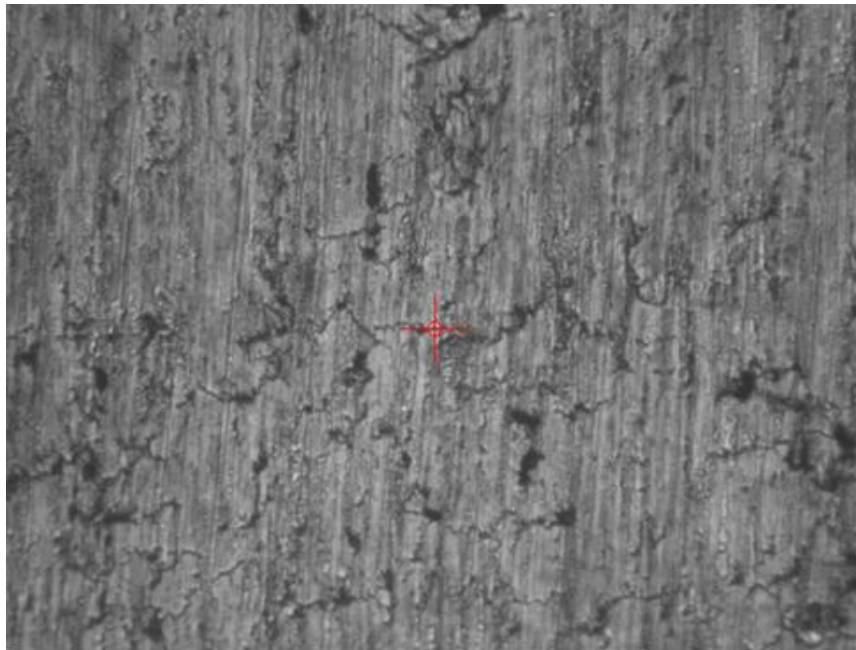


Figure 0.141: RCF-1-12, Surface Condition

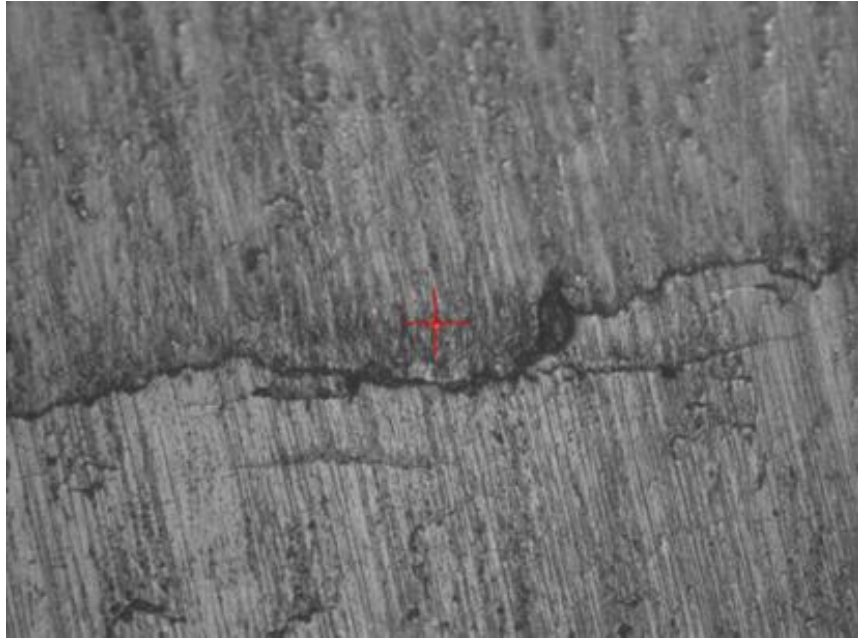


Figure 0.15: RCF-1-13, 42.0% Increased Contact Width, crack 1.7mm

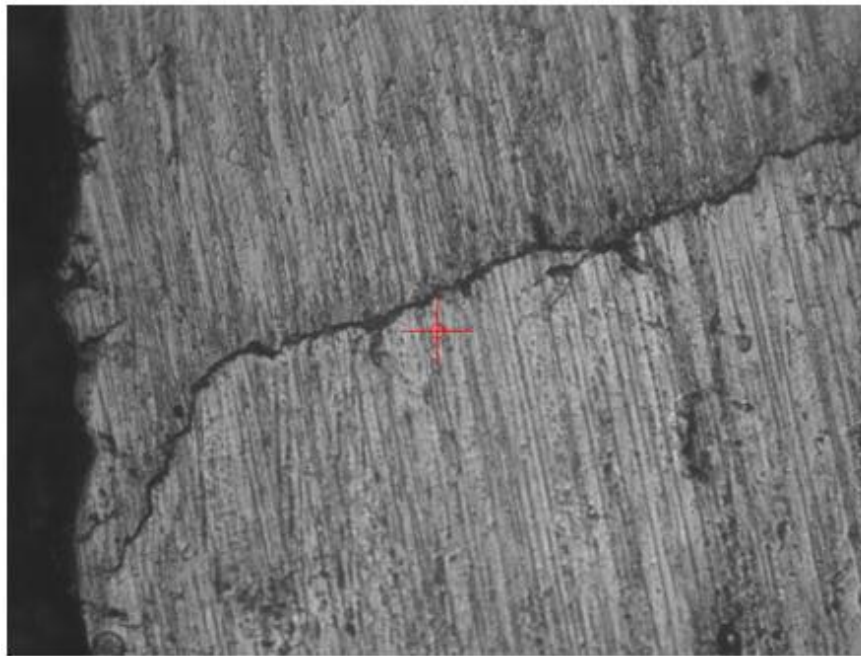


Figure 0.16: RCF-1-13, Crack Tip at Edge of Rolling Surface

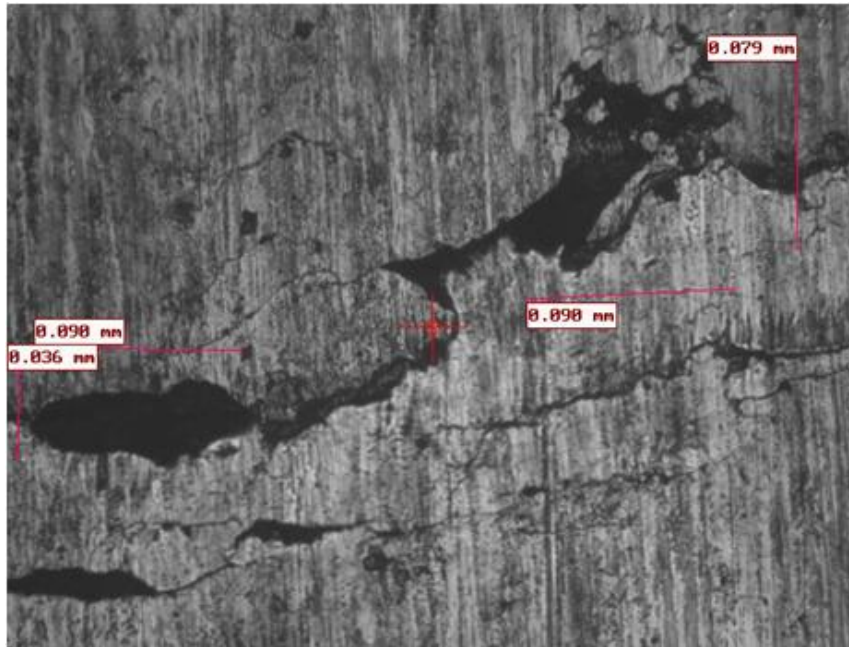


Figure 0.17: RCF-1-14, 37.8% Increased Contact Width, crack 3mm

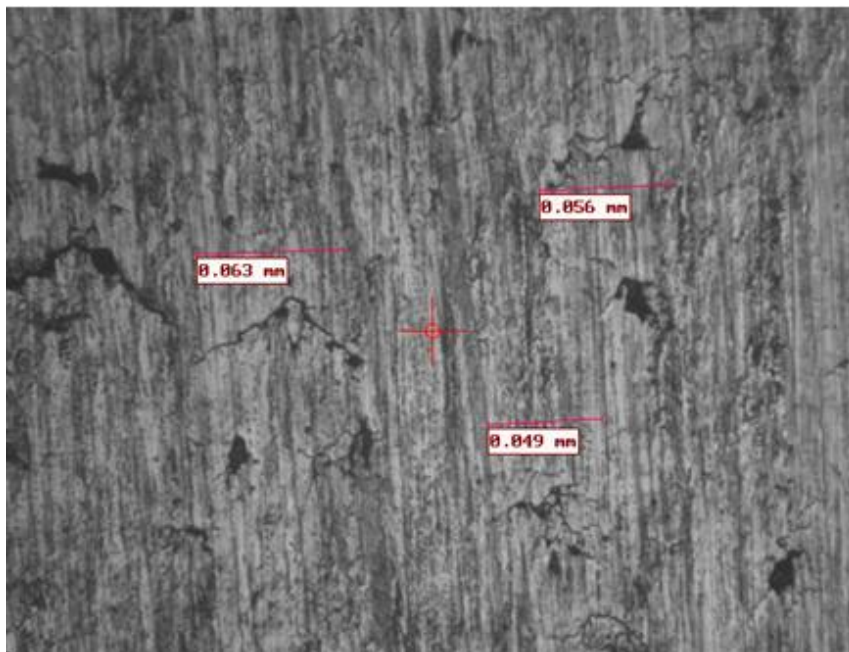


Figure 0.18: RCF-1-14, Surface Condition



Figure 0.19: RCF-1-15, 38.5% Increased Contact Width, crack 1.3mm

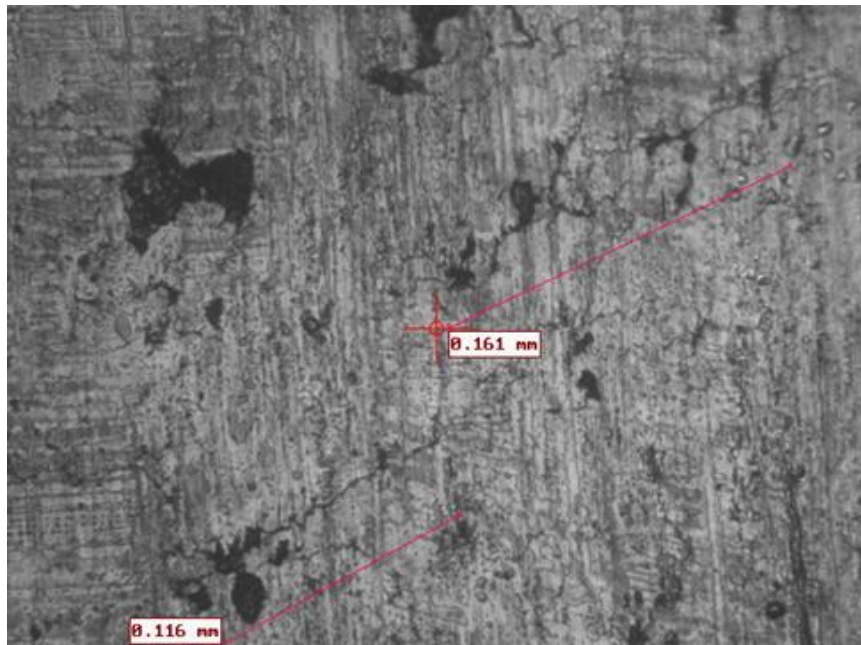


Figure 0.20: RCF-1-15, Surface Condition

Appendix B: Rolling Surface evaluation of RCF-2-XX

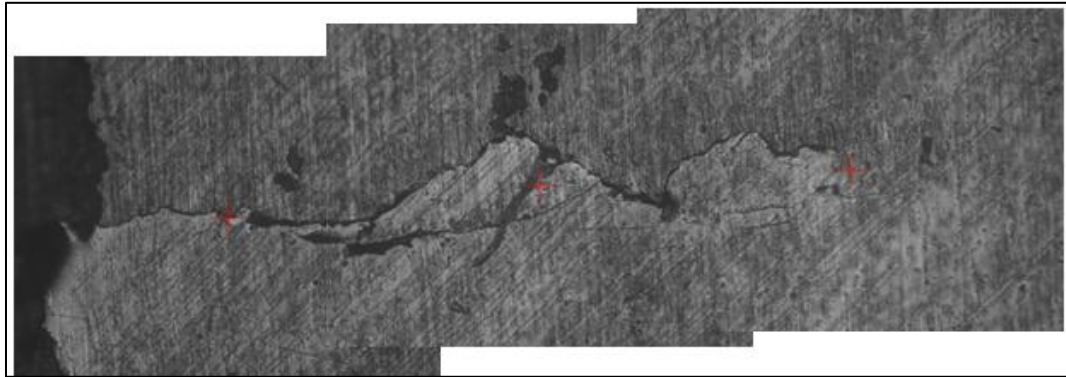


Figure 0.1: RCF-2-01, 11.8% Increased Contact Width, crack 1.4mm

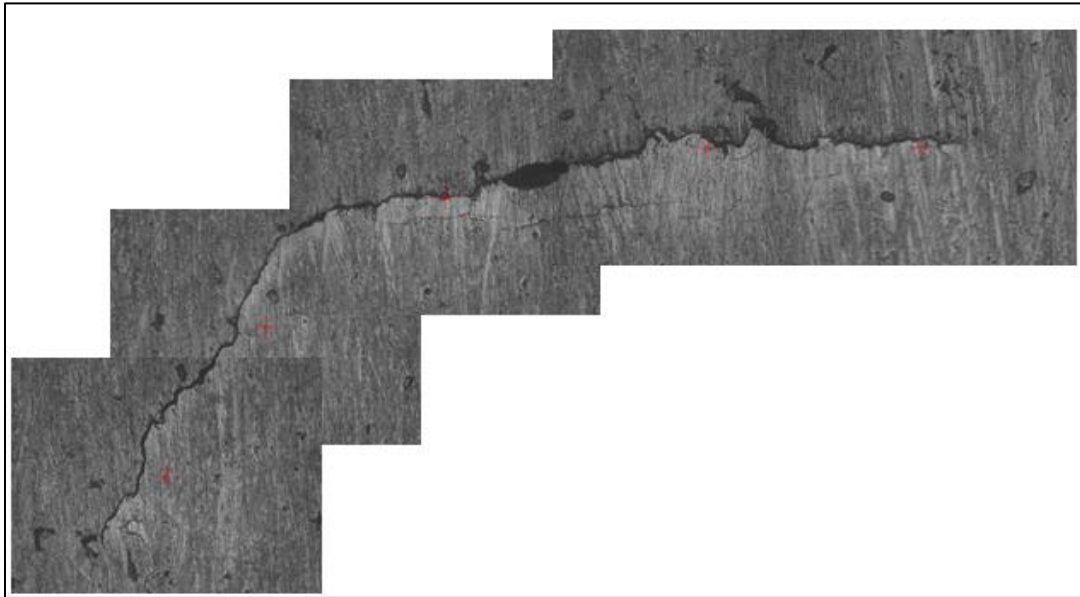


Figure 0.2: RCF-2-02, 9.8% Increased Contact Width, crack 2.15mm

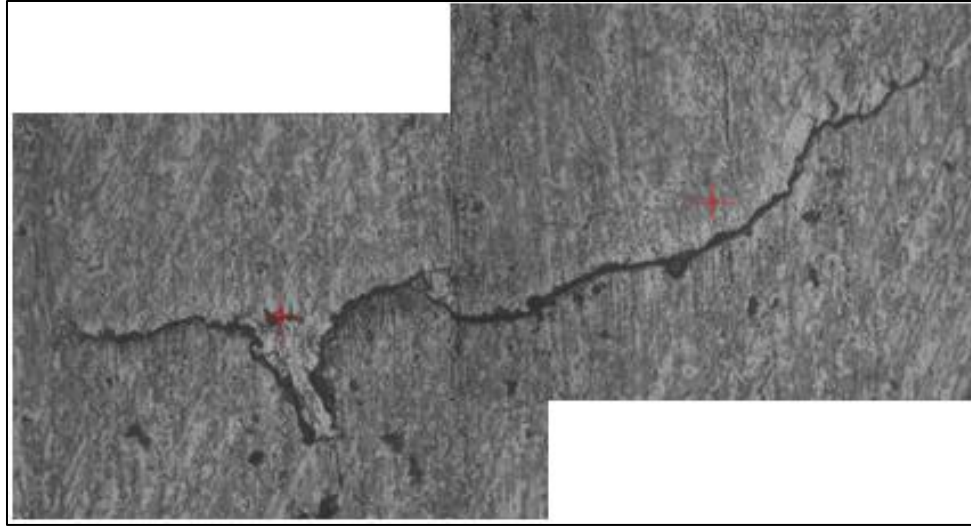


Figure 0.3: RCF-2-03, 11.8% Increased Contact Width, crack 1.2mm

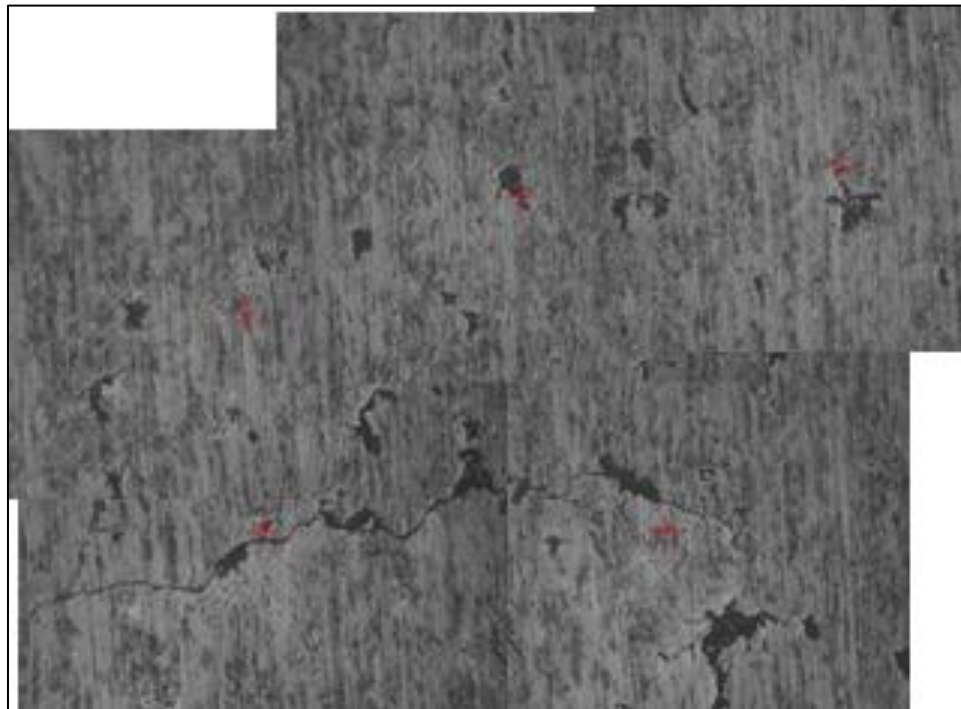


Figure 0.4: RCF-2-04, 11.8% Increased Contact Width, crack unknown

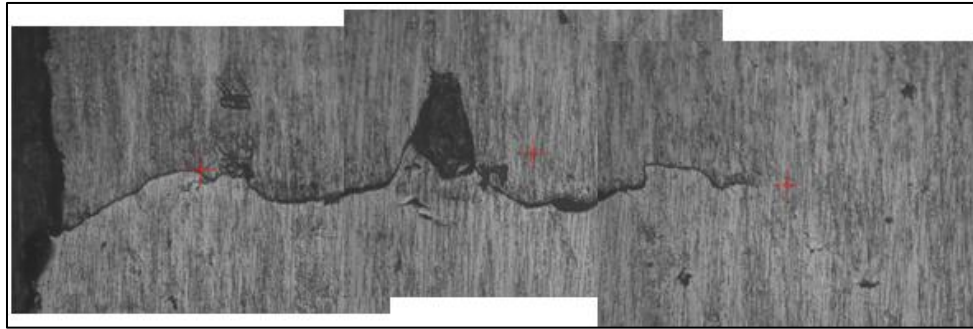


Figure 0.5: RCF-2-05, 11.8% Increased Contact Width, crack 1.4mm

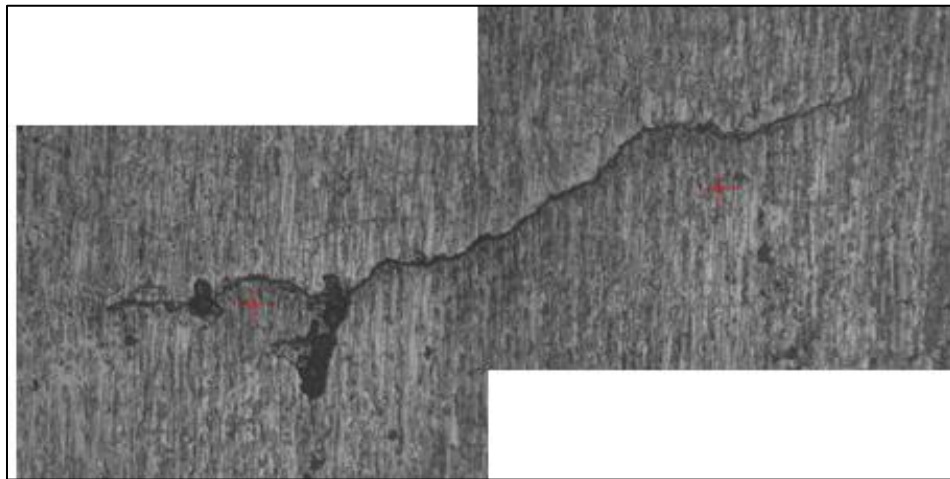


Figure 0.6: RCF-2-06, 17.6% Increased Contact Width, crack 1.1mm

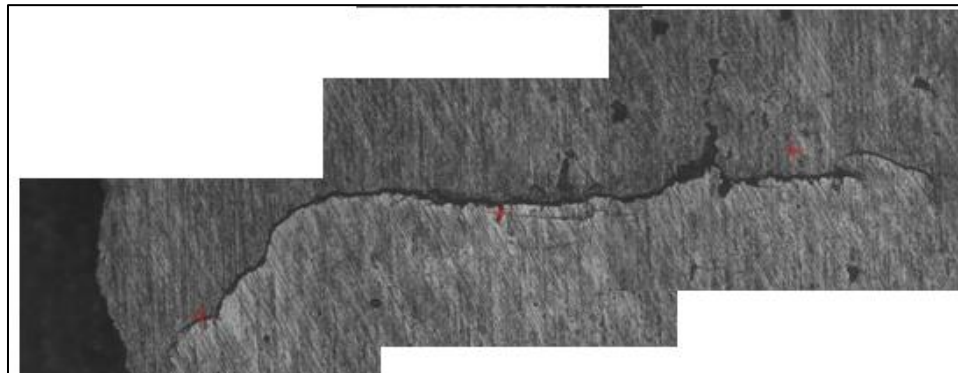


Figure 0.7: RCF-2-07, 17.6% Increased Contact Width, crack 1.5mm

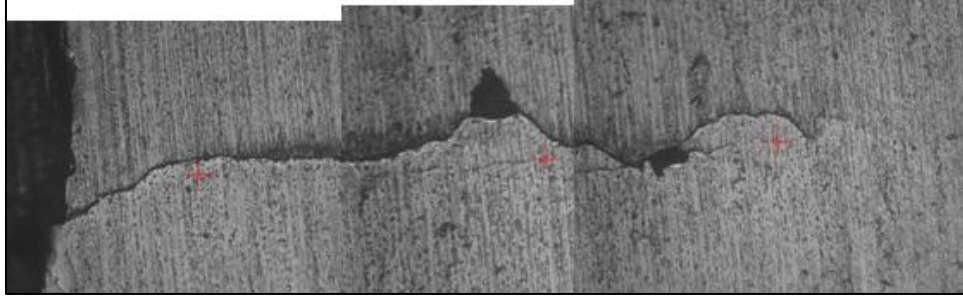


Figure 0.8: RCF-2-08, 13.7% Increased Contact Width, crack 1.5mm

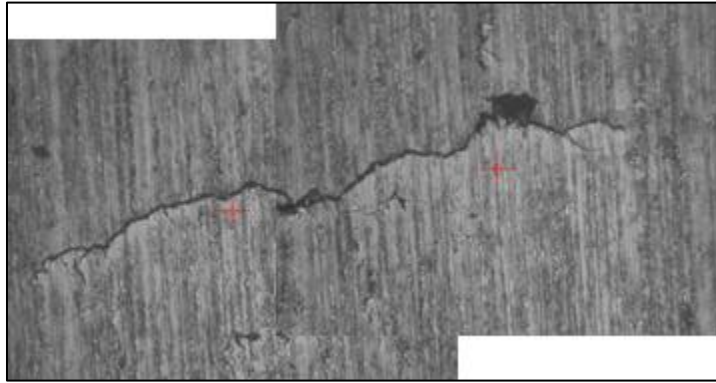


Figure 0.9: RCF-2-09, 17.6% Increased Contact Width, crack 1.0mm

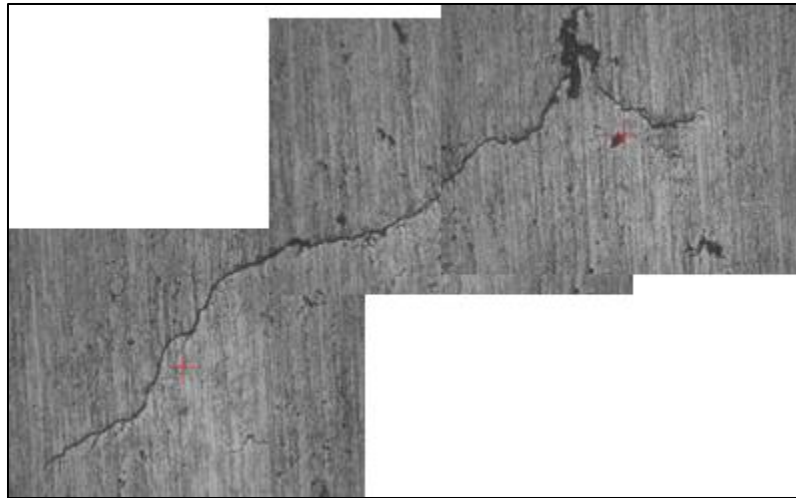


Figure 0.10: RCF-2-10, 17.6% Increased Contact Width, crack 1.3mm

Appendix C: Rolling Surface evaluation of RCF-3-XX

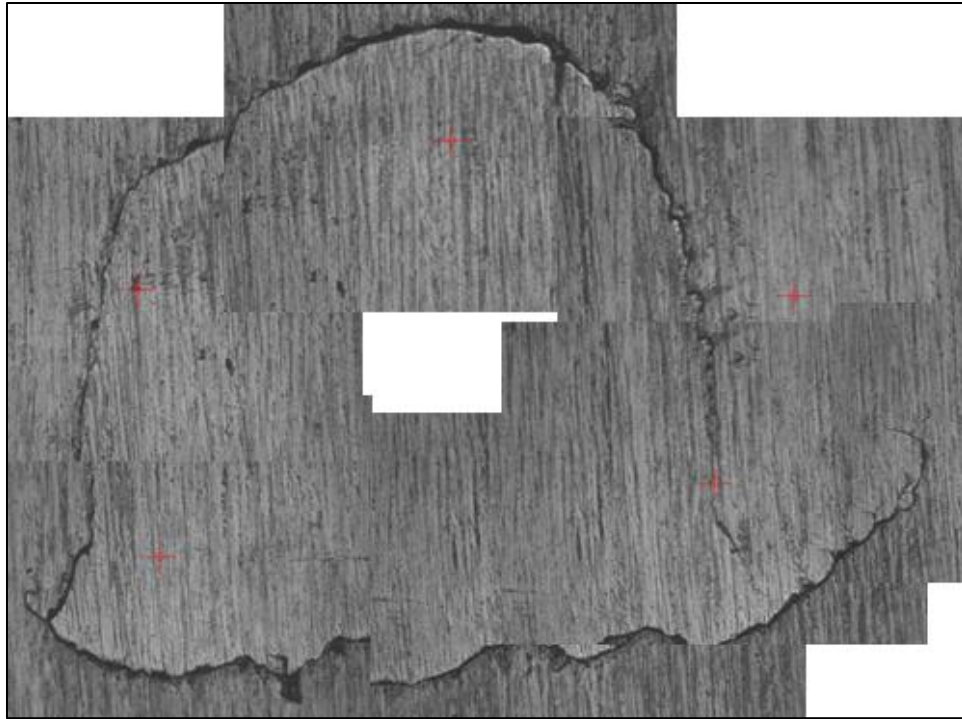


Figure 0.1: RCF-3-04, 9.4% Increased Contact Width, crack 1.9mm

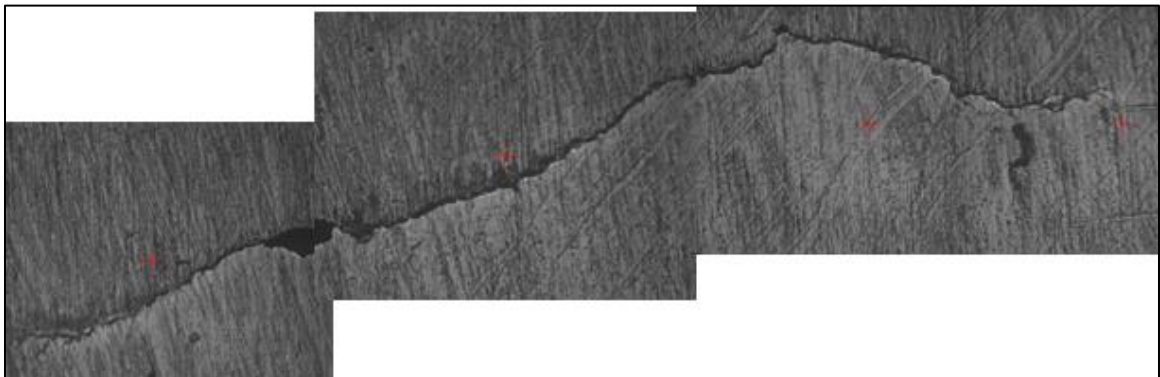


Figure 0.2: RCF-3-05, 7.8% Increased Contact Width, crack 2.2mm

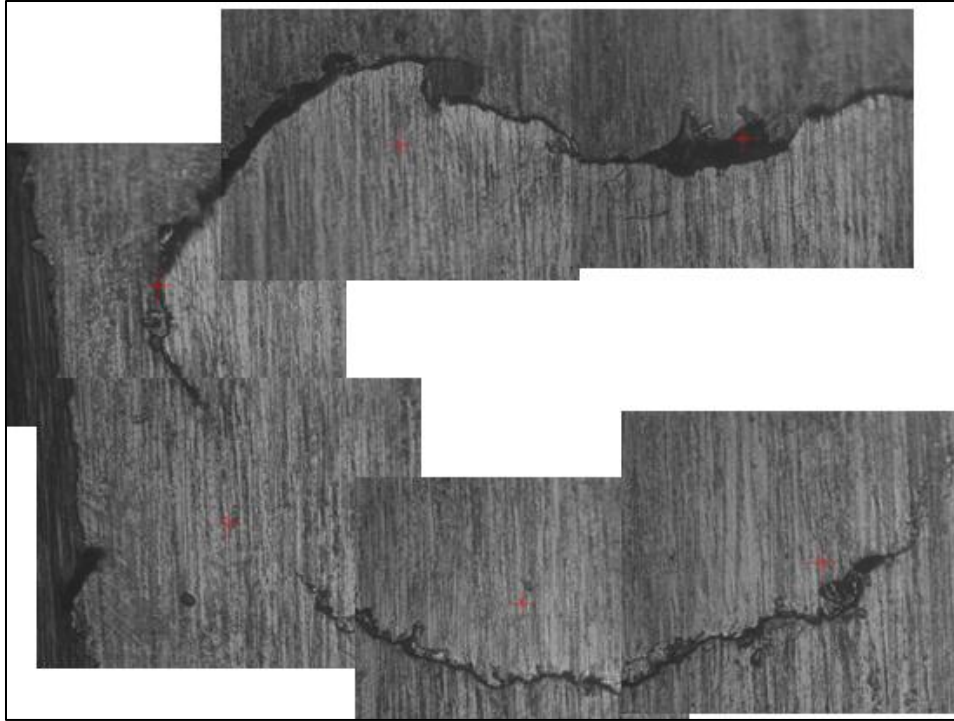


Figure 0.3: RCF-3-06, 7.3% Increased Contact Width, crack 1mm

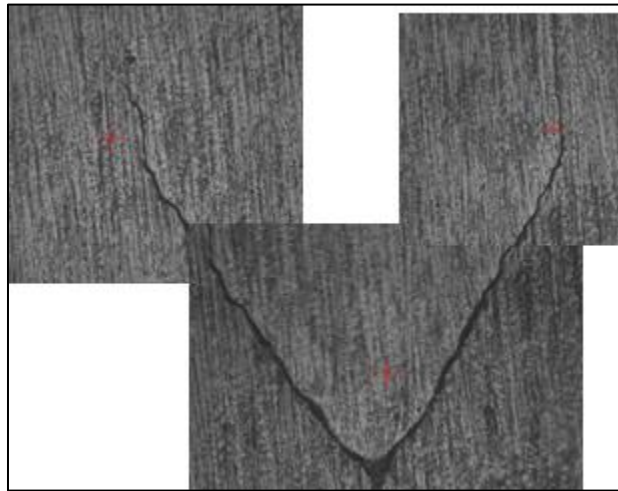


Figure 0.4: RCF-3-07, 9.2% Increased Contact Width, crack 0.62mm

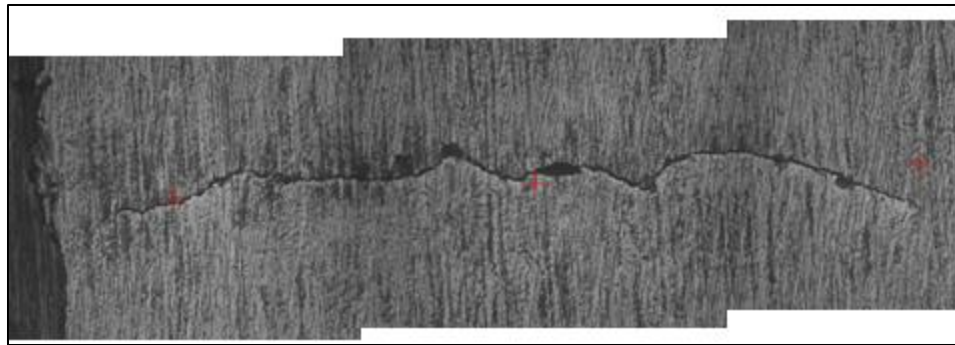


Figure 0.5: RCF-3-08, 4.9% Increased Contact Width, crack 1.5mm

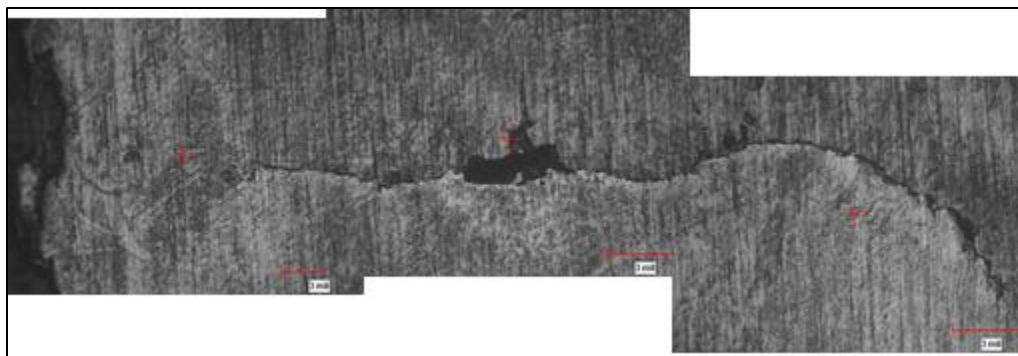


Figure 0.6: RCF-3-09, 9.8% Increased Contact Width, crack 1.5mm

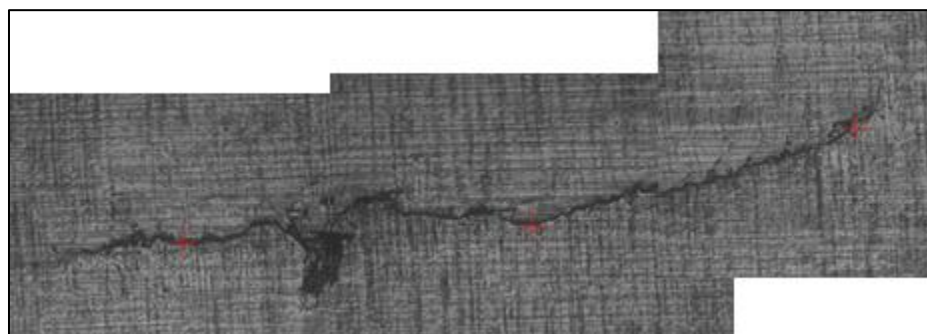


Figure 0.7: RCF-3-10, 9.8% Increased Contact Width, crack 1.5mm

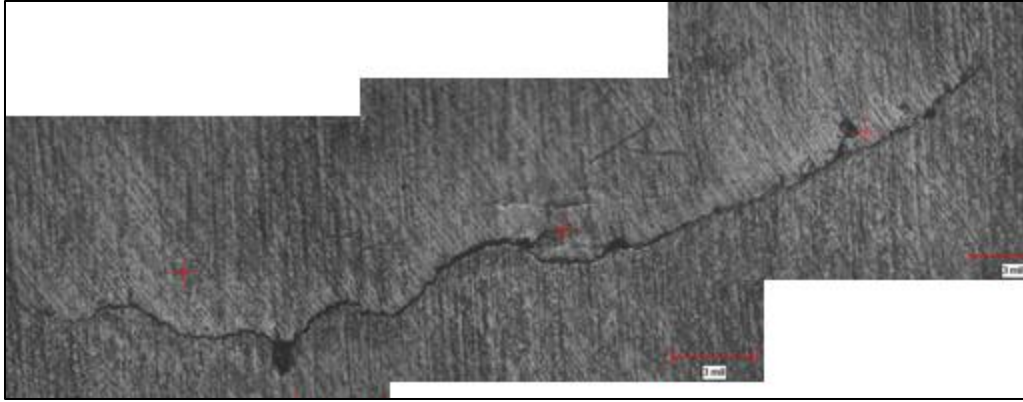


Figure 0.8: RCF-3-11, 7.8% Increased Contact Width, crack 1.7mm

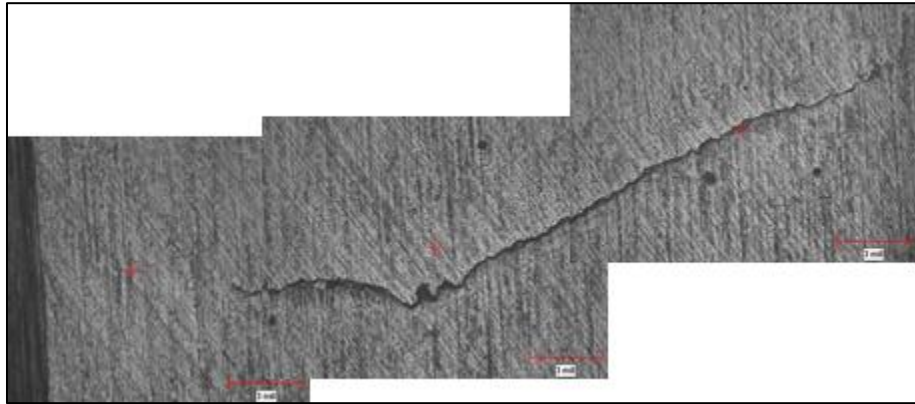


Figure 0.9: RCF-3-11, 9.8% Increased Contact Width, crack 1.35mm

Appendix D: Rolling Surface evaluation of RCF-4-XX

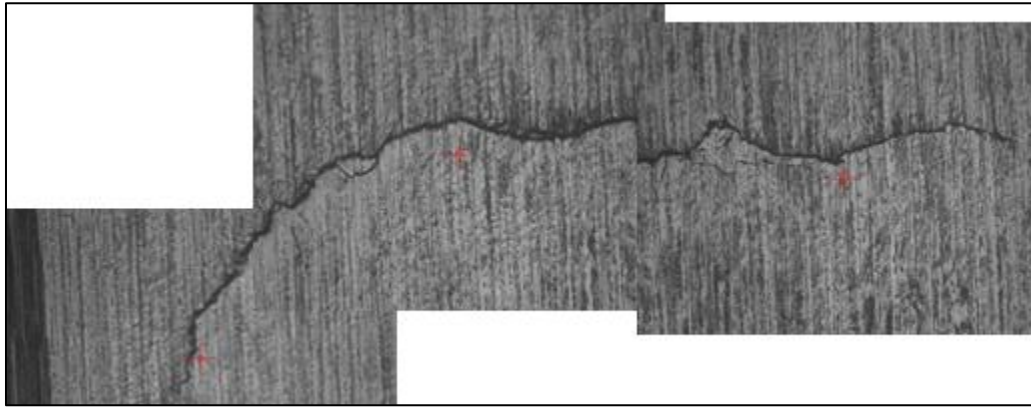


Figure 0.1: RCF-4-03, 11.2% Increased Contact Width, crack 1.5mm

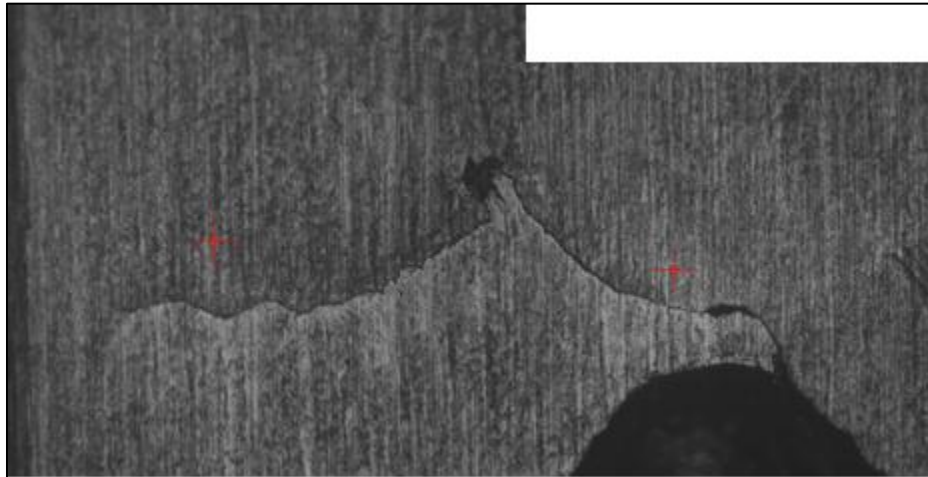


Figure 0.2: RCF-4-04, 11.6% Increased Contact Width, crack 0.7mm, Chunk Missing

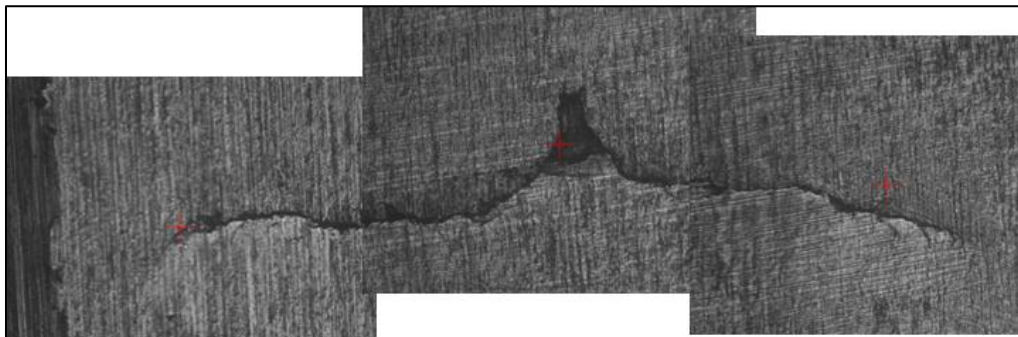


Figure 0.3: RCF-4-05, 8.4% Increased Contact Width, crack 1.5mm

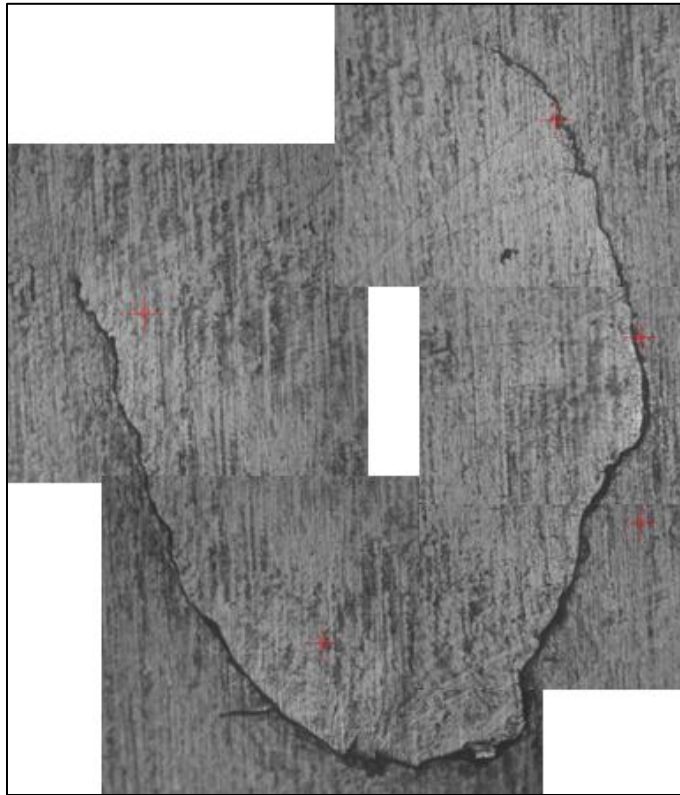


Figure 0.4: RCF-4-06, 12.2% Increased Contact Width, crack 0.9x1.2mm

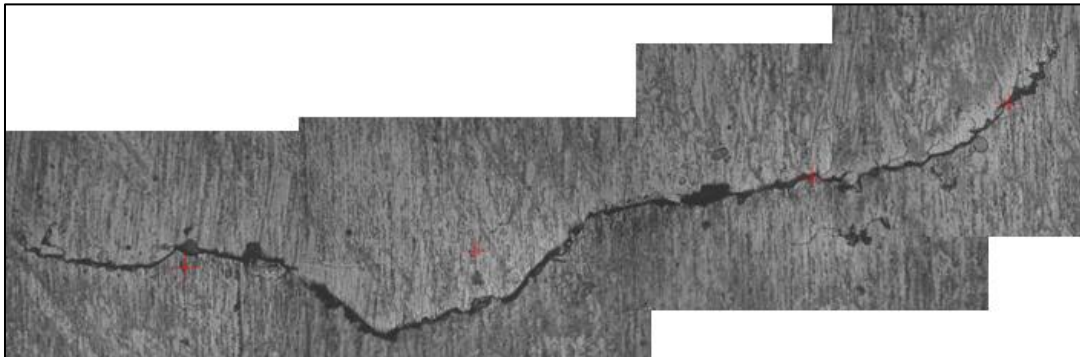


Figure 0.5: RCF-4-07, 14.7% Increased Contact Width, crack 2.1mm

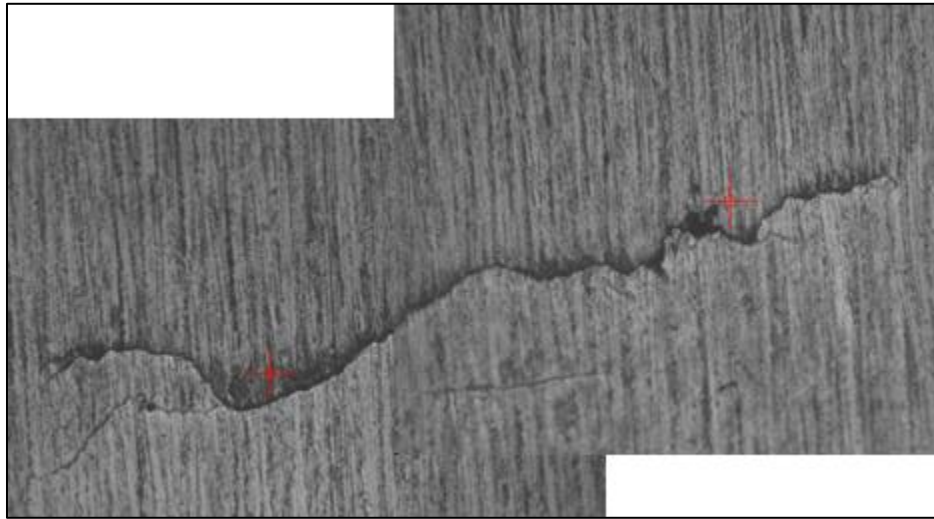


Figure 0.6: RCF-4-08, 7.8% Increased Contact Width, crack 1mm

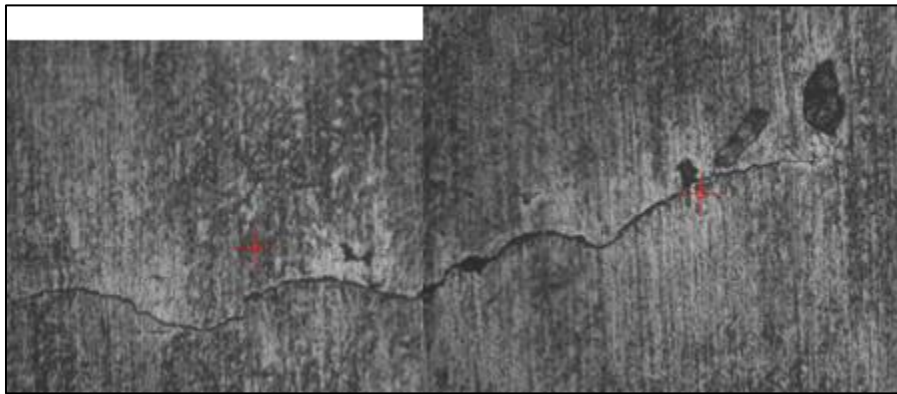


Figure 0.7: RCF-4-10, 8.8% Increased Contact Width, crack 1.1mm

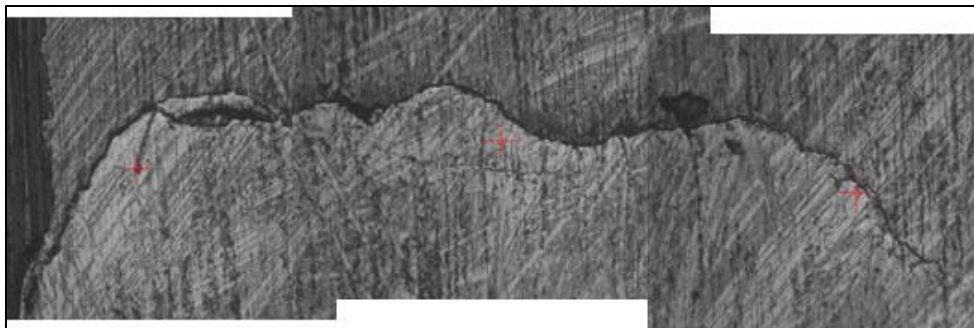


Figure 0.8: RCF-4-12, 19.6% Increased Contact Width, crack 1.5mm

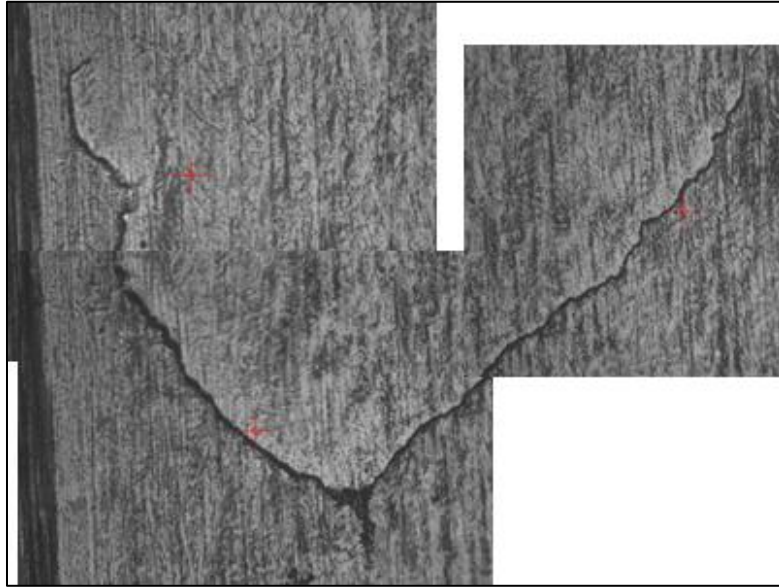


Figure 0.9: RCF-4-14, 14.9% Increased Contact Width, crack 1x0.6mm

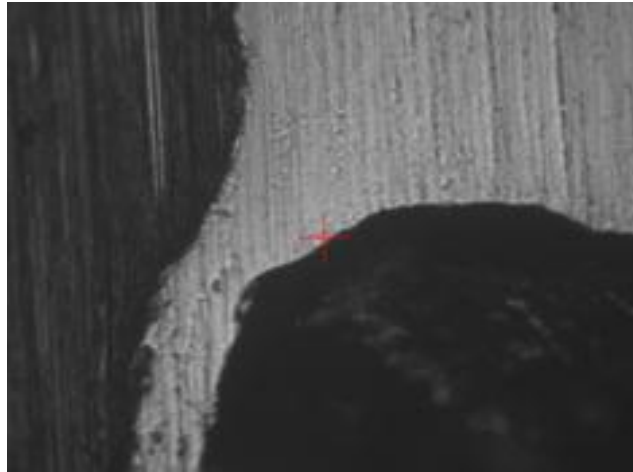


Figure 0.10: RCF-4-15, 7.6% Increased Contact Width, Missing Chunk 2.2x2.1mm

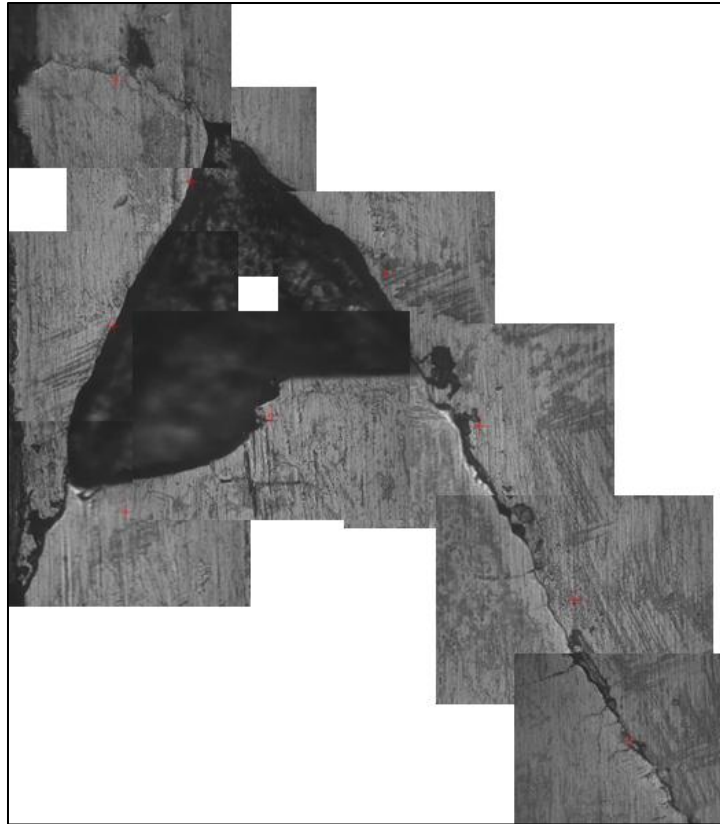


Figure 0.11: RCF-4-16, 7.8% Increased Contact Width

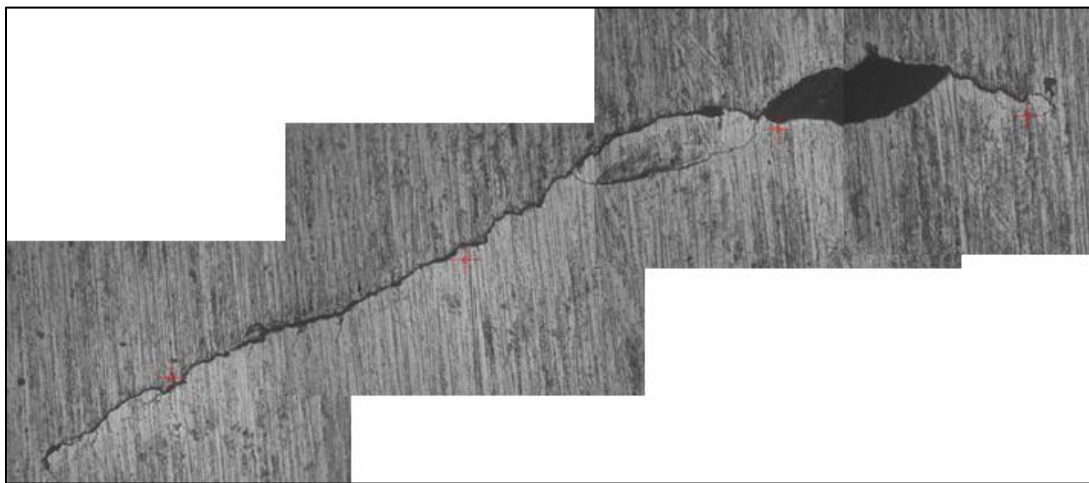


Figure 0.12: RCF-4-18, 12.5% Increased Contact Width, crack 2.1mm



Figure 0.13: RCF-4-19, 10.2% Increased Contact Width, crack 1.2mm

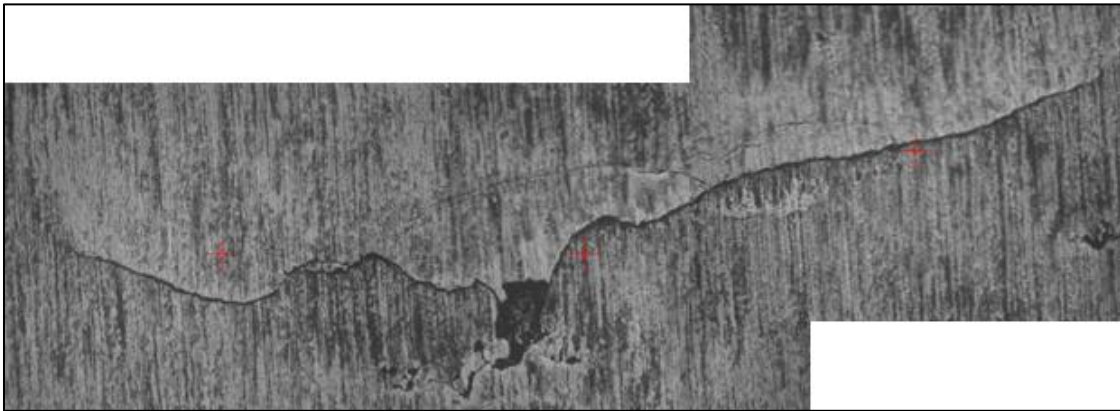


Figure 0.14: RCF-4-21, 13.9% Increased Contact Width, crack 1.7mm

Appendix E: Rolling Surface evaluation of RCF-5-XX

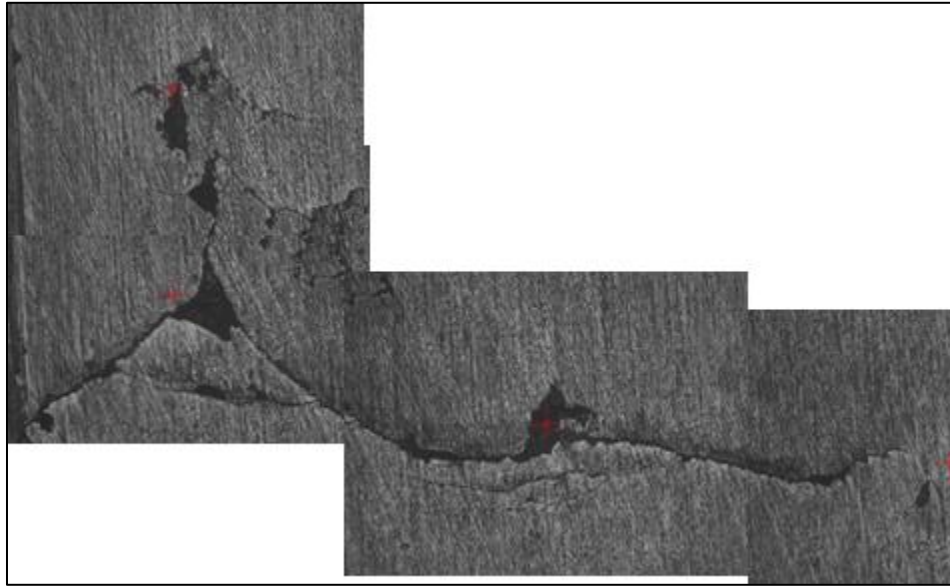


Figure 0.1: RCF-5-01, 17.6% Increased Contact Width, crack 1.5mm

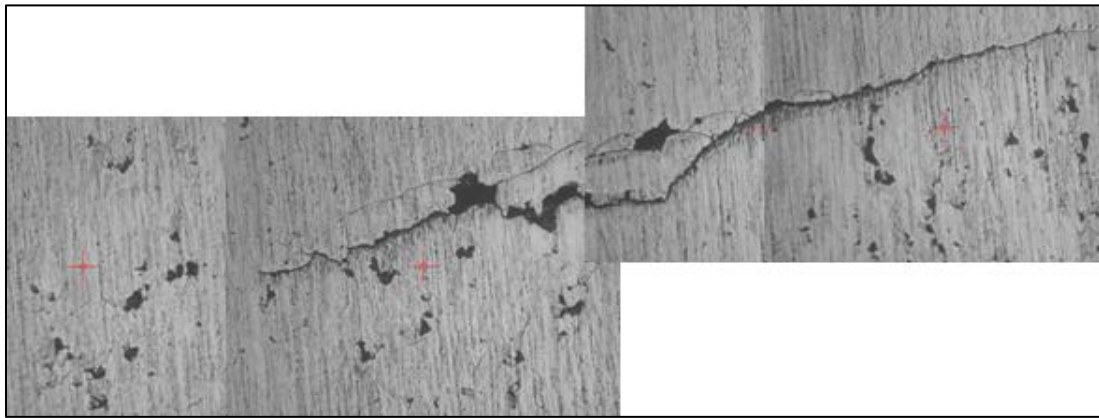


Figure 0.2: RCF-5-02, 5.1% Increased Contact Width

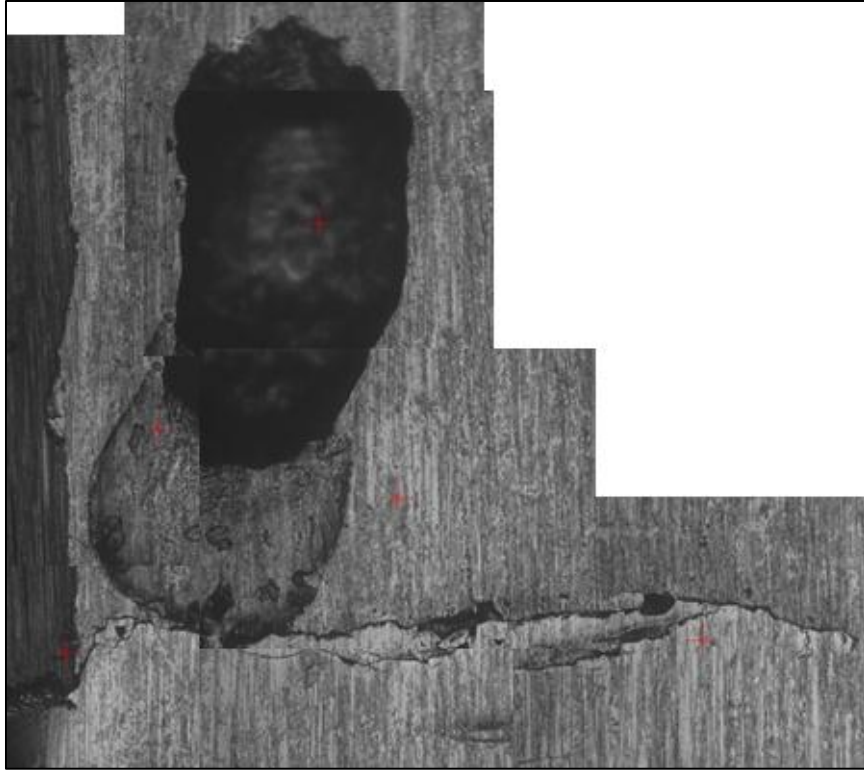


Figure 0.3: RCF-5-04, 4.9% Increased Contact Width, Crack 1.6mm

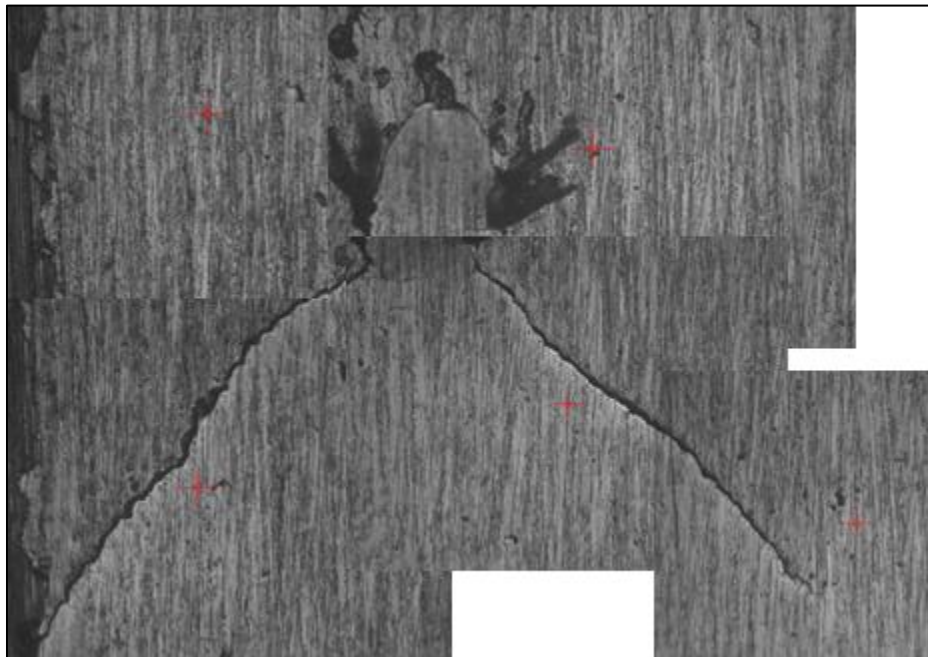


Figure 0.4: RCF-5-05, 3.5% Increased Contact Width, Crack 1.2mm



Figure 0.5: RCF-5-06, 3.9% Increased Contact Width, Crack 1.5mm

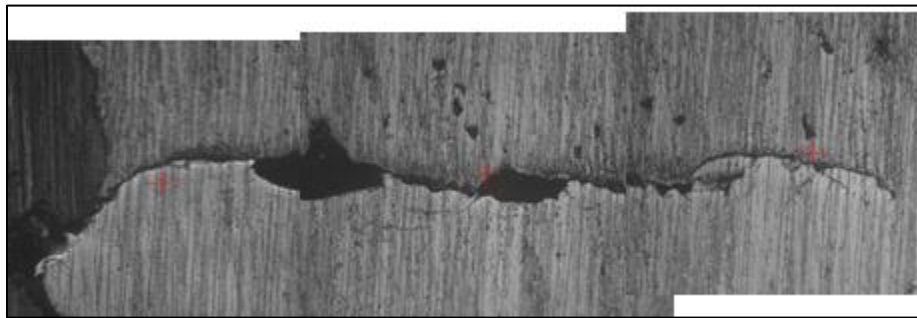


Figure 0.6: RCF-5-08, 6.9% Increased Contact Width, Crack 1.5mm

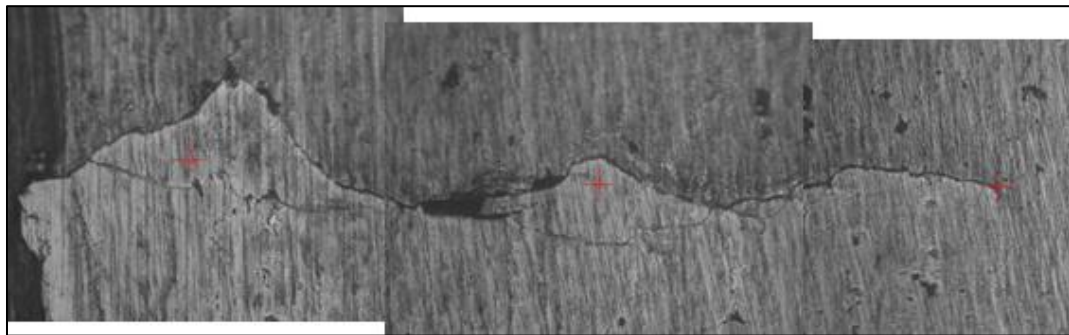


Figure 0.7: RCF-5-09, 4.7% Increased Contact Width, Crack 1.6mm

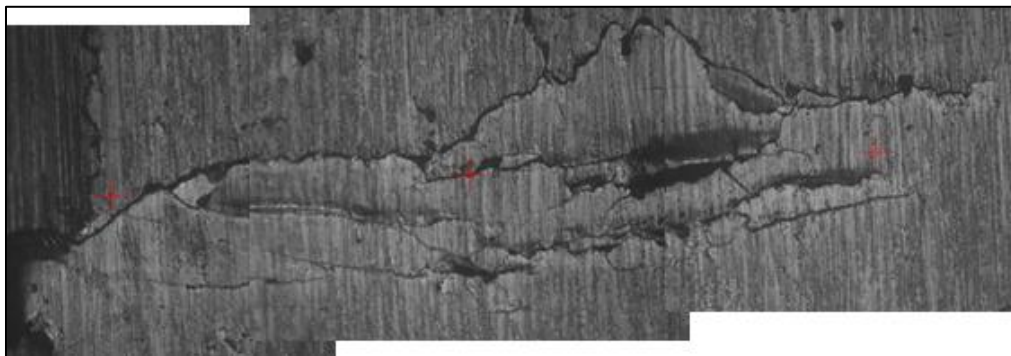


Figure 0.8: RCF-5-10, 4.1% Increased Contact Width, Crack 1.5mm



Figure 0.9: RCF-5-11, 4.1% Increased Contact Width

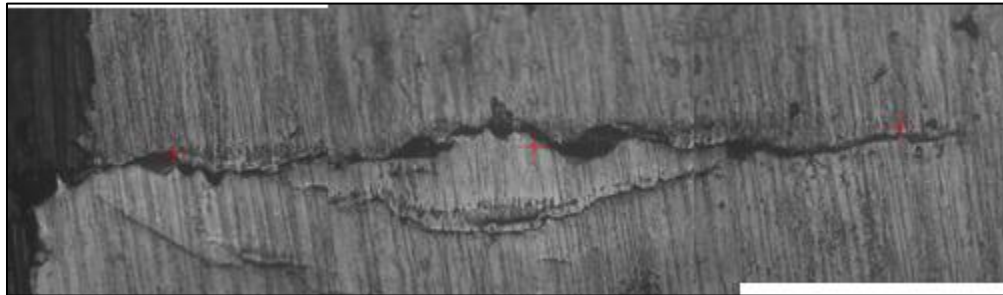


Figure 0.10: RCF-5-11, 4.1% Increased Contact Width, Crack 1.5mm

Appendix F: Weibull Curve

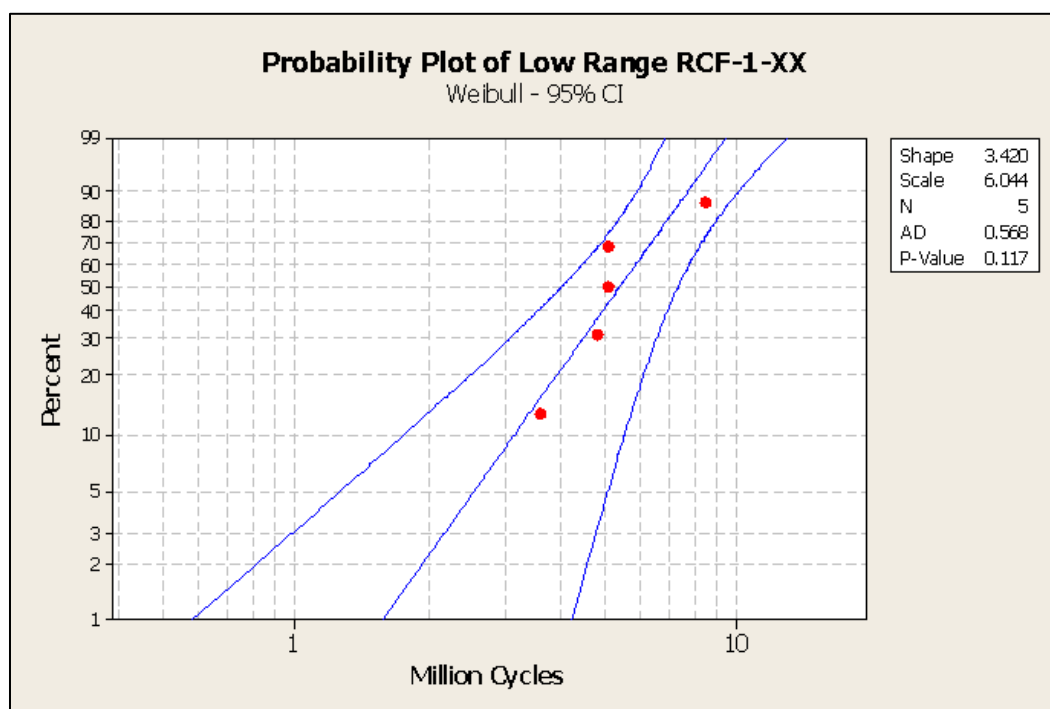


Figure 0.1: RCF-1-XX, Low Range, Weibull Plot

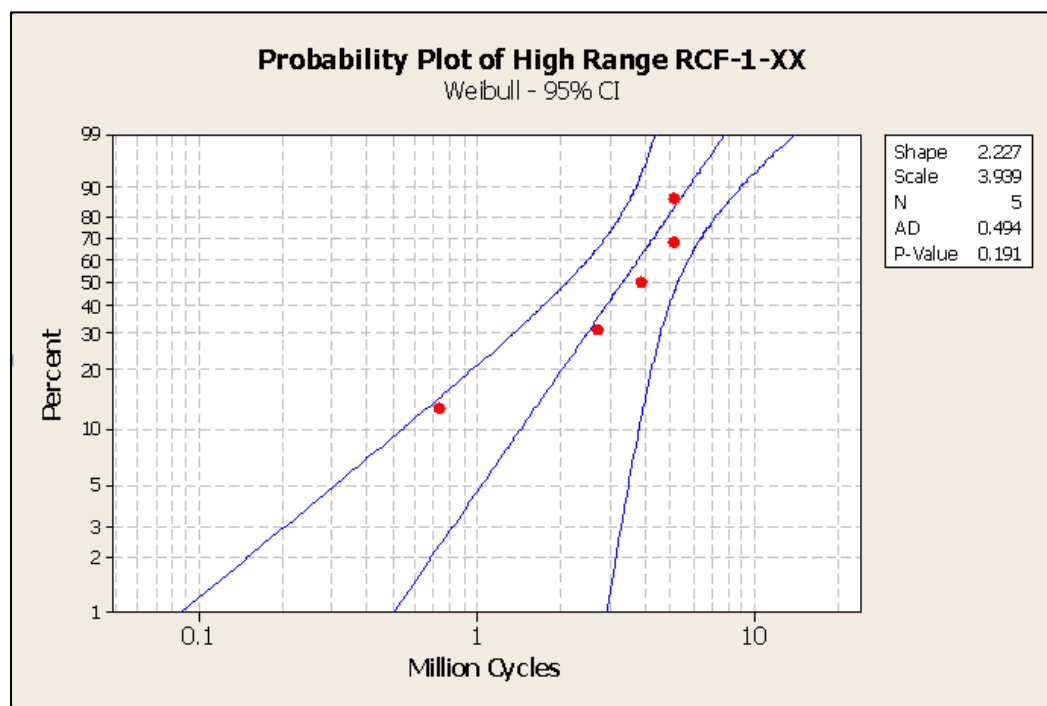


Figure 0.2: RCF-1-XX, High Range, Weibull Plot

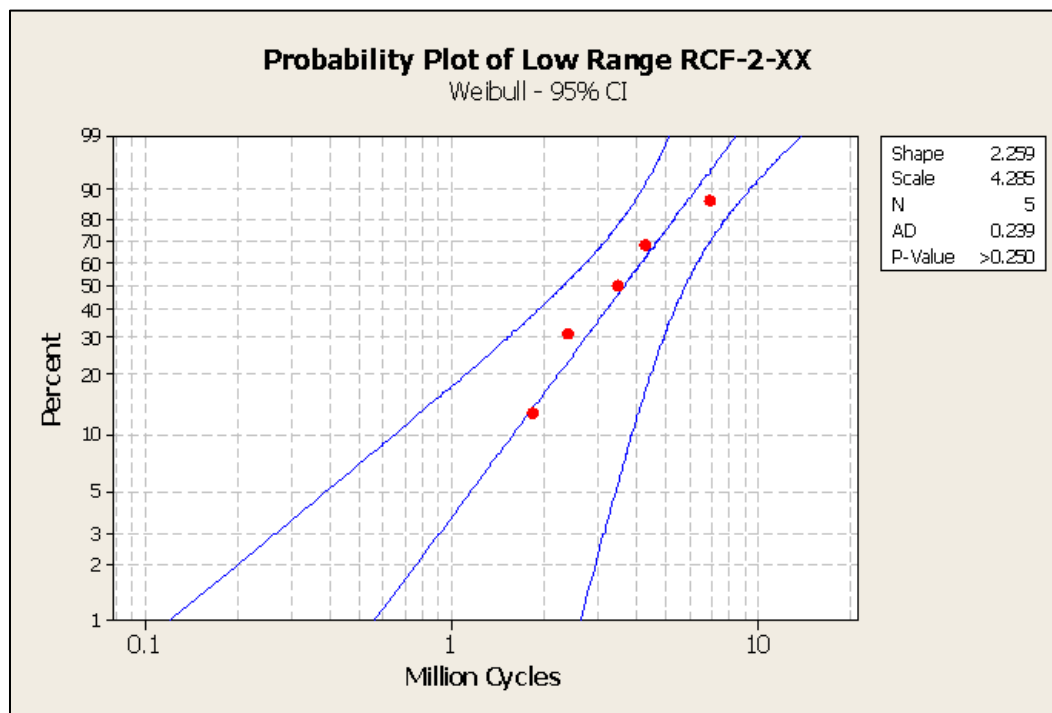


Figure 0.3: RCF-2-XX, Low Range, Weibull Plot

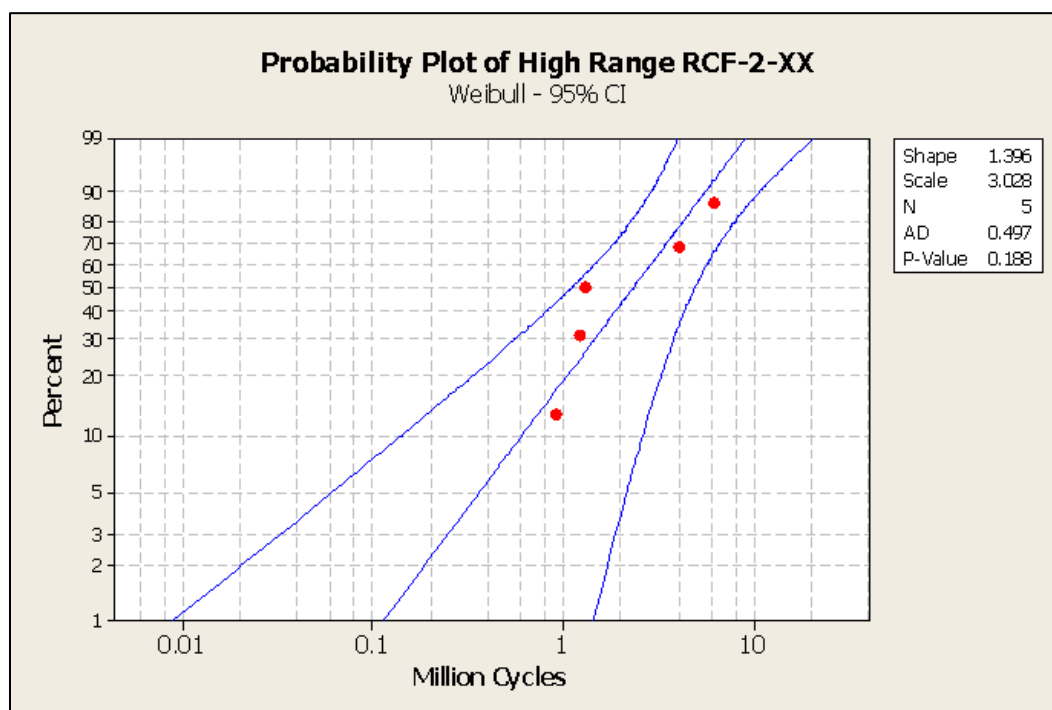


Figure 0.4: RCF-2-XX, High Range, Weibull Plot

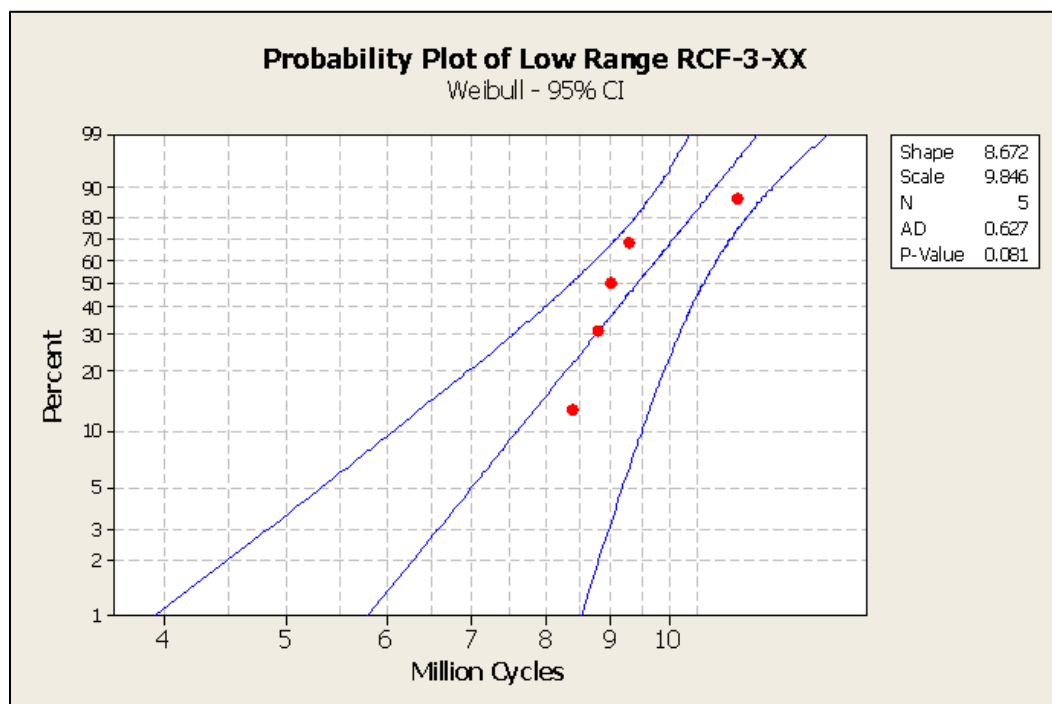


Figure 0.5: RCF-3-XX, Low Range, Weibull Plot

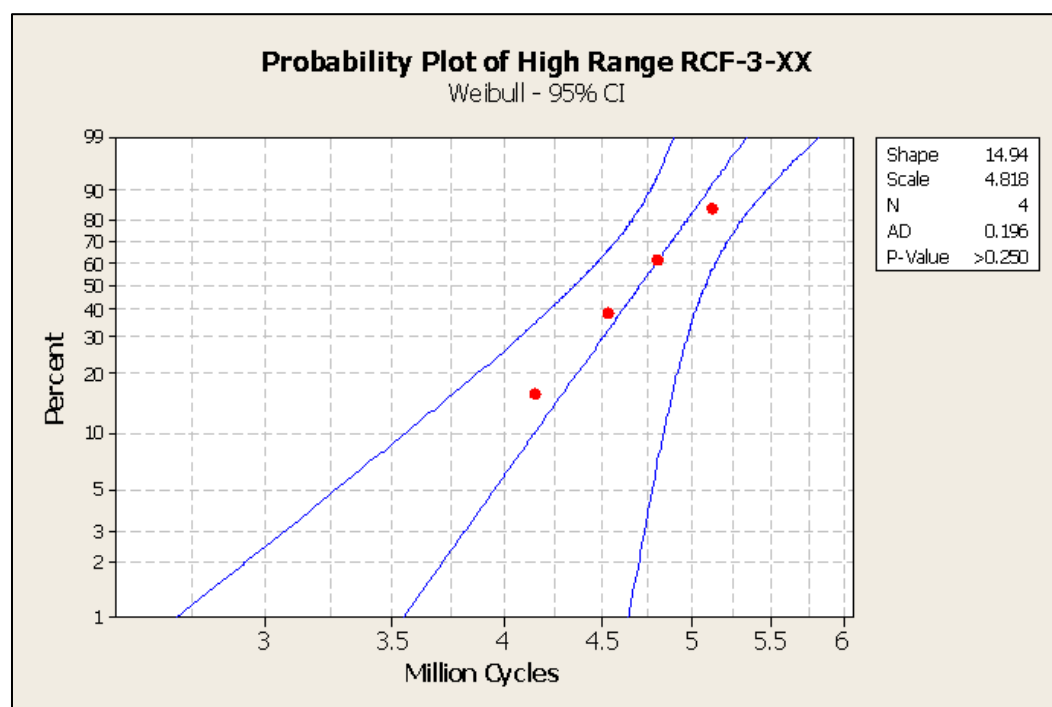


Figure 0.6: RCF-3-XX, High Range, Weibull Plot

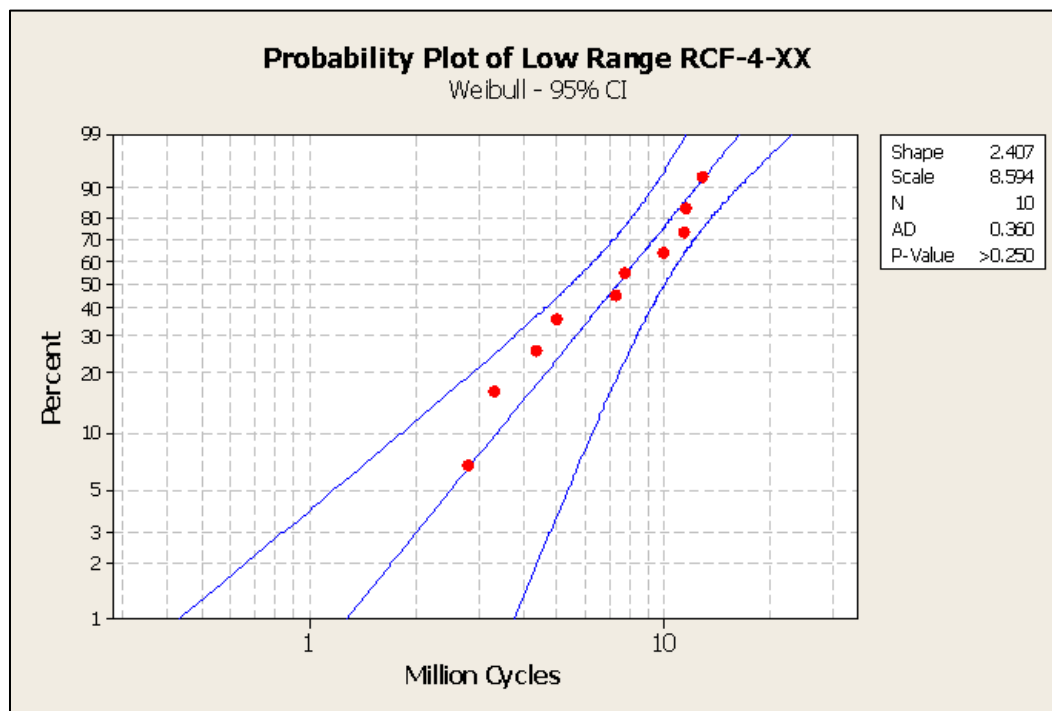


Figure 0.7: RCF-4-XX, Low Range, Weibull Plot

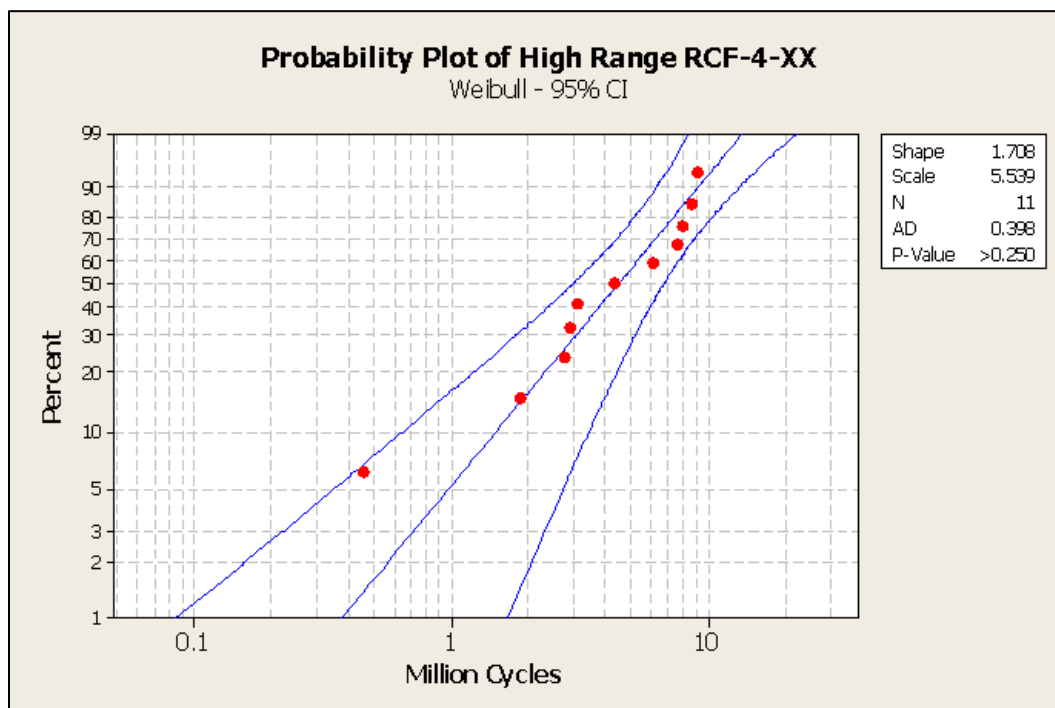


Figure 0.8: RCF-4-XX, High Range, Weibull Plot

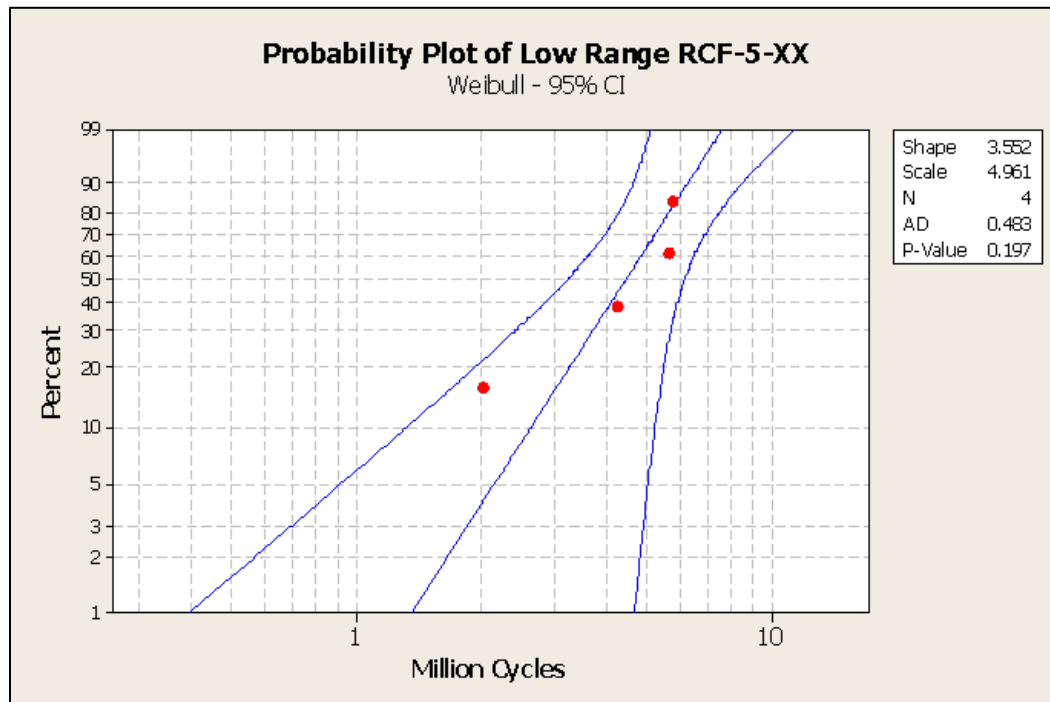


Figure 0.9: RCF-5-XX, Low Range, Weibull Plot

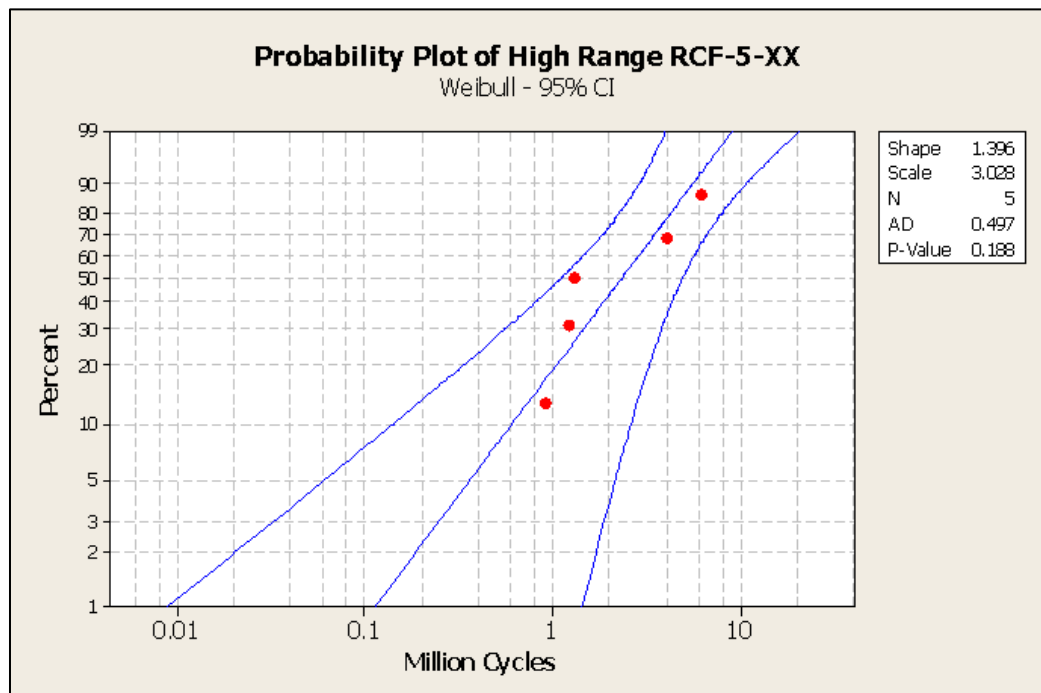


Figure 0.10: RCF-5-XX, High Rang, Weilbull Plot